Adile YÜRÜK

Ph.D. Thesis

AGU 2024

PREPARATION and CHARACTERIZATION of A NEW GENERATION CARDIAC PATCH

Ph.D. THESIS
SUBMITTED TO THE DEPARTMENT OF BIOENGINEERING
AND THE GRADUATE SCHOOL OF ENGINEERING AND SCIENCE
OF ABDULLAH GUL UNIVERSITY
IN PARTIAL FULFILLMENT OF THE REQUIREMENTS
FOR THE DEGREE OF
DOCTOR OF PHILOSOPHY

By
Adile YÜRÜK
December 2024

PREPARATION and CHARACTERIZATION of A NEW GENERATION CARDIAC PATCH

Ph.D. THESIS
SUBMITTED TO THE DEPARTMENT OF BIOENGINEERING
AND THE GRADUATE SCHOOL OF ENGINEERING AND SCIENCE OF
ABDULLAH GUL UNIVERSITY
IN PARTIAL FULFILLMENT OF THE REQUIREMENTS
FOR THE DEGREE OF
DOCTOR OF PHILOSOPHY

By
Adile YÜRÜK
December 2024

SCIENTIFIC ETHICS COMPLIANCE

I hereby declare that all information in this document has been obtained in accordance with academic rules and ethical conduct. I also declare that, as required by these rules and conduct, I have fully cited and referenced all materials and results that are not original to this work.

Name-Surname: Adile YÜRÜK

Signature :

REGULATORY COMPLIANCE

Ph.D. thesis titled Preparation and Characterization of a New Generation Cardiac Patch has been prepared in accordance with the Thesis Writing Guidelines of the Abdullah Gül University, Graduate School of Engineering & Science.

Prepared By	Advisor
Adile YÜRÜK	Assoc. Prof. İsmail Alper İŞOĞLU
Signature	Signature

Head of the Bioengineering Program
Assist. Prof. Emel Başak GENCER AKÇOK
Signature

ACCEPTANCE AND APPROVAL

Ph.D. thesis titled Preparation and Characterization of a New Generation Cardiac Patch and prepared by Adile YÜRÜK has been accepted by the jury in the Bioengineering Graduate Program at Abdullah Gül University, Graduate School of Engineering & Science.

20/12/2024

(Thesis Defense Exam Date)

JURY:

Advisor : Assoc. Prof. İsmail Alper İŞOĞLU

Member : Prof. Dr. Sevil DİNÇER İŞOĞLU

Member : Assoc. Prof. Ömer AYDIN

Member : Assoc. Prof. Murat TOPUZOĞULLARI

Member : Assist. Prof. Tuğrul Tolga DEMİRTAŞ

APPROVAL:

The acceptance of this Ph.D. thesis has been approved by the decision of the Abdullah Gül University, Graduate School of Engineering & Science, Executive Board dated ….. /….. / …….. and numbered ……..……. .

…….. /…….. / ……..

Graduate School Dean

Prof. İrfan ALAN

ABSTRACT

PREPARATION and CHARACTERIZATION of A NEW GENERATION CARDIAC PATCH

Adile YÜRÜK
Ph.D. in Bioengineering
Advisor: Assoc. Prof. İsmail Alper İŞOĞLU
December 2024

Cardiovascular diseases (CVDs) are the leading cause of deaths worldwide, CVDs-based myocardial defects lead to mechanical, electrical, and structural dysfunctions in the heart. Therefore, cardiac patches hold great promise for the treatment of myocardial defects. In this thesis, we developed a bilayered cardiac patch comprising a first layer of polyaniline (PANI) nanoparticle coated decellularized pericardium and a second layer of a poly (lactic-co-glycolic acid (PLGA))/gelatin electrospun membrane containing vascular endothelial growth factor (VEGF) and hawthorn extract. For the second layer, membranes having the fiber diameters between 850-1200 nm demonstrated the controlled release behaviour within 28 days. Following the layers were prepared and characterized separately, they were integrated via a biocompatible tissue adhesive. The bilayered cardiac patch demonstrated the conductivity of $9.093\pm8.6x10^{-4}$ S/cm, anticoagulant ability of 331±65.1 APTT time, tensile strength of 22.70±6.33 MPa, elongation of %53.58±10.63, hemolysis ratio of %0.421±0.191, and over 90% cell viability with cardiomyocytes. In the final part of thesis, cardiac patch efficiency was investigated in rat myocardial infarction (MI) model for 28 days. The patch implanted groups demonstrated an improvement in cardiac functions, with fractional shortening increasing from 44.35% to 50.46% and ejection fraction rising from 80.73% to 87.99% when compared to the MI group. The heart sections were histologically examined by Hematoxylin-Eosin (H&E) and Masson's Trichrome staining, scar sizes and left ventricle wall thickness were determined for all groups. The immunofluorescence staining was applied to determine the vessel formations, actin filaments of muscle cells, cardiac cells and macrophage markers using von Willebrand Factor (vwf), αSMA, CD31, GATA4 CD34, and CD68 antibodies. The obtained results support the proposed cardiac patch can be a promising candidate for the treatment of myocardial defects.

Keywords:cardiac patch, myocardial defect, pericardium, electrospinning, PLGA/gelatin

ÖZET

YENİ NESİL BİR KARDİYAK YAMANIN HAZIRLANMASI ve KARAKTERİZASYONU

Adile YÜRÜK
Biyomühendislik Anabilim Dalı Doktora
Tez Danışmanı: Doç. Dr. İsmail Alper İŞOĞLU
Aralık 2024

Dünya genelinde ölümlerin büyük çoğunluğunu kardiyovasküler hastalıklar (KVH) oluşturmaktadır, KVH kaynaklı miyokard hasarları kalpte mekanik, elektriksel ve yapısal işlev bozukluklarına sebep olmaktadır. Bu sebepten kardiyak yamalar miyokard hasarlarının tedavisinde umut vadetmektedir. Bu tez çalışmasında, ilk katmanı hücresizleştirilmiş perikardın poli-anilin (PANI) nanopartikülleri ile kaplanması ile, ikinci katman ise büyüme faktörü ve alıç özütü içeren poli (laktik-ko-glikolik asit (PLGA))/jelatin elektroeğrilmiş membrandan oluşmaktadır. İkinci katman için membranların fiber çapları 850-1200 nm arasında elde edilmiş ve 28 gün boyunca kontrollü salınım davranışı sergilemişlerdir. Katmanlar hazırlanıp karakterize edildikten sonra biyouyumlu bir doku yapıştırıcısı ile entegre edilmiştir. Çift katmanlı kardiyak yama, $9.093\pm8.6\text{x}10^{-4}$ S/cm iletkenlik, 331±65.1 APTT süresi antikoagülan özellik, 22.70±6.33 MPa çekme dayanımı, %53.58±10.63 uzama oranı, %0.421±0.191 hemoliz oranı ve kardiyomiyosit hücreleri ile %90'dan fazla hücre canlılığı göstermiştir. Tezin son bölümünde, kardiyak yamanın etkinliği sıçan miyokard enfarktüsü (MI) modelinde 28 gün için incelenmiştir. Yama uygulanan gruplar MI grubu ile karşılaştırıldığında fraksiyonel kısalma oranının %44.35'ten %50.46'ya ve ejeksiyon fraksiyonunun %80.73'ten %87.99'a yükseldiğini gösteren kardiyak fonksiyonlarda iyileşme sergilemiştir. Kalp kesitleri, Hematoksilen-Eozin (H&E) ve Masson Trikom boyama yöntemleriyle histolojik olarak incelenmiş, tüm gruplar için miyokard hasar boyutları ve sol ventrikül duvar kalınlıkları belirlenmiştir. Damar oluşumlarını, kas hücrelerinin aktin filamentlerini, kardiyak hücreleri ve makrofaj işaretçilerini belirlemek için von Willebrand Faktörü (vwf), αSMA, CD31, GATA4, CD34 ve CD68 antikorları kullanılarak immünofloresan boyama yapılmıştır. Elde edilen sonuçlar, önerilen kardiyak yamanın miyokard hasarlarının tedavisi için umut verici bir aday olabileceğini desteklemektedir.

Anahtar kelimeler: kardiyak yama, miyokard hasarı, perikard, elektroeğirme, PLGA/jelatine

Acknowledgements

I would like to express my deepest gratitude to my esteemed advisor Assoc. Prof. İsmail Alper İŞOĞLU for his endless support, invaluable knowledge, and guidance throughout my PhD. His expertise, professionalism, patience, and encouragement have been a constant source of inspiration for me, I am truly grateful for his unwavering support and for always being there for me.

I would like to thank to the Higher Education Council of Turkey for their support to me through the "YÖK100/2000, Micro and Nanotechnology" scholarship program. I extend my gratitude to the relevant authorities for the support provided to me through The Scientific and Technological Research Council of Turkey (TÜBİTAK) Scientist Support Programs Directorate (BİDEB) 2211-Domestic Graduate Scholarship Program. Additionally, I would like many thanks to TÜBİTAK programs that BİDEB-2250, BİDEB 2244-B, and ARDEB (1003, Project no: 216S639) for their financial supports to me. I am also grateful to the European Federation of Biochemistry (FEBS) for awarding me twice with "Young Scientist Travel Grants". This thesis project was financially supported by TÜBİTAK within the scope of ARDEB-1001 program with 122M020 project number, we would like to thank to TÜBİTAK.

I would like to thank to my thesis progress committee Assoc. Prof. Ömer AYDIN and Prof. Dr Sevil DİNÇER İŞOĞLU. I would like to thank to Burhan KABATAŞ and Graduate School of Science team of Abdullah Gül University for their unwavering support during my PhD. I would like to thank to Prof. Dr Ayhan DÜZLER, Assist. Prof. Osman Okan ÖZOCAK, Assist. Prof. Gonca KAMACI ÖZOCAK, Dr. Gülden SARI, Prof. Dr. Ali BAYKAL, Prof. Dr Feyzullah BEYAZ, Dr. Fatma KÖSE, Orhan BAHAR, and Ahmet CABİR for their contributions to our *in vivo* studies.

Lastly, I want to express my deepest thanks to everyone who supported me throughout my PhD journey. I want to extend my heartfelt gratitude to my beloved family for their unwavering support, love, and encouragement, which have been my constant source of strength.

Adile YÜRÜK

TABLE OF CONTENTS

LIST OF FIGURES

LIST OF TABLES

LIST OF ABBREVIATIONS

ACE	Angiotensin-Converting Enzyme
αSMA	Alpha-Smooth Muscle Actin
ANI	Aniline
APTT	Activated Partial Thromboplastin Time
APS	Ammonium Peroxide Sulphate
ATR	Attenuated Total Reflectance
AV Node	Atrioventricular Node
CHAPS	3-[(3-cholamidopropyl)dimethylammonium]-1-propanesulfonate
CMs	Cardiomyocytes
CVD	Cardiovascular Diseases
DAPI	Diamidino-2-Phenylindole
DBSA	Dodecylbenzene Sulfonic Acid
DP	Decellularized Pericardium
DMEM	Dulbecco's Modified Eagle Medium
DLS	Dynamic Light Scattering Spectrometer
EDV	End-Diastolic Volume
ECG	Electrocardiogram
ECM	Extracellular Matrix
EF	Ejection Fraction
ESV	End-Systolic Volume
FDA	Food and Drug Association
FBS	Fetal Bovine Serum
FS	Fractional Shortening
FTIR	Fourier Transform Infrared Spectrophotometer
GC-MS	Gas Chromatography-Mass Spectroscopy
GATA4	GATA Binding Protein 4
H&E	Hematoxylin-Eosin
HFIP	1,1,1,3,3,3-Hexafluoro-2-Propanol
LAD	Left Anterior Descending Artery
LV	Left Ventricular

LVEDd	Left Ventricular End-Diastolic Diameter
LVESd	Left Ventricular End-Systolic Diameter
MI	Myocardial Infarction
MTS	Cell Proliferation Assay
NP	Native Pericardium
PANI	Polyaniline
PBS	Phosphate Buffered Saline
PCL	Polycaprolactone
PGA	Poly Glycolic Acid
PEG	Polyethylene Glycol
PEUU	Polyester Urethane Urea
PLA	Polylactic Acid
PLCL	Polypropylene-co-ε-Caprolactone
PLA	Polylactic Acid
PLCL	Polypropylene-co-ε-Caprolactone
PLGA	Poly (Lactic-co-Glycolic Acid)
PPP	Platelet-Poor Plasma
PTh	Polythiophene
PTFE	Poly-Tetrafluoroethylene
PVA	Polyvinyl Alcohol
PPy	Polypyrrole
RLU	Relative Luminescence Unit
SA	Sinoatrial Node
SB-10	Sulfobetaine-10
SB-16	Sulfobetaine-16
SD	Sodium Deoxycholate
SDS	Sodium Dodecyl Sulphate
SDGs	Sustainable Development Goals
SDG 3	Good Health and Well-Being
SDG 9	Industry, Innovation, and Infrastructure
SEM	Scanning Electron Microscope
SF	Physiological Saline
UTS	Ultimate Tensile Strength

VADs	Ventricular Assist Devices
VEGF	Vascular Endothelial Growth Factor
vwf	von Willebrand Factor

To all the workers who work hard but did not receive what they truly deserve

Chapter 1

Introduction

1.1 The Heart

1.1.1 Heart Anatomy

The heart is a pinecone-shaped organ located in the thoracic cavity between the lungs and separated from other organs by the pericardial sac. The average size of a human heart is about the size of a clenched your fist and its weight can vary between approximately 250-350 grams depending on age, gender, and physical factors [1]. The primary function of the heart is pump blood to whole body, an adult human heart pumps approximately 75 times per minute, which totals to around 108,000 times in a day. Each of the primary pumping chambers of the heart expels around 70 mL of blood with each contraction of the heart [2, 3].

1.1.2 Heart Chambers

The human heart is consisting of left atrium, right atrium, left ventricle and right ventricle. The atrium contracts to force blood into the lower chambers where the left and right ventricles are located. These ventricles are the heart's primary pumping organs, circulating blood throughout the body or to the lungs [4].

1.1.3 Circulatory System

The human circulatory system basically comprises two interconnected circuits: the pulmonary circuit, which returns deoxygenated blood to the heart and provides oxygenated blood to bodily tissues, and the pulmonary circuit, which moves blood to and from the lungs for gas exchange. In the pulmonary circuit, the right ventricle pumps deoxygenated blood to the lungs through the pulmonary trunk and arteries, where it taken up oxygen and releases carbon dioxide.

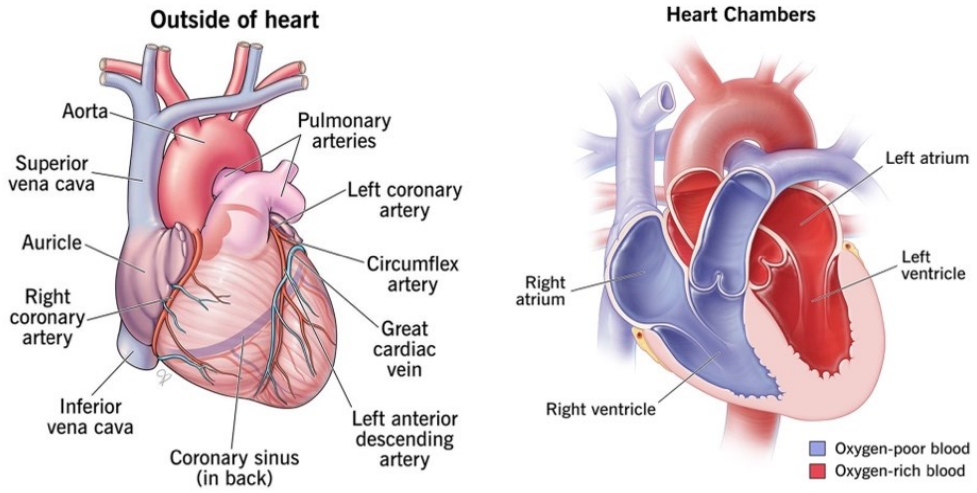

Figure 1.1 The heart's structure and chambers [5-7].

The pulmonary veins then carry oxygenated blood back to the heart, where it passes via the left atrium and ventricle before being pushed into the systemic circuit through the aorta. Throughout the systemic circuit, oxygen and nutrients are delivered to tissue and the carbon dioxide and waste products is taken away from tissues. Deoxygenated blood is eventually returned to the heart via systemic veins, such as the superior and inferior vena cava, completing the circulation. This blood circulation process persists for the duration of the individual's life [8, 9].

1.1.4 The Layers of Heart Wall

The heart's wall compromises three layers, namely the epicardium, myocardium, and endocardium, each with different thicknesses. The pericardium is the outermost layer of heart, separates the heart from other organs. The endocardium is the innermost layer of the heart, surrounds the heart valves and lines the chambers where blood flows. Endothelin's secreted from the endocardium create an environment regulating ionic concentrations and contraction states in the surrounding tissue fluids [3, 10].

1.1.4.1 Myocardium

The myocardium, predominantly composed of cardiac muscle cells, is the thickest and middle layer of the heart. It is situated upon the framework of collagen fibers, blood vessels nourishing the heart, and nerve fibers aiding in heart regulation. Through the contraction of the myocardium, the function of pumping blood into the heart and main

arteries is performed. The heart muscle cells wrap around the chambers and major vessels in a figure-eight pattern (Figure 1.2b), allowing the heart to pump blood more effectively than a linear arrangement would. The left ventricle has a thicker wall than the right ventricle due to generate a significant amount of pressure for pumping blood throughout the body [3, 10] .

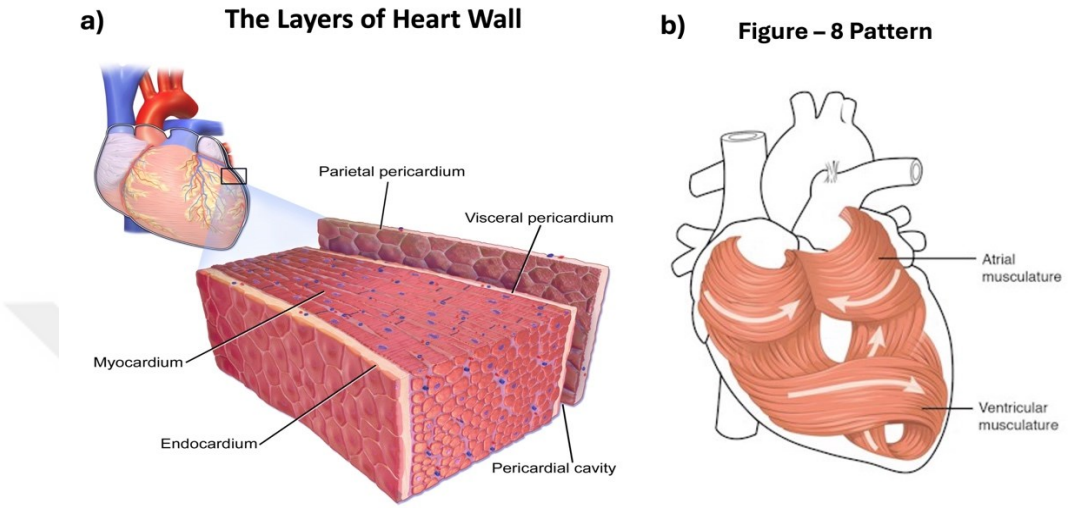

Figure 1.2 a) The representation of heart layers [11], b) The image of figure-8 patterns of heart [12].

1.1.4.2 Pericardium

The pericardium is a sac consisting of visceral and parietal components that envelops the outer surface of the heart, separating it from other organs. The visceral pericardium is connected to the heart's epicardial layer by a layer of mesothelial cells, and within the space it forms between itself, and the heart lies pericardial fluid. Although the amount of pericardial fluid can change based on the factors like age and gender, it is typically around 50 mL. This fluid is an ultrafiltrate of plasma and may also include lymph drainage. The thickness of the pericardial membrane varies by region, typically ranging from about 0.8 mm to 2.0 mm. On the other side of the pericardial membrane lies the fibrous pericardium, known for its dense collagen fibers. Histologically, the pericardial tissue contains dense type 1 and type 3 collagen fibers compressed between short elastin fibers. The abundance of collagen matrix provides the pericardial tissue with viscoelastic mechanical properties [13].

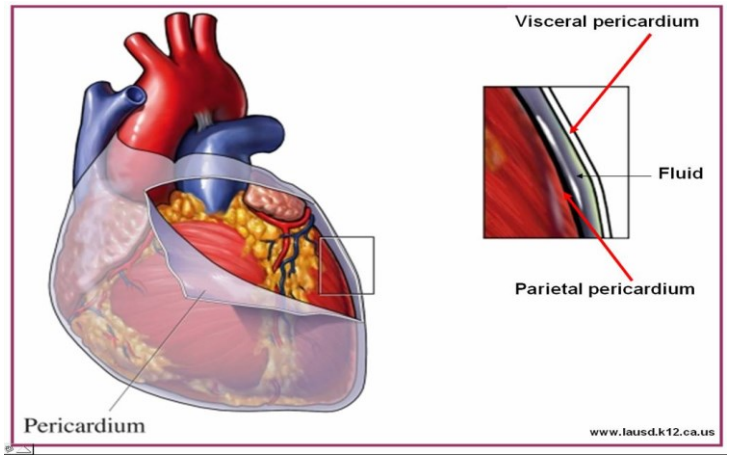

Figure 1.3 Illustration of the pericardium [14].

1.1.5 Conduction System

The heart' conduction system is a physiological system in which myocardium, pacemaker cells and heart muscle cells play an active role. The pacemaker cells in the sinoatrial (SA) node initiate the cardiac stimulation, and electrical conduction spreads throughout the heart cells in the myocardial layer. The heart cells have the capacity to transmit cardiac impulses, this phenomenon is due to the electrical connection points of heart cells called gap-junctions. Stimulation of heart cells with cardiac impulse causes the atrial and ventricular myocardium to contract. The cardiac impulse begins in the sinoatrial (SA) node, and travels through the heart cells in the atria and is transmitted to the atrioventricular (AV) node via the intermodal pathway. At this stage, contraction of the atria occurs. Electrical conduction in the AV node slows down a little, the reason for this is to gain time for the blood in the contracting atria to fill the ventricles. Electrical conduction is transmitted from the AV to all ventricular cells through branched Purkinje networks, also known as the bundle of His, and the ventricular contraction is achieved [15].

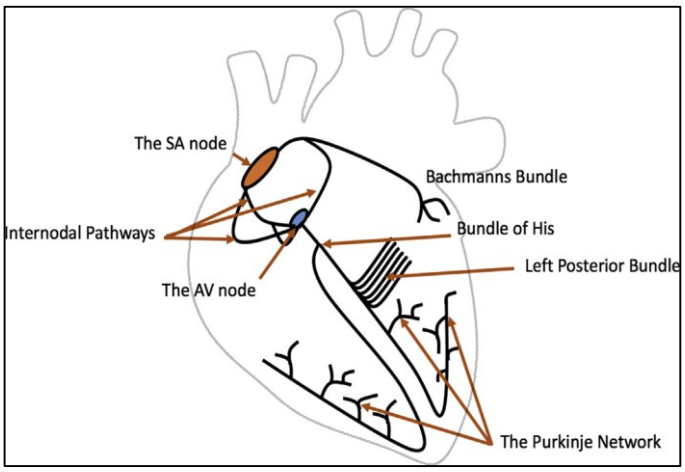

Figure 1.4 The representation of the heart' cardiac conduction system [15].

1.1.5.1 Cardiomyocytes

Cardiomyocytes (CMs) are the heart muscle cells characterized by their cylindrical rod-shaped and beating ability, which provide myocardium's contraction-relaxation function. CMs consist of myofibrils, which act as contractile apparatus. These myofibrils composed of repeated sarcomeres which knows as minimal contractile units including thick and thin filaments. The thin filament contains actin and titin, while the thick filaments include myosin. The ends of the myosin connect with actin, forming cross bridges. The ends of the actin filaments called Z-discs, have high electron density. The I-band, with low electron density, includes actin and titin filaments, while the A-band, which is electron-dense band, consists of the parallel-aligned myosin and actin filaments. The relationship between the myosin and actin filaments initiates sarcomere contraction [16]. Each CMs connects with each other's through the intercalated disks, which provide the mechanical and electrical linkage between cells via cell-cell adhesion molecules like N-cadherin [17, 18].

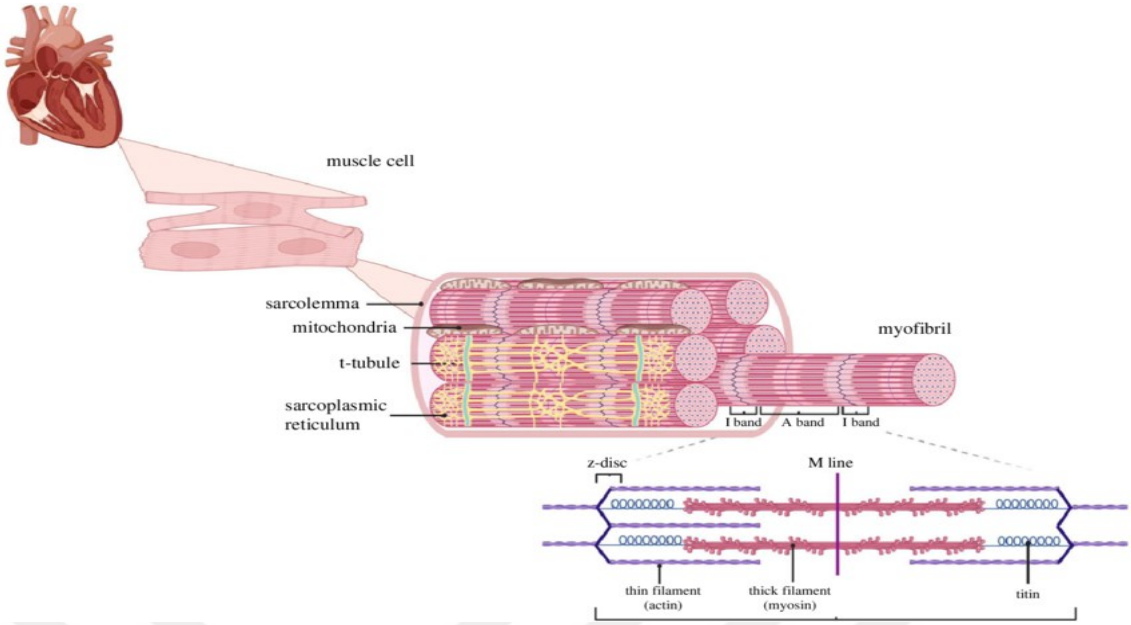

Figure 1.5 Illustration of the structures of myofibril and sarcomere [19].

1.1.5.2 Action Potential

Heart cells transmit electrical impulses by passing electrolytes through the cell membrane. Especially, sodium, potassium and calcium are the most important electrolytes for the electrical transmission on cardiomyocytes. These electrolytes move in and out of the cell membrane through ion channels and ion pumps on the membrane [15]. Pacemaker cells are located in AV and SA nodes and have the capability to rhythmically depolarize and initiate action potential. Basically, the action potential consists of intracellular and extracellular electrolyte movements on the pacemaker cells. While the action potential in pacemaker cells occurs in 3 stages, it occurs in 5 stages in the cardiomyocytes, which is due to the faster conduction provided by pacemaker cells. At resting state, the inside of the cell has a potential of -90 mV, and this phase is called Phase 4. During phase 0, stimulated Na+ channels open, permitting Na+ ions enter the cell, thus the intracellular potential reaches to +20 mV. Thus, the action potential is initiated by the depolarization wave, and this depolarization wave spreads from cell to cell throughout the heart. After depolarization, phase 1 is initiated by repolarization of cells where Ca^{+2} ion channels open. There is a slight decrease in potential in this phase, since the velocity of Ca^{+2} ions is slower than Na^{+} ions. Phase 2 is known as the stabilization phase, has a potential of approximately +10 mV, Na^{+} channels close here. By the end of phase 2, Ca^{+2} concentration inside the cell increases, leading to mechanical contraction. Following to

contraction, calcium channels close and potassium channels open in Phase 3, then cells re-polarized, returning the potential to -90 mV resting state [15, 20] .

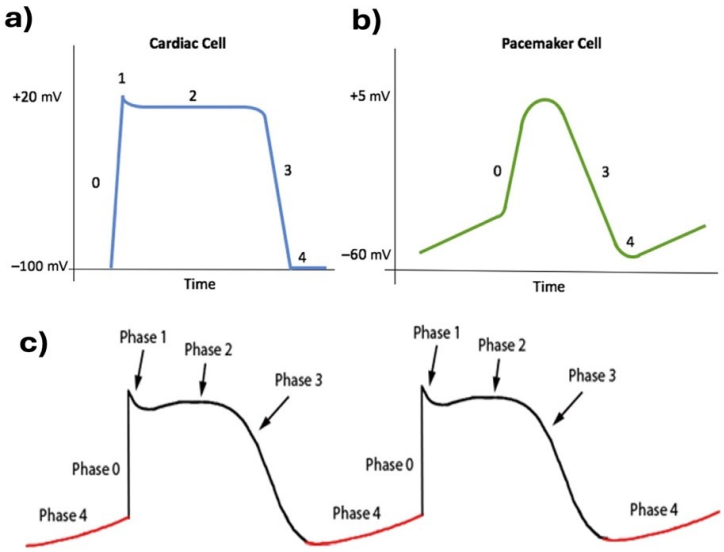

Figure 1.6 The action potential of a) cardiac cells, b) pacemaker cells, and c) action potential phases [21].

1.1.5.3 Electrocardiogram

Electrocardiogram (ECG) is a method of reading the electrical activity of a heart through conductive electrodes from the skin surface, generally a 12-lead electrocardiography device is used in clinical applications. There are 5 main waves in the ECG, labeled as "PQRST", herein P wave indicates the atrial depolarization, which means contraction, while P-Q interval gives the period of arterial systole. The QRS waves represent the trasmission of the cardiac stimuli and ventricular myocardial depolarization. Finally, T wave indicates repolarization in the myocardium and the return of cardiac cells to resting potential [15]. Changes in the heart's electrical conduction system can lead to cardiac arrhythmias, which can be detected by abnormalities in ECG signals. For example, when myocardial defect occurs, it can cause bradycardia in the heart rhythm or irregular heartbeat known as arrhythmia, and these changes can be seen on the ECG graph [15, 20] .

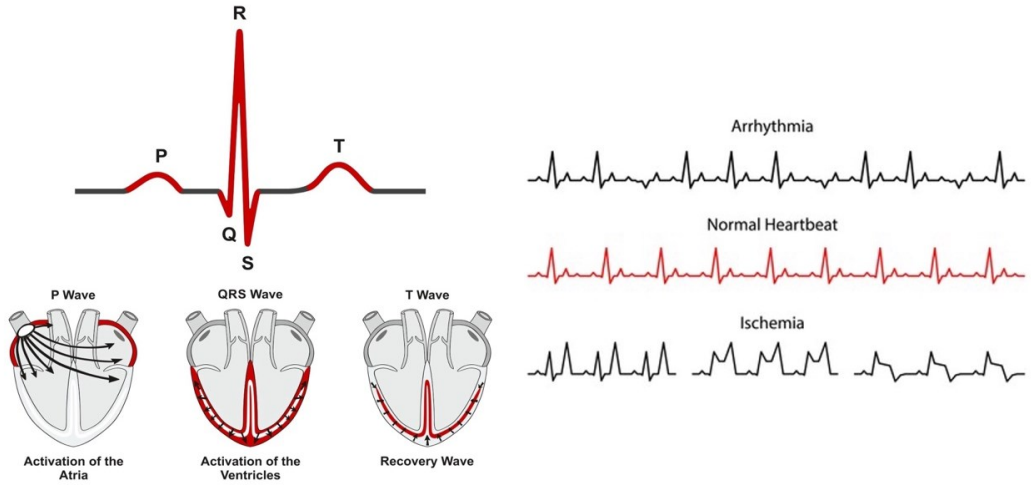

Figure 1.7 Illustration of ECG waves in normal, arrhythmia and ischemic conditions [22, 23] .

1.1.5.4 Echocardiography

In the ischemic conditions in myocardium, CMs cells die and collagen deposition increase, and then the scar formation expanses. This dense scar lead the weakness of mechanical and electrophsiological properties of myocardium. The decrease in heart functions, left ventricular dilation, arrhytmia and heart failure are main results of this scar. The heart's functions can be determined by echocardiography measurement, the changes in heart's functions is the main indicators for heart failure. Basically, end-systolic volume (ESV) and end-diastolic volume (EDV), venticule diameters, fractional shortening, ejection fractions can be measured by echocardiography [24].

1.2 Heart Diseases

Cardiovascular diseases (CVD) keep going to be leading primary cause of death worldwide, imposing a substantial burden on public health systems and economies worldwide [25, 26]. Recent statistics underscore the magnitude of this issue, with a predicted 18.6 million deaths attributed to CVDs in 2019 alone, representing a significant proportion of total global mortality [27]. The World Health Organization further reports that CVDs accounted for 27% of all deaths between 2000 and 2019, highlighting the enduring impact of these conditions on global health [28]. In 2020, the American Heart Association documented 19 million deaths globally attributable to CVDs, further

emphasizing the scale of this epidemic. Beyond the human toll, CVDs also exact a substantial economic toll, with an estimated annual cost of $378.0 billion in the United States alone [26]. According to the data from the Turkish Statistical Institute, it is known that 38% of deaths in Turkey were caused by ischemic heart diseases in 2018 [29].

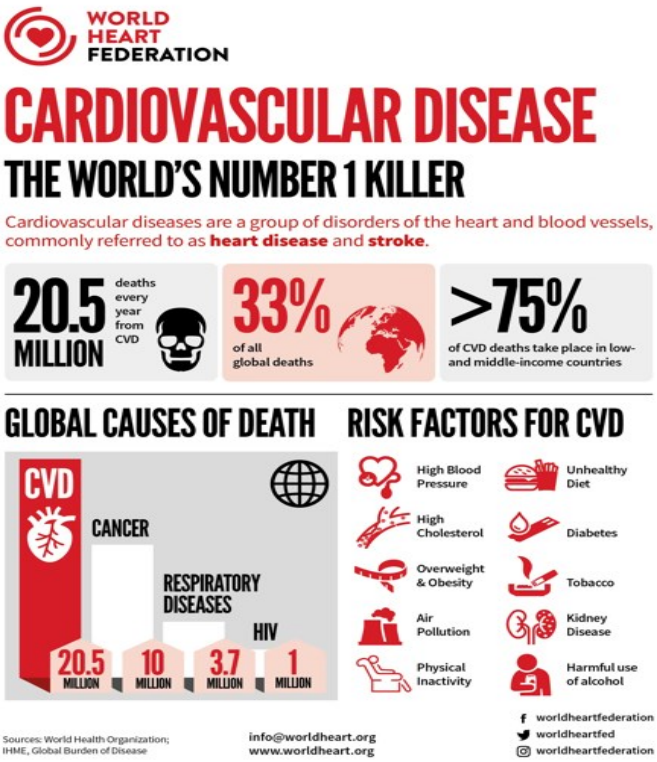

Figure 1.8 The World Heart Federation report for Cardiovascular Diseases [30].

Cardiovascular diseases are the general term for diseases of the heart and blood vessels affected by conditions such as coronary artery disease, stroke, peripheral arterial disease, aortic disease, abnormal heart rhythms (arrhythmias), congenital heart disease, deep vein thrombosis and pulmonary embolism, heart attack, heart failure, heart muscle disease (cardiomyopathy), heart valve disease, pericardial disease, peripheral vascular disease, rheumatic heart disease and myocardial infarction [31]. These diseases often arise from a complex interplay of risk factors, including tobacco use, unhealthy diet, obesity, physical inactivity, hypertension, diabetes, and hyperlipidaemia [32].

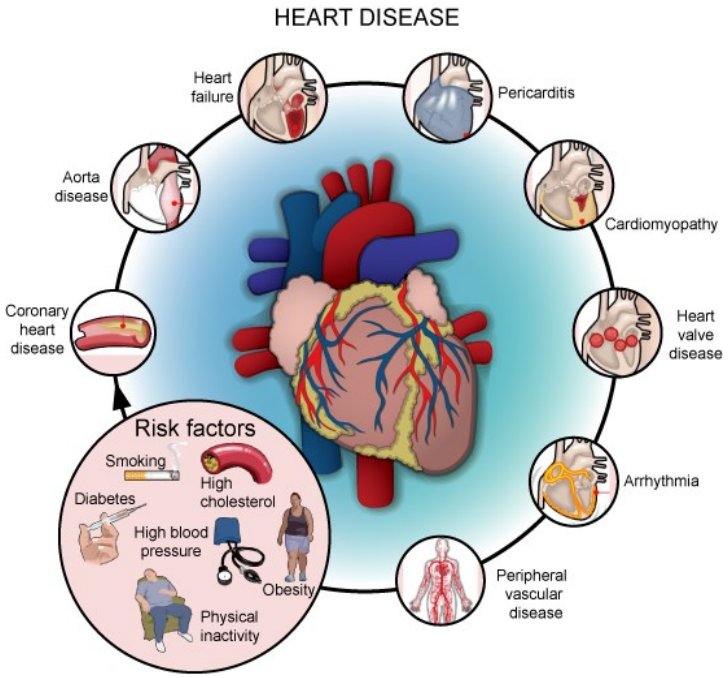

Figure 1.9 The type of heart diseases and risk factors [32].

1.2.1 Myocardial Defects

Cardiomyocytes, the predominant cell type in the heart, are more abundant in the ventricles compared to the atria. In the adult human heart, the ventricular region, including the apex and interventricular septum, consists of approximately 49.2% cardiomyocytes, 21.2% vascular smooth muscle cells, 15.5% fibroblasts, 7.8% endocardial cells, and 5.3% immune cells [33]. Like other cells, cardiomyocyte cells also require circulation to provide them with nutrients and oxygen and to remove cellular waste. This circulation occurs through the coronary arteries in the heart. The coronary arteries branch off from the aorta and deliver blood to the myocardium and other components of the heart through coronary circulation. The main artery that distributes blood to the left atrium, ventricle, and interventricular septum on the left side of the heart is the left coronary artery that is the left anterior descending artery (LAD).

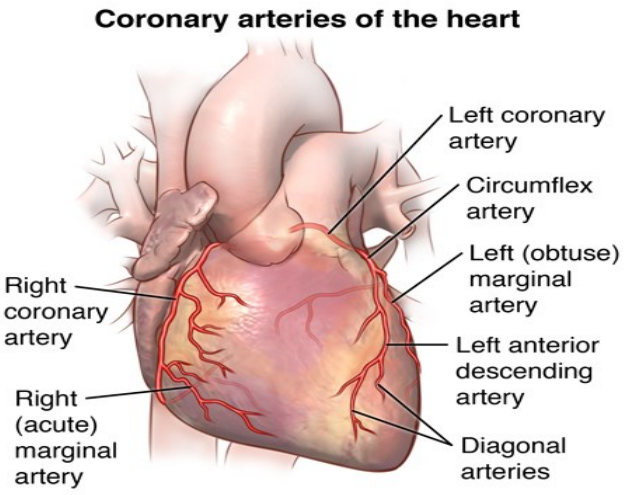

Figure 1.10 The illustratin of heart coronary arteries [34].

When the coronary arteries are blocked, blood flow to the tissues is restricted, and cells cannot receive nutrients and oxygen. The condition where cells cannot access blood flow and oxygen is referred to as ischemia and hypoxia, respectively. If the blockage of coronary arteries is left untreated, it can lead to myocardial infarction (MI) [33]. In the event of a myocardial infarction, millions of cardiomyocyte cells can be lost and cause the formation of myocardial defect, cardiomyocyte cannot repair the defected tissue due to the limited regenerative properties [35]. Fibroblasts and endothelial cells create granulation tissue and a thick collagenous scar over the course of the next weeks to months, which impairs the heart's ability to contract and ultimately results in a pathological remodelling and, frequently, heart failure [36].

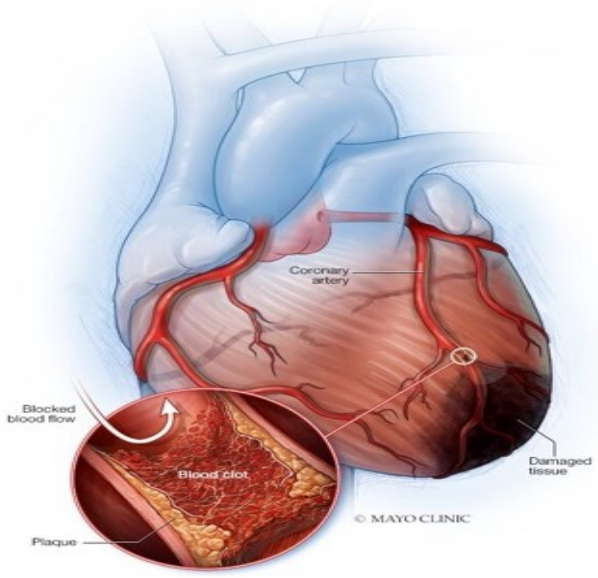

Figure 1.11 Representation of myocardial defect [37].

1.3 Therapeutic Approaches of Myocardial Defects

1.3.1 Traditional Therapeutic Approaches of Myocardial Defects

In the early stages of myocardial defects, reperfusion treatment is applied, which aim is to regulate blood flow, including the pharmacological treatments and invasive surgical techniques Firstly, aspirin can be used to prevent blood clotting in the vein again and nitro-glycerine can be used to relieve chest pain. Afterwards, angioplasty can be applied to open the blocked vessels, if there is more than one blocked vein, bypass method is applied. [38]. In long-term treatment, the aim is to regulate the heartbeat, relieve the load on the myocardium and reduce the fat and plaque in the veins by drugs [39]. Basically, angiotensin-converting enzyme (ACE) inhibitors, angiotensin receptor-neprilysin inhibitors, β-blockers, and mineralocorticoid receptor antagonists are used in the pharmacological drug approaches used [40, 41]. Anticoagulant and antiplatelet effective drugs such as Aspirin, clopidogrel, Heparin and Coumarin based drugs are used for most patients to prevent the formation of plaque and clot molecules in the blood [38]. Beta-blockers reduce the heart rate by affecting the sympathetic nervous system, thus reducing blood pressure and reducing the load on the myocardium [15]. ACE inhibitors and Ca channel blockers are used to reduce the heart's oxygen need by lowering blood pressure. Drugs containing Digitalis glycosides, such as Digocin, are also used to strengthen the contractile function of the heart muscle [38]. However, this approach cannot provide adequate recovery in myocardial scar because the drug molecules aims to regulate heart rate, decreasing workload on myocardium, having short half-lives, and side effects such as slowing the heart rate, creating edema, hypotension, and kidney failure [40, 42].

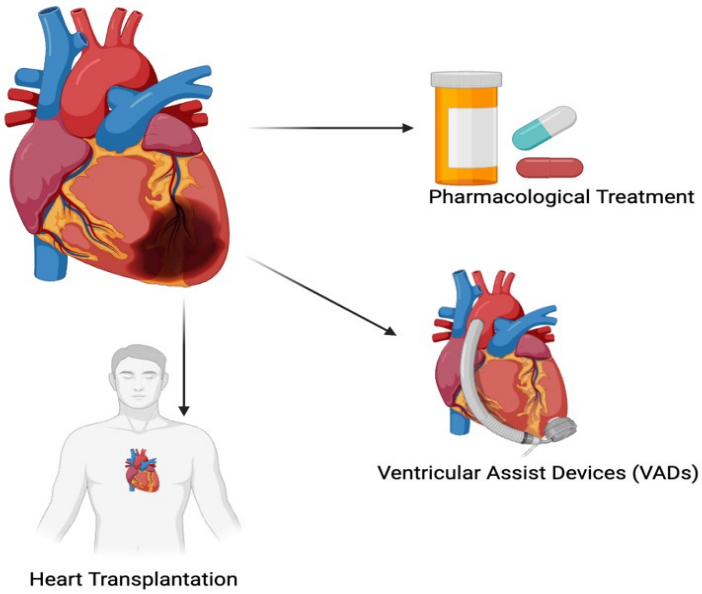

Figure 1.12 Traditional therapeutic approaches of myocardial defects (Figure was drawn in Biorender).

The ventricular assist devices (VADs) and heart transplantation methods are used at the last stage of heart failure. The many patients die while waiting for the heart transplantion due to the inadequate number of donors [43]. Ventricular assist devices are generally applied to patients when waiting for a transplantation. The pump of VADs placed in the heart pumps blood into the aorta and helps transmit blood to the whole body [44]. However, these supporting devices are not permanent solution for repearing of myocaridal defects, also they have side effects such as thrombosis, infection, and gastrointestinal bleeding. Its disadvantages include permanently encapsulation of the heart and cannot be applied to every patient group [45].

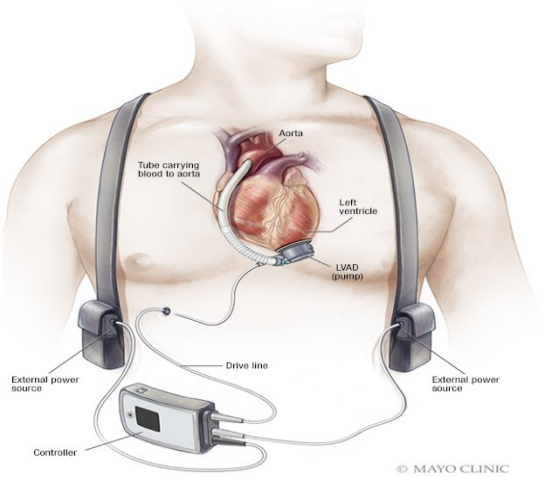

Figure 1.13 The representation of ventricular assist devices (VADs) [46].

1.3.2 Modern Therapeutic Approaches for the Treatment of Myocardial Defects

The current conventional treatments of myocardial defects do not meet the expectations for healing of defected area since the limited regenerative capacity of heart [47]. Therefore, the development of the modern therapeutic approaches and smart materials has gained considerable attention in order to restore or regenerate damaged tissues by applying biomaterials and tissue engineering principles. Tissue engineering aims to regenerate or repair to defected tissue by mimicking native tissue's extracellular matrix (ECM). The tissue engineering princible based on the three main components, the cells, a three dimentional scaffold to guide tissue formation, and bioactive molecules. The scaffold can be fabricated from biomaterials, and its structure, chemical compositions, physical and mechanical properties are the determine factors of cell behaviours [48]. Therefore, the desing of scaffolding materials are important step to provide repearing and restoring of tissues. The modern therapeutic approaches for the treatment of myocardial defects are the cell injections, injectable hydrogels and cardiac patch implantations [49].

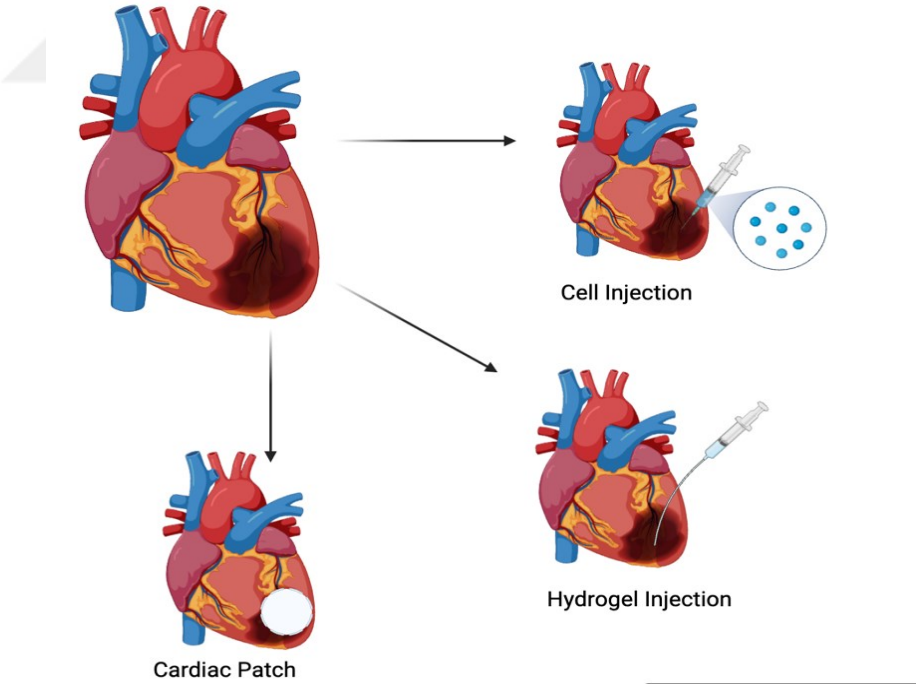

Figure 1.14 Modern therapeutic approaches for the treatment of myocardial defects (Figure was drawn in Biorender).

1.3.2.1 Cell Injections

Due to the limited regenerative capabilities of cardiomyocyte cells, the cell injection technique can be apply to the infarcted area. The cell-based cardiac treatment was initiated by the injection of the autologous skeletal muscle satellite cells, which known as myoblasts, due to differentiation to cardiomyocytes. Clinical and animal studies demonstrated that the injection of myoblasts improved cardiac function in heart [50]. Also, the embryonic, mesenchymal, pluripotent, bone marrow cells are high preferabe cell types to injections for cardiac repair [36]. In the literature, the injection of the fetal or neonatal cardiomyocyte cells improved the left ventircular thickness and fuction in animal model studies [51, 52]. The injected cardiomyocyte cells can interact with host cardiomyocyte intercalated disks and gap junctions. However, there are limited clinical outcome and ethical concerns about human fetal or neonatal cardiomyocyte transplantations. Therefore, scientist focus on to find clinically relevable cell source [36]. Afzal et al. injected the adult bone marrow stem cells to ischemic heart of patient, they reported the treatment improved the ejection franction and reduced the infarct size [53]. The human pluripotent stem cell has the ability to differantiate to CMs, therefore it can be applied clinically without ethical concern [36]. However, cell injections provide less improvement than expected due to technical inadequacies in the application. The main reason for the low expected success is that the injected cells cannot adhere to the tissue and then cannot achieve the expected compliance, the 90% of injected cells dying or being removed from the injected area [36, 54]. Therefore, biomaterials mediated three dimentional ECM-like cardiac therepies are needed to accelarate healing of myocardial defects.

1.3.2.2 Injectable Gels

The hydrogel injections can be promising approaches after MI since easily applicability via syringe or cathater [55]. Basically, the hydrogels are polymeric materials with a three-dimensional porous structure and high-water holding capacity. Generally, monomers or polymers link with each other by crosslinkers to achieve a gel form of a hydrogel, the density of monomers, the type and concentration of crosslinker, and environmental factors are the essential parameters for hydrogel synthesis [56]. The hydrogels can be combined with the cells, bioactive molecules, growth factors, or drugs to improve myocardium healing after MI. The natural and synthetic polymer based

injectable hydrogels can be obtained from collagen, fibrin, chitosan, alginate, gelatin, laminin, Matrigel, hyaluronic acid, polyethylene glycol, poly(N-isopropylacrylamide), aniline and methacrylated gelatin. Additionally, the hydrogels can be synthesized from decellularized ECM materials such as myocardium or pericardium. [57]. In a study, collagen based inectable hydrogel was applied in mice MI model, and it reported its postive effects on the cardiac functions [58]. In another study, human induced pluripotent stem cell based cardiomyocytes were encapsulated into polyethylene glycol hydrogel and applied on the rat MI model to improve cardiac functions and healing of myocardium [59]. The natural polymer based injectable hydrogels are preferred since their high biocompatibility, while the synthetics are preferred since their adjustable mechanic strenght, porosity, and easily availability. However, the natural polymers possess the disadvantages such as poor mechanical properties, rapid degradation, late gelation time, risk to immune response, lack of electrical conductivity, while the synthetics have low biocompatibility. The injectable hydrogels for cardiac applications still have difficulties and the expected healing in myocardial defects could not be achieved due to their low mechanical strength, fast degradation rate, and limitations such as gelation time and fluidity [57].

1.3.2.3 Cardiac Patch Applications

Cardiac patch applications are promising approach for the treatment of myocardial defects, act as artificial ECM for cellular attachment and regenerate defected myocardium. Basically, the cardiac patches are polymeric or biological materials, can be adhered or sutured to the defected zone of the heart, and should be mimic the damaged tissue biologically, mechanically, or physiologically and provide tissue healing [60, 61]. The cardiac pacth implantation includes surgically suturing which is more invasive surgical process than injection techniques, but it enable to more control of patch properties such as mechanical, structural, physical and electrophysiology [24]. Additionally, cardiac patches have excellent advantages such as providing mechanical support, avoiding dilation and decrease in heart's wall stress [24].
There are important criteria designing a cardiac patch, an ideal cardiac patch should be;

- Biocompatible, it does not show toxic or carcinogenic effects and is accepted by the immune system [62, 63]. The noncompatible materials can initiate the foreign-body response, resulting with rejection and necrosis [64].

- Biodegradable or Bioabsorbable in order to replace with regenerated tissue, and the degradation products must be nontoxic, and they can be removed safely from the body without inflammation [54].
- Have suitable morphology to mimics the heart tissue in terms of microporosity to allow cells to adhere and proliferate and provide tissue healing and new vessel formation [65, 66].
- Have appropriate elasticity and mechanical strength to ensure the contraction and relaxation dynamics of the heart [24]
- Electrically conductive [24, 65]
- prevent inflammation and coagulation with the substances it contains
- Enhance vascularization [24, 54]
- Support mechanically during organizing cells into tissue in early stages, while it was recommended the degradation in later stages [24, 64].

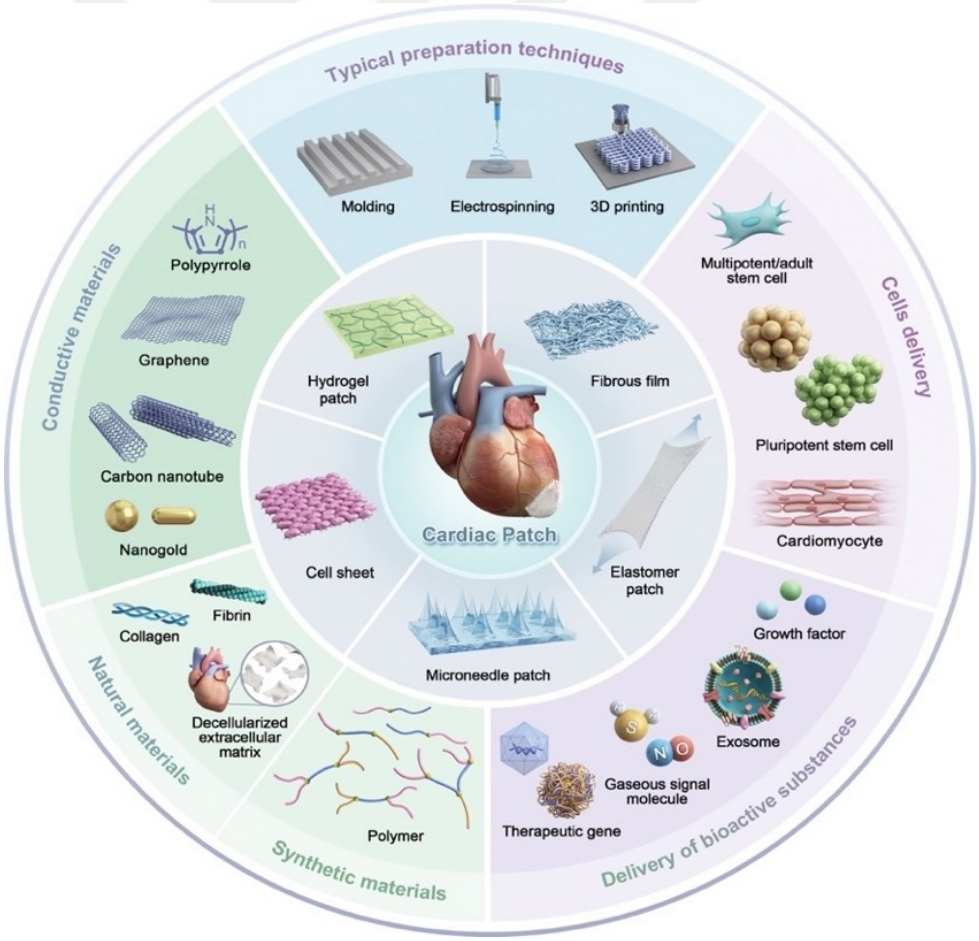

Figure 1.15 Representation of materials and fabrication techniques for cardiac patches [67].

Cardiac patches can be fabricated from synthetic and natural polymers, or obtained by native tissues [60, 68]. The complex functional and structural properties of the myocardium requires the suitable therapeutic scaffolding patches. Herein, the polymers are good candidates for fabricating a patch with the adjustable morhphology, degradation rate, mechanical strengh, and surface functionalizations to mimic ECM and restoration of myocardium. Therefore, the chosen the right type of polymers and right fabrication techniques are vital to achieve threupetic effects of cardiac patch [69].

1.4 Polymeric Cardiac Patches

1.4.1 Natural Polymers for Cardiac Patches

The natural polymers are obtained from mammalian or biological sources, they are a type of protein or polysaccaride. The mammalian derived polymers are collagen, gelatin, fibrin, matrigel, the other sources derived polymers are alginate, cellulose, chitosan, hyaluronic acid, and silk [24]. These polymers are mostly preferred in cardiac tissue engineering applications [70, 71]. Chrobak et al. developed a fibrin-based cardiac patch, fibronectin is a biocompatible protein, insoluble in water, it was reported that the fibrin patch improved the cell oriantation in defected myocardium [72, 73]. Silk fibroin can be derived from silk, higly preferable since high biocompatibility and degradablity properties. Chitosan is a polysaccharide based poylmers derived from chitin, it has several advantages such as biocompatibility, mechanic properties, antibacterial properties and hemostatic properties [73]. In a study, chitosan based scaffold improved the cardiomyogenic differentiation [74] . Alginate is derived from algae, purificated alginate is biocompatible polysaccharide, its structure similar with ECM [73]. In a study, alginate based scaffold was applied rat MI model, important development in cardiac function was obtained after 28 day implantation [75]. Another polysaccharide is hyaluronic acid, it is an acidic polysaccharide, can be obtained from animal sources and microbial production [73]. In a study, 3D printed hyaluronic acid and gelatin cardiac patch enriched with cardiac-derived progenitor cells and applied to mouse MI model. The presence of vascular markers and improvement of cardiac fucntion was reported after implantation patch [76]. Collagen and gelatin are main proteins in animal body, the hyrolysis of collagen resulted

with gelatin, they are higly preferable in cardiac patch applications since familarities high cell adhesion [77].

1.4.1.1 Gelatin

Gelatin is a natural protein-based polymer, obtained from hydrolized collagen which is the important native ECM component. Gelatin offers excellent biocompatibility thanks to the its denaturated structure, because mitigated aromatic groups of collagen regarding immune response, inflammation and rejection. Also, gelatin improve the elacticity, viscocity, water solubility and conductivity of polymers. Gelatin includes the carboxylic and amino groups, which provide ability to chemically crosslink or conjugate with several molecules [78]. However, using gelatin alone is not recommended for cardiac applications due to weak mechanical properties and susceptibility to enzymatic degradation [79] .

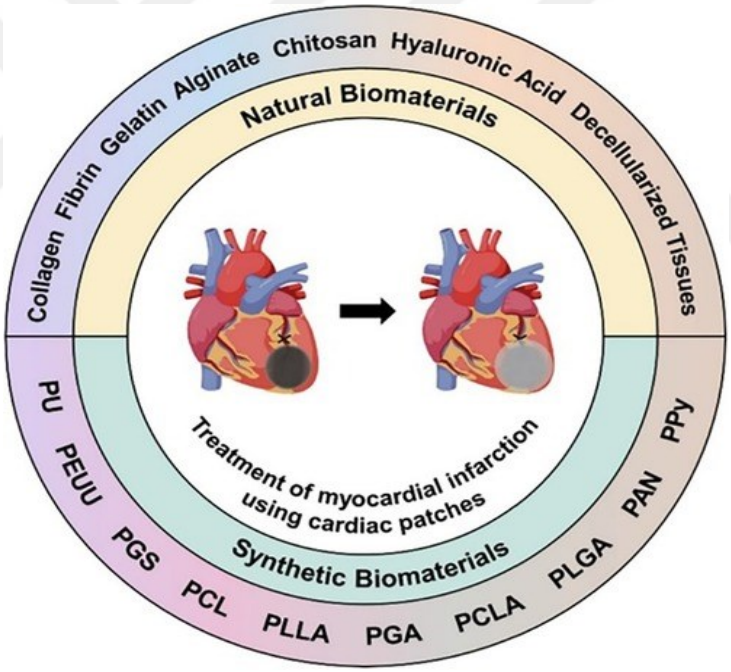

Figure 1.16 The natural and synthetic polymers for cardiac patch applications [80].

1.4.2 Synthetic Polymers for Cardiac Patches

Synthetic polymers can be categorized as polyesters, polyacids, polyol, etc. depending on the their matrix type, higly preferable in cardiac applications due to low cost, easy manufacturing, stable structure and adjustable degradation and mechanical properties [73]. The common synthetic polymers are polylactic acid (PLA), poly glycolic

acid (PGA), poly (lactic-co-glycolic acid) (PLGA), polycaprolactone (PCL), poly (glycerol sebacate), polyurethane (PU), polyester urethane urea (PEUU), polyvinyl alcohol (PVA), polyacrylamide, poly-tetrafluoroethylene (PTFE), which are most prefereble polymers in cardiac patches applications [60]. The PGS is biodegradable elastic polyester, including glycerol and sebacic acid, was developed by Robert Langer [70]. PCL, PGA, and PLA or their copolymers are a type of polyester polymers, while the PU is the elastomeric polymer [81]. PCL is like a cornerstone of tissue engineering scaffolds since good biocompatibility, adjustable mechanical properties and degradation rate, easily manufacturing in desired morhphologhy. [73]. PCL can be used as blended form like Polypropylene-co-ε-caprolactone (PLCL) [67]. PLCL and PGA were combined in cardiac patch scaffold to improve myocardial healing and promote cardiomyocyte regeneration [82]. The PLA and PLGA are the main polyacid substrates with high biocompatibility, biodegradability, adjustable mechanical properties [73].

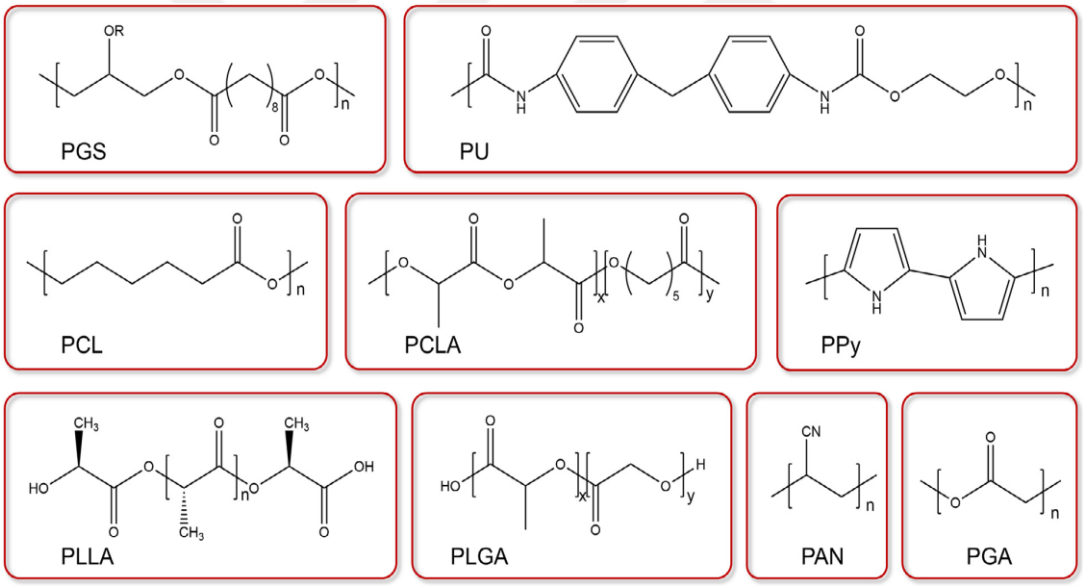

Figure 1.17 The chemical structures of synthetic polymers used in cardiac patch applications [83].

1.4.2.1 PLGA

PLGA is a Food and Drug Association (FDA) approved synthetic polymer used in several biomedical applications. PLGA is a water non-soluble polymer, its biodegradation process run with hydrolytic degradation since its ester bond in polymer chain. PLGA's properties such as molecular weight, mechanical property, crystallinity, degradation rate, glass transition temperature depends on its glycolide and lactide content on polymer

chain. PLGA is high preferable polymers due to its adjustable biodegradation and mechanical properties for biomedicine applications [84]. In a study, stem cell loaded PLGA scaffold promoted the cell adhesion and proliferation and cardiac proteins expression was reported [85]. In another study, electrospun PLGA/gelatin cardiac patch demonstrated the integration of cardiomyocyte cells with the functional cardiac protein expressions [86]. Wee et al. developed a stem cell loaded PLGA/collagen cardiac patch in rabbit MI model, they reported the fabricated cardiac patch improved cardiac function and increased stem cell retention capacity [87].

1.4.3 Natural and Synthetic Blend Polymers for Cardiac Patches

The natural polymers higly preferable for cardiac tissue enginnering since their have superior biocompatibility, and capability to enhance cell adhesion and proliferation since similar nature with ECM [71]. However, natural polymers have drawbacks such as fast degradation rate and low mechanical strength. On the other hand, synthetic polymers are favorable because of being easily produced in the desired morphology, structurally stable, adjustable mechanical properties, and controlled degradation rate [69]. However, the rigid synthetic polymers can not integrate to contraction-relaxation function of heart since their high stiffness and rigidity, also they have high hydrophobicity, their use alone is insufficient for cell adhesion and proliferation, the synthetic patch needs to improve their bioactivity [24, 60]. For this reason, synthetic and natural polymers should be used as a mixture in cardiac patch applications [73, 88]. In a study, collagen, elastin, and PCL blend polymers were used to fabricate cardiac patch, and investigated in vivo mice MI model. It was reported that the cardiac-mimicking patch improved the cardiac function and reduced ischemic area after 4 weeks of patch implantation [89]. In a study, GelMA/PCL/PPY composite conductive cardiac patch was studied in MI model, it was reported that the patch improved neovascularization and decreased the scar size [90].

1.5 ECM-Based Cardiac Patches

The challenge of copying the compexity of the heart architecture directed the researchers to use native ECM as biologic scaffold [45]. The native ECM includes the structural and biochemical supportive macromolecules such as collagen, glycoproteins

and glycosaminoglycans [83]. The native ECM could be ideal scaffold for cardiac applications due to its vascular architecture and high macromolecular content [45].

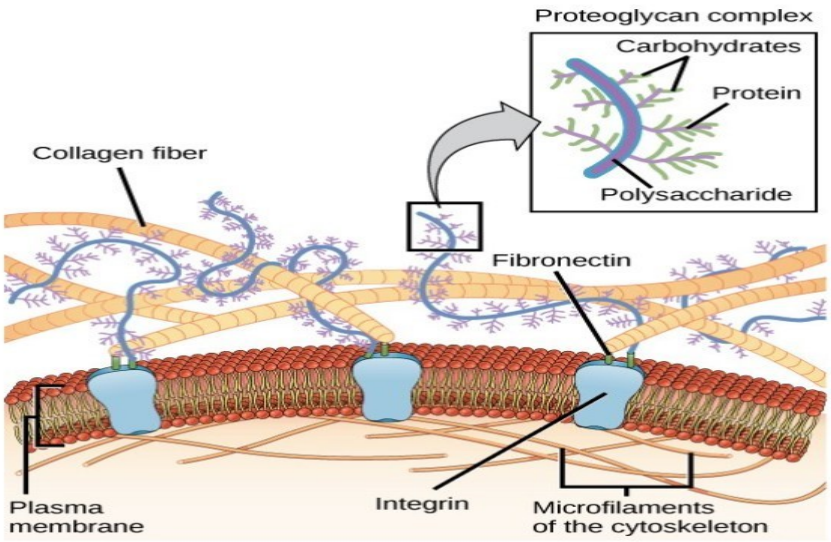

Figure 1.18 Extracellular matrix components [91].

The most significant advantages of ECM-based patches are that they quickly provide tissue-material compatibility, regeneration, repair, and remodeling of defected tissues [62]. In the literature, myocardium, pericardium, bladder, and small intestinal submucosa tissues were used for cardiac patch applications [83, 92]. The ECM-based scaffold can be obtained from allogeneic or xenogeneic tissues [83]. However, the allogeneic and xenogeneic tissue's cellular antigens induced immune-mediated rejection due to recognizing as foreign by the host tissue. Therefore, the native ECM is used either fixed with crosslinker or decellularized in order to hold down of that antigens [93].

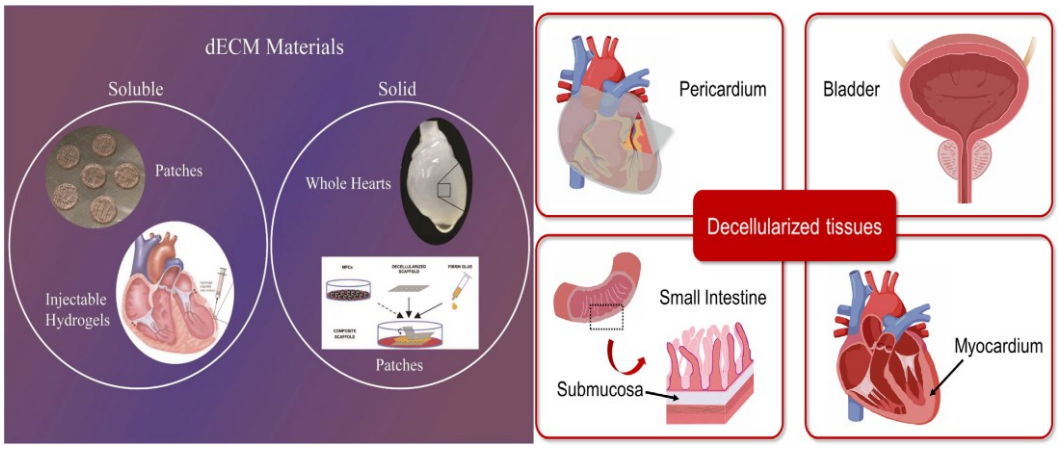

Figure 1.19 Decellularized tissues for cardiac applications [62].

1.5.1 Pericardium for Cardiac Patches

Tissue selection for decellularized cardiac patches is crucial, the structure and properties of the tissue should be considered for the selection of tissue. The cardiac patch should support the function and regeneration of myocardium, match the elasticity and mechanical strenght of myocardium, provide host cell integration and vascularization, and avoid immune reactions [68]. The pericardium is an essential and advantageous tissue for cardiac patches thanks to its high collagen content provides high mechanical strength and elasticity. The pericardium is a fibrous sac that surrounds the heart, mainly composed of compact collagen and elastin fibers [94]. The pericardium consists of three layers: serosa, the thin inner layer composed of mesothelial cells; fibrosa, which is the thicker layer formed by collagen and elastin bundles; and epi-pericardial connective tissue layer [13]. Also, there are commercial available pericardium-based biomeshes for several biomedical applications such as Bioripar® and Tutomesh® [94]. Pericardium-based cardiac patches have many advantages over synthetic patches such as lower cost, flexibility, functionality, easy integration into the host tissue, biocompatibility, less suture bleeding, and reduction in infection rates [95]. However, the mechanical and fiber structure of the ECM could be defected during the current decellularization methods, that's why the desing of decellularization protocol is critial [93]. In a study, acellular pericardium cardiac patch enriched with mesenchymal stem cell and investigated on rat MI model. They reported that the natural acellular scaffold as cell delivery patch demosntrated the neo-vessels [96].

1.6 Hybrid Materials for Cardiac Patch

The polymeric cardiac patches are attractive since their easy fabricability, low cost, adjustable morphological, physical properties, biodegradable behaviour, however they could have low biocompatibility, weak mechanical property, and high hydrophobicity. On the other hand, ECM-based cardiac patches can provide excellent biocopatibility, tissue-material integrity, mechanical support for injured myocardium, however, the obtained ECM-based patch suffer from lack of conductivity. Therefore, the cardiac patches should be designed with the capabilities to fulfill the requirements of an ideal cardiac patch such as; high biocompatibility, fully integration with body, appropriate degradation rate, bioactivity, enhanced vascularization, appropriate mechanical strenght,

and conductivity. The combination of hybrid polymeric and biologic scaffolds can be versatile for cardiac patch applications. In a study, a cardiac patch was fabricated from silk and ECM, the hybrid scaffold was enriched with gold nanoparticles and mesenchymal stem cells, then its efficiency was investigated, the improvement of cardiomyocyte cell adhesion, proliferation and increase ventricular thickness was obtained in mice MI model [97]. In another study, a bilayered PECUU/ECM patch was fabricated and investigated in animal MI model. They highlighted that the patch has positive effect on angiogenesis, decreasign LV compliance and alleviating scar formation [98] .

1.7 Fabrication Techniques for Cardiac Patches

Tissue engineered scaffolds play an important role in cardiac patch applications in that mimic ECM structure of myocardium, providing mechanical support, enhancing cell adhesion, proliferation, differentiation and orientation, contolled degradation rate and controlled release of bioactive molecules [73]. Considering these criteria, the fabrication techniques play important role to cardiac patch's morphological and physical properties. Cardiac patches with various morphologies can be fabricated by utilizing several methods such as electrospinning, 3D printing, molding, freeze-drying, decellularization and solvent-film casting [99]. The working principle of freeze-drying depends on the drying of frozen materials, applying high vacuum to water molecules transfers from solid to gaseous state. In this way, the porosity can be achieved in freeze-dried scaffolds. The 3D printing is another technology to produce a cardiac patch, the biomaterials, cells, growth factors and bioactive components can be printed layer by layer. The ink solution of 3D printing can be prepared from polymeric solutions or native ECM solutions [73].

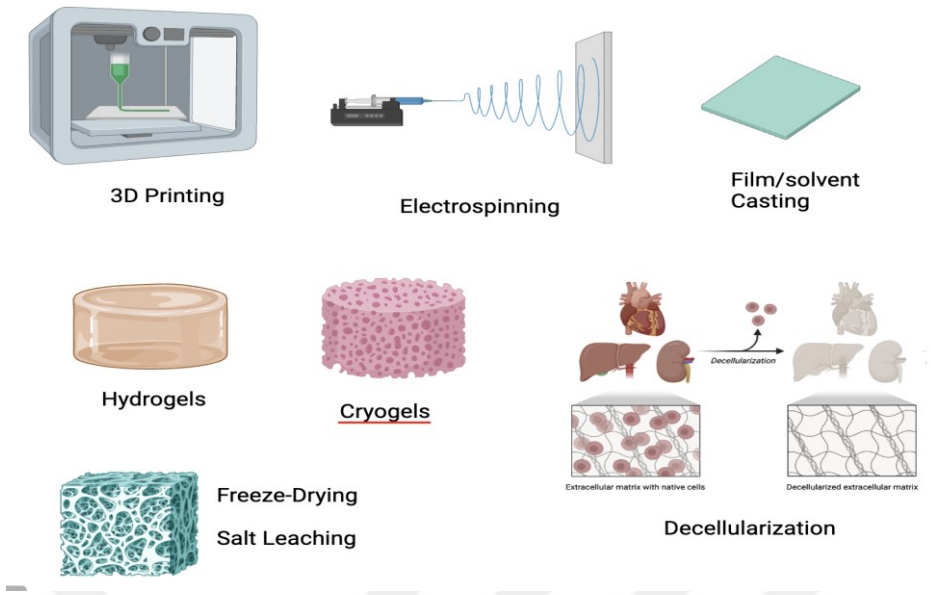

Figure 1.20 The fabrication techniques for cardiac patches (Figure was drawn in Biorender).

1.7.1 Electrospinning

Electrospinning is one of the versatile methods used to produce ultrafine fibers with diameters from nanometer to micrometers [63]. Electrospinning can be classifed into solution electrospinning and melt electrospinning, working principles depend on the applying high voltage static electricity to polymer solution at the tip [73]. The electrospinning components are a syringe pump, a power-voltage supply, a spinneret that conductive needle tip, and a grounded conductive collector. The polymer solution can be fed with a stable flow rate by syringe pump, the needle is connected with an electrode of power supply to charge polymer droplet. The other one is connected to the grounded collector [100]. When the polymer droplet is loaded with high voltage, the surface tension of polymer droplet becomes electrostatically charged at the tip of spinnered. By this way, the droplets unders the two electrostatic forces, one is Coulombic force by applied electric field, and second is electrostatic repulsions from surface charces of droplet. The droplet elongates into conical shape which known as Taylor cone by these two forces. When the electric field exceed the critical value, electrostatic forces bypass the surface tension of polymer solution, it push the polymer solution to jump from Taylor cone. The liquid jet elongates continuosly in the direction of electric field, and during its spinning movement the solvent evaporates and the polymer fibers collected randomly on collector as an electrospun mat. The fabricated elelctrospun mats fiber diameters and mat's pore

structure depends on the electrospinning parameters such as solution concentration, molecular weight of polymer, polymer solution composition, solution flow rate, applied voltage, and the distance between the tip and collector The formation of beads in polymeric fibers is an essential problem of electrospinning, it can be solve by optimizing electrospinning parameters. [101].

The electrospun membranes can imitate the structure and biological functions of ECM thanks to their properties such as adjustable fiber diameters, high surface area and porosity, and 3-dimensional network structure. In addition, electrospun nanofibrous scaffolds can be used as 3-dimensional structures that create environmental conditions which allow cell adhesion, migration, and differentiation, thus providing tissue regeneration function of ECM in the body. It has been shown that electrospun cardiac patches used with agents such as bioactive molecules, growth factors, drugs, and stem cells are more effective in treating myocardial defects [63].

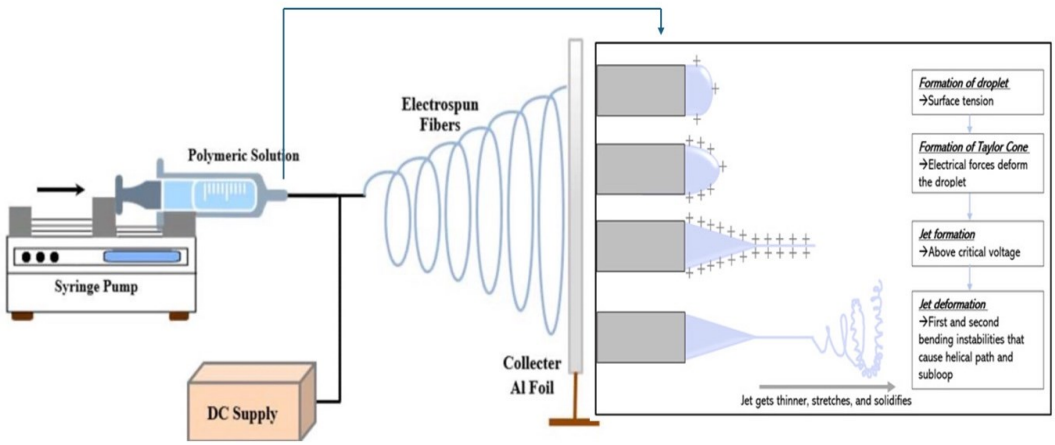

Figure 1.21 The illustration of electrospinning apparatus and formation of fibers [94, 95]**.**

1.7.2 Decellularization

Decellularization is the important methods of obtaining ECM-based scaffolds from organ or tissue parts [104]. The decellularization method aims to remove all cells and genetic materials from the ECM and obtain a biological scaffold while preserving its structural, biochemical, and biomechanical properties [93]. Generally, decellularization techniques are adapted to preserve different physical and biochemical properties of ECM, including tissue thickness, the density of ECM molecules, mechanical integrity, and 3-dimensional configuration [105]. Decellularization procedures often include a

combination of physical, chemical, and enzymatic strategies. The physical methods contain the mechanically agitation, pressure, or massage, sonication, and frezing-thawing, principles depends on the distrupting cell membrane, then releasing of cell content. However, the physical treatments have failed to completely decellularization, therefore they combined with chemical and enzymatic methods [98, 101]. The enzymatic and chemical methods includes the use of ionic solutions or detergents in order to lysis of cell membrane. Its principle depends on the distrupting cell membrane, then releasing of cell content and removing cell residue from tissue. Basically, tyripsin is the most common enzymes that can cleave the carbon bonds of arginine and lysine. Moreover, the alkaline or acid solutions can be preferable for chemical methods to solubilize cytoplasmic component. Basically, acetic acit, paracetic acit, hydrochloric acid, ammonium hydroxide and sulfuric acid are used for decellularization, but they could be damage the ECM structural components. The non-ionic detergents such as Triton X-100 can be break lipid-lipid or lipid-protein interactions, but its higher concentrations can lead to loss of ECM protein components. The ionic detergents such as sodium dodecyl sulfate (SDS), sodium deoxycholate (SD), are versatile to solubilize cytoplasmic and cellular membranes, but they can denaturate the proteins. The zwitterionic detergents demonstrates the both ionic and non-ionic detergents properties, 3-[(3-cholamidopropyl)dimethylammonio]-1-propanesulfonate (CHAPS), sulfobetaine-10 (SB-10), and sulfobetaine-16 (SB-16) are the main zwitterionic detergents for decellularization. The osmotic shock can be used with hypertonic(deionize water) and hypotonic (Trizma/EDTA) solutions for decellularization [93].

The success of the decellularization procedure depends on the completely removal of cells and genetic materials and the preservation of tissue integrity, microstructure, and mechanical structure [107]. The decellularized tissues also known as acellular scaffolds, have advantages than native tissue on behalf of low immune reaction, low cost, long shelf life, off-the-shelf availibility for quick implantation [68]. In a study, rat placenta matrix was decellularized and implanted on the rat heart after MI, it demonstrated the significant improvement in cardiac functions [108]. In another study, the porcine heart tissue was decellularized and used as a hydrogel form for cardiaovascular applications [109].

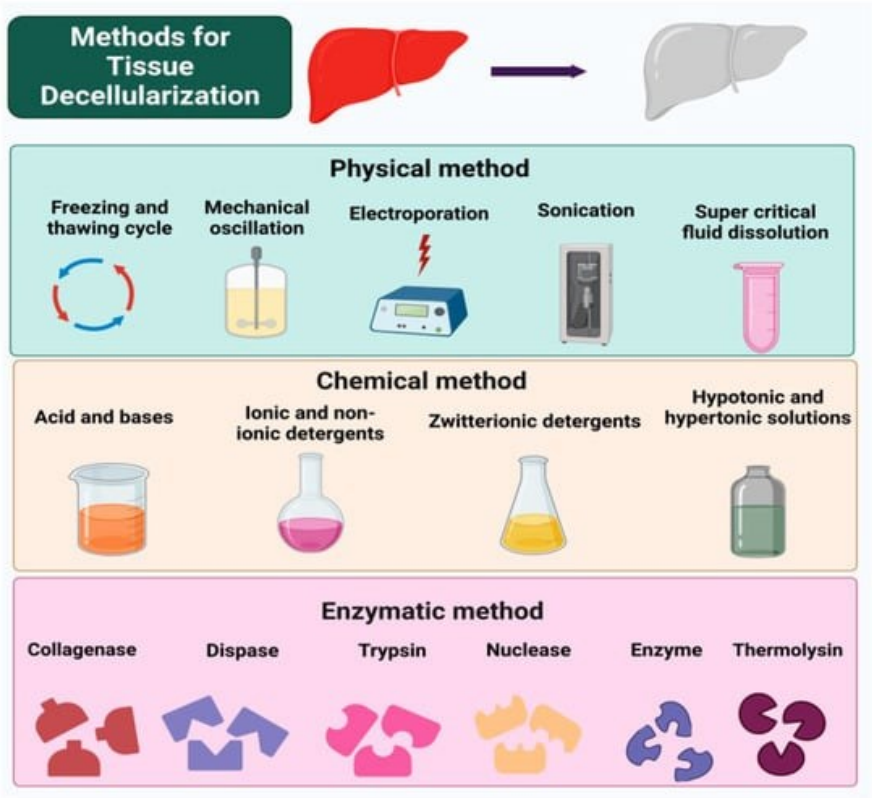

Figure 1.22 Ilustration of physical, chemical and enymatic decellularization methods [110].

1.8 Conductivity Criteria for Cardiac Patch

Considering the critical component in the heart's structure, a cardiac pacth should be electrically conductive [111]. The contraction-relaxation behavior of the heart results from the synchronous propagation of electrical signals through the cardiomyocytes. In recent years, electrically conductive polymers have had an important role in tissue engineering, especially for cardiac patch applications [112]. Many researchers try to imitate and improve the functionality of the heart by using electrically active particles or conductive polymers for cardiac applications. A fully integrated cardiac patch should be conductive, non-toxic, biologically active and have the ability to withstand the dynamic forces of the heart especially the contraction, torsion, and tension forces. Basically, carbon-based nanomaterials such as carbon nanotupes, or carbon nanofibers, graphene derivatives, metalic nanoparticles such as gold nanoparticles and silver nanoparticles, and electroactive polymers are most preferable for cardiac applications [111]. The electrically conductive polymers are a type of synthetic polymers with distinctive electro-active

properties. Their polymers have π-conjugated chain that alternate the single and double bonds that means delocalized electron can move along the polymer chain. The electro-optic properties depend on the polarizable and delocalized π-electrons in their chain [113]. In the doping process, electrons can be injected or removed that is provides movable charge carriers such as electrons or hole in the molecules achieving conductivity [114]. Firstly, Alan Heeger, Alan MacDiarmid, and Hideki Shirakawai discovered a conductive polyacetylene polymer by doping polyacetylene with iodine in 1977. By the way that study has a Nobel Prize in chemistry in 2000 [113]. Mainly, polyaniline (PANI), polypyrrole (PPy), and polythiophene (PTh) and their derivatives or composites are attractive conductive polymers for cardiac patch applications due to their biocompatibility, easy synthesis, low cost and modifiability conductivity, and charming electro-optic properties [112, 113]. However, the conductive polymers have a brittle structure and are very difficult to use alone in scaffolding production, nondegradable properties, and they may cause toxicity in long-term application [112]. Therefore, they should be used with blending with other polymers especially in cardiac applications. In a study, PANI blended with PLA in nanofibrous membrane for cardiac patch applications [115]. In a study, PCL film was coated with conductive PPy, the fabricated cardiac patch demostrated the 1.0 ± 0.4 kΩ cm. resistivity, which is similar to native heart resistivity [116].

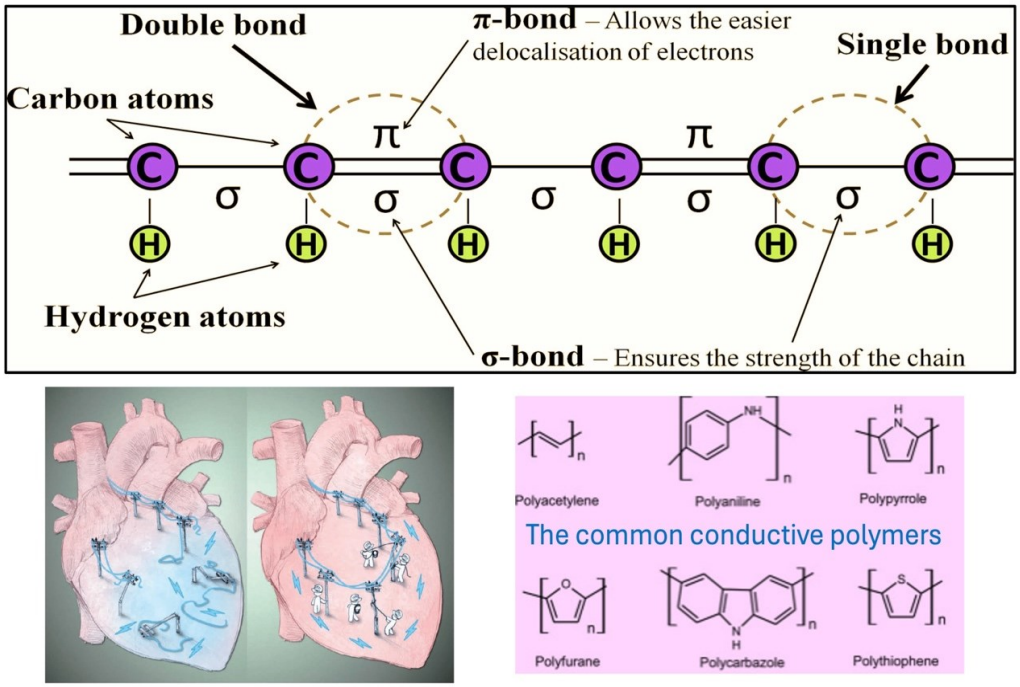

Figure 1.23 The common conductive polymers and π-conjugated polymer chain [71, 117, 118].

1.8.1 PANI

PANI is one of the charming polymers preferred in various industrial and biomedical applications due to its low cost, easy preparation, controllable conductivity, and low toxicity [113]. PANI can be synthesized by oxidative polymerization of aniline, existing different forms based on the oxidation level. The full-oxidized base form is known as pernigraniline, and the half-oxidized form is emeraldine. The emeraldine is conductive and stable form of aniline [111]. The dodecyl benzene sulfonic acid (DBSA) is a dopant for PANI, the lipophilic group in DBSA provides solubility in many organic solvents, that's why PANI has been preferable in many studies [113]. In a study, PANI contained gelatin scaffold was fabricated by electrospinning, it supported the cardiomyocyte cell adhesion and prolfieration on scaffold [119]. In another study, electrically conductive nanofibers were fabricated from PCL/PANI by electrospinning, the PANI integration improved the conductivity of nanofibers up to 63.6 ± 6.6 mS/cm [120]. In another study, PANI nanoparticles was coated on the PCL-based scaffold by ink-jet printing [121].

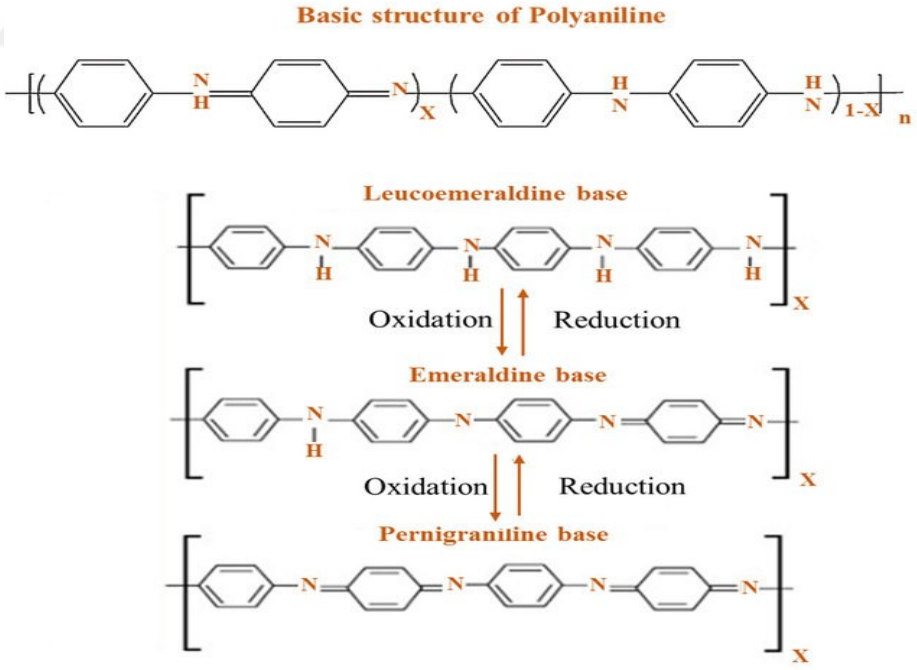

Figure 1.24 The chemical structure of polyaniline [122].

1.9 Bioactivity of Cardiac Patch

1.9.1 Vascularization Criteria

Vascularization is one of the major challenge of cardiac tissue engineering applications. The heart contains numerous capillaries, which surround the cardiomyocytes to facilitate efficient mass transfer. The blood vessel formation can be stimulated by several methods such as gene theraphy, stem cells or delivering growth factors on the infarcted myocardium [123]. The vascular enthothelial growth factor (VEGF) is a growth factor acting as a signaling molucule to enhance angiogenesis in biomaterials. Basically, VEGF binds to VEGF-receptor and activates it, the ligand-activated VEGFR generates the angiogenic signals, then several pathways can be initiated respectivelly. Then, the endothelial cell migration is activated by these pathways to form of vessels [124]. Additionally, the scaffold-based approach is critial to provide suitable porosity to formation of blood vessels [125]. Miyagi et al. developed a collagen-based cardiac patch, they immobilized VEGF covalently to patch to provide fast vascularization response in vivo [126]. In a study, VEGF growth factor was encapsulated into PLGA and combined into a acelllular myocardium scaffold to increase capillary density on animal model [127]. In another study, PCL/PGS electrospun membrane was functionalized with VEGF to gain bioactivity for cardiac patch applications [128].

1.9.2 Bioactive Plants

Several plants have bioactive and anticoagulant effects, such as cinnamon, parsley, liverwort, hawthorn, etc., have been used as alternative medicine in heart disease [129]. Especially hawthorn, also known as deer thistle and crataegus oxyacantha, is a plant widely used to treat gastrointestinal disorders and cardiovascular problems such as angina, hypertension, hyperlipidemia, arrhythmia, and functional class II congestive heart failure [130–132]. Hawthorn contains many pharmacologically active substances such as polyphenols (chlorogenic acid, proanthocyanidin B2, epicatechin), flavonoids (proanthocyanidins, mucoxanthin, quercetin, rutin), and pentacyclic triterpenoids (ursolic acid, hawthornic acid, oleanolic acid) and phenol carboxylic acids [78]. In the literature, there are several *in vivo* and *in vitro* studies regarding the hawthorn extract's cardioprotective effect and antioxidant properties [133]. It was reported that the

hawthorn’s antiplatelet or anti-coagulant properties depeds on its preventive effect on the platelets agregation [134]. On the other han, oxidative stress is an undesirable event in defected myocardium, hawthorn can provide positive effect on the protection of myocardium by reducing oxidative stress [135] . Therefore, hawthorn extract could be good bioactive molecules for cardiac patch applications.

Chapter 2

Materials & Methods

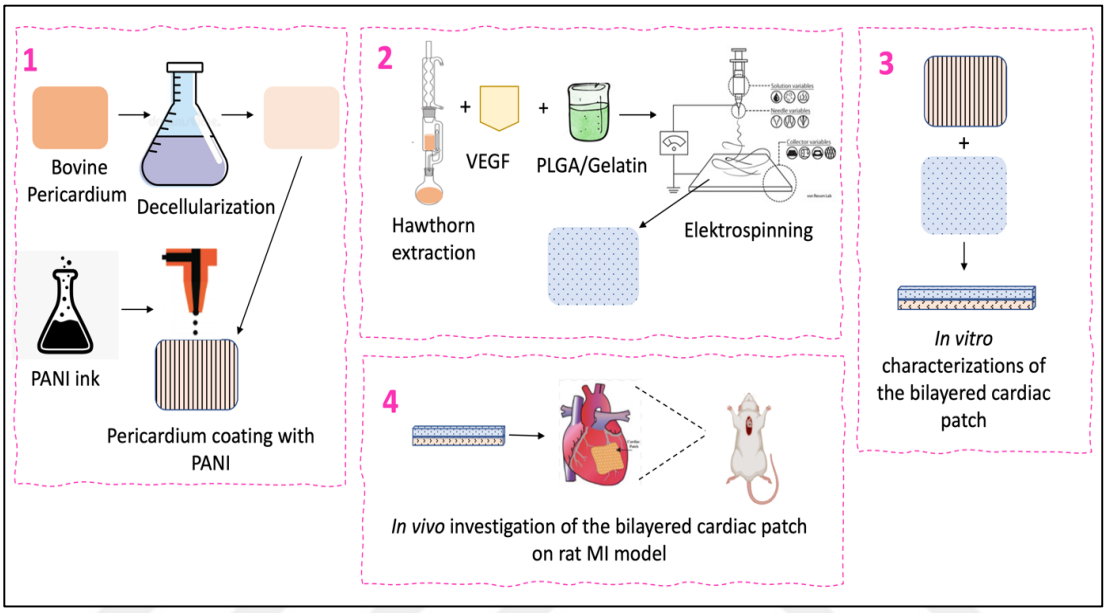

Figure 2.1 Graphical representation of the bilayered cardiac patch fabrication and methods parts.

2.1 Materials

The bovine pericardium used in this study was donated from Erciyes University Faculty of Veterinary Medicine slaughterhouse. Various reagents and materials were acquired from reputable suppliers, with details as follows: phosphate buffered saline (PBS), penicillin/ streptomycin, trypsin/ EDTA, pepsin, sodium chloride (NaCl), Aniline (ANI), ammonium peroxydisulfate ((NH4)2S2O8), Dodecylbenzene sulfonic acid (DBSA), sodium dodecyl sulphate (SDS), Genipin, gelatin (Derived from Bovine Skin, CAS No.9000-70-8) $225g Bloom, Type B) were obtained from Sigma. DNase and RNase were procured from Thermo Fisher, and diamidino-2-phenylindole (DAPI, Thermo Fisher), Hematoxylin-Eosin (H&E, Roth Fast Staining Kit), Sircol Soluble Collagen Assay Kit (Biocolor, S1000), One-4-All Genomic DNA Miniprep Kit(BS88503, BioBasic Canada), 1,1,1,3,3,3-hexafluoro-2-propanol (HFIP, Chem

Solute), Poly-L-lactide-co-glycolide (PLGA, 75/25, Mw:120.000, Purasorb), Paraffin (TEKKIM), deoxycholic acid (CAYMAN), Tris (BioBasic), VEGF165, (Z02689-50, Genscript), VEGF165-Eliza Kit (MyBiosource), (Triton X-100 (AppliChem), rat cardiomyocyte cell line (ATCC, H9c2, CRL-1446™), Dulbecco's Modified Eagle Medium-Low Glucose (DMEM, Serox), RPMI (Serox), L-glutamine (Capricorn), Fetal Bovine Serum (FBS, Serox), CellTiter 96® AQueous One Solution Cell Proliferation Assay ((MTS), Promega), APTT (Atlas Medical), VEGF Bioassay (Promega GA2001), tissue adhesive (Glubran®) were sourced from several brands. Additionally, hawthorn was purchased from local plant stores. Xylene, Methanol, Ethanol and Formalin were purchased from Merck.

For *in vivo* studies, the ketamine (Ketasol®), xylazine (Xylazinbio®), and disposable sterile materials were purchased from several brands, the sutures (4-0, 3-0, 1-0, 6-0, 7-0) were purchased from Doğsan™. Hematoxylin & Eosin Fast Staining Kit was purchased form Roth™, Masson's Trichrome Stain Set was purchased from Zag™. The antibodies: VWF Polyclonal Antibody (BS-0586R), GATA4 Polyclonal Antibody (BS-1778R), CD68 Polyclonal Antibody (BS-0649R), CD34 Polyclonal Antibody (BS-0646R), CD31 Polyclonal Antibody (BS-0468R) were purchased from Bioss™, α-SMA Polyclonal Antibody (E-AB-34268), Goat Anti-Rabbit IgG(H+L) (Elab Fluor®488 conjugated, E-AB-1055), Goat Anti-Rabbit IgG(H+L)(Elab Fluor®647 conjugated, E-AB-1075) were purchased from Elabscience™. Citrate buffer was obtained from Scytek™, anti-fade fluorescence mounting medium was purchased from Abcam. DAPI (2-(4-Carbamimidoylphenyl)-1H-indole-6-carboximidamide dihydrochloride, 98%, BD123448) was purchased from BLD Pharma™.

2.2 Preparation and Characterization of First Layer

2.2.1 Decellularization of Bovine Pericardium

Bovine pericardium was taken from Erciyes University Faculty of Veterinary Medicine slaughterhouse and processed in accordance with the established protocol [136]. To achieve decellularization, the pericardium underwent treatment with a 10 mM Tris buffer (pH 7.4) containing Triton X-100 (1%, v/v), SDS (0.2%, w/v), 150 mM NaCl, deoxycholic acid (1%, w/v) for a duration of 72 hours. Subsequently, a hypotonic 10 mM Tris buffer, incorporating trypsin/EDTA (0.5%/0.2), RNase (20 µg/ml) and DNase (0.2

mg/ml), was applied for an additional 48 hours at 37°C. Following the decellularization process, thorough rinsing with distilled water was carried out to eliminate detergent residues [137]. The processed pericardium was then subjected to drying using a freeze-dryer (Labconco, FreeZone) and stored at -20°C for further use.

2.2.1.1 DNA Analysis of Pericardium

The commercial DNA Assay kit (BioBasic, BS88503) was employed to quantify the DNA content in both decellularized and native pericardium samples. Following the kit protocol, 15 mg of dried tissues were extracted using the "BioBasic DNA Kit (BS88503)", and the resultant DNA was dissolved in 50 µl of dilution buffer. Subsequently, the DNA concentration was defined by NanoDrop spectrometer (NanoDrop2000, Thermo Scientific), yielding a concentration of 1 ng/µl at 260 nm [138]. The ng DNA per mg dry tissue weight was calculated using the following equation, and the results were presented comparatively [139].

$$\text{DNA amount (ng/mg)} = \frac{\text{Concentration of DNA at 260 nm } \left(\frac{\text{ng}}{\mu\text{l}}\right) \text{ x Volume of dilution buffer (µl)}}{\text{Sample weight (mg)}} \quad \textbf{(2.1)}$$

2.2.1.2 Collagen Analysis of Pericardium

The impact of decellularization on collagen content was assessed using commercial Sircol Soluble Collagen Assay Kit (S1000). The pericardium underwent digestion in 0.5 M acetic acid solution containing 1 mg/ml pepsin, conducted overnight at 4°C. The resulting digested solutions were subjected to centrifugation at 3000 rpm, and 100 µl of the supernatants were then incubated with 1 mL of Sircol dye reagent for 30 minutes at room temperature. Following the precipitation and washing step using kit buffers, the final collagen solution's absorbance was measured at 555 nm using a microplate reader [140].

2.2.1.3 Histological Staining of Pericardium

Both decellularized and native pericardium were subjected to histological analysis using diamidino-2-phenylindole (DAPI, Thermo Fisher) and Hematoxylin&Eosin (H&E, Roth Fast Staining Kit) staining techniques. Formalin-fixed samples were embedded in paraffin, and 5 µm tissue sections were prepared. Initially, the tissue sections were stained with DAPI (300 nM), followed by a 5-minute incubation period, and subsequently

examined under a confocal microscope at 20X magnification [137]. Subsequently, the tissue sections were subjected to H&E staining and observed using an optical microscope (Olympus, DP72).

2.2.1.4 Mechanical and Morphological Characterizations of Pericardium

The mechanical strength of the pericardium was investigated by uniaxial tensile test (Shimadzu, AGS-X 10 kN). Samples, cut to dimensions of 41 mm in length and 4.0 mm in width with following ISO 37 standards, underwent tensile testing at a strain rate of 5 mm/ using a 10 N per load capacity device [141]. Tensile strength, elastic modulus, and elongation ratios were calculated from stress-strain curve in accordance with ASTM 638D standards. To investigate the decellularization effect on the ECM structure, the pericardium's thickness was measured using a micrometer. Additionally, the serous and fibrous layers of the pericardium were examined via scanning electron microscopy (SEM, Carl Zeiss EVO LS10, Germany). The pericardium, dried by freeze-dryer (Labconco, FreeZone), underwent a gold coating process under vacuum with a 5 kV acceleration voltage. SEM images were captured to discern the impact of decellularization on the ECM fibers [141–143] .

2.2.2 Synthesis and Characterization of PANI Nanoparticles

The PANI ink solution was synthesized through oxidative polymerization in water, using aniline (ANI) as the monomer, dodecyl benzene sulfonic acid (DBSA) as the anionic surfactant, and ammonium peroxide sulphate ($(NH4)_2S_2O_8$, APS) as the initiator agent. Aniline, APS, and DBSA were mixed at a ratio of 1:0.5:1.6 and stirred for 2.5 hours. Subsequently, the mixture underwent dialysis against water for 48 hours, and the PANI ink solution was obtained following centrifugation at 8000 rpm for 30 minutes [144]. The chemical structure of the resulting PANI was characterized using Fourier Transform Infrared Spectrophotometer (FTIR, Thermo Fisher) utilizing the Attenuated Total Reflectance (ATR) technique within the range of 400-4000 cm^{-1}. Furthermore, the particle size of PANI nanoparticle was determined using a dynamic light scattering spectrometer (Malvern Zetasizer NanoZS DLS). The instrument, equipped with a 4 mV He-Ne laser operating at $\lambda = 633$ nm, performed measurements at a backscattering angle of 173°.

2.2.3 Pericardium coating with PANI

The decellularized bovine pericardium's surface was coated with PANI nanoparticle ink using ink-printing method, applying a pressure of 2.1 psi and a 0,25 mm inner diameter needle. The coating process involved applying PANI nanoparticles in parallel lines on the pericardium. Subsequent to coating, the pericardium was dried at 37ºC for 30 minutes and crosslinked using %1 genipin solution (w/v in (70:30) ethanol: water). Following crosslinking, the pericardium underwent multiple washes with PBS and then subjected to freeze-dryer. The crosslinking efficiency was evaluated through FTIR analysis.

Morphological examination of the PANI-coated pericardium was conducted via SEM, while its mechanical properties were assessed through a tensile test. The electrical conductivity of the PANI-coated pericardium was measured using a 4-point device (KEITHLEY 2400 SourceMeter). This technique relies on the principle of determining the sheet resistance of the material. The resistivity of the material was derived from the measured resistance value, and the conductivity was expressed in Siemens per centimeter (S/cm). The calculations followed established equation based on previous studies in the literature [145].

$$R_{sheet} = \frac{R}{t} \qquad \text{Conductivity (S/cm)} = \frac{1}{R} \quad \textbf{(2.2)}$$

(R; resistance (ohm), t; tissue thickness)

2.3 Preparation and Characterization of Second Layer of Cardiac Patch

2.3.1 Obtaining and Characterization of Hawthorn Extract

A quantity of 50 g of dried hawthorn was subjected to extraction using 500 ml of 70% ethanol at 63°C for 4 hours, employing a Soxhlet extraction system [146]. The resultant extract-ethanol mixture underwent treatment in a rotary evaporator at 40ºC to eliminate ethanol and water. The final hawthorn extract was then stored at -18ºC for further use.

The chemical structure of the hawthorn extract was elucidated through FTIR utilizing the ATR technique within the range of 400-4000 cm^{-1}. Gas Chromatography-

Mass Spectroscopy (GC-MS) analysis was conducted to identify the compounds present in the hawthorn. The analysis, performed using a Shimadzu GCMS-QP2010 ULTRA instrument with helium gas as a carrier gas, utilized an Rtx®-5MS column (30 m x 250 µm 0.25 µm) at a flow rate of 3 ml/min. The temperature range for analysis spanned from 40ºC to 280ºC, with a rate of temperature increase set at 15ºC/min.

2.3.2 Fabrication of Electrospun Membranes

The polymer solutions for the electrospinning were prepared from a (15%, w/v) PLGA/gelatin mixture (9:1) in 1,1,1,3,3,3-hexafluoro-2-propanol (HFIP) as a solvent. Subsequently, hawthorn extract at a concentration of 1%, 5%, 10%, and 15% (w/v) were individually incorporated into the solutions. Solutions containing VEGF were prepared from a (15%, w/v) PLGA/gelatin and 10% (w/v) of hawthorn extracts mixture in HFIP, with VEGF concentrations set at 0.1 µg/ml, 0.5 µg/ml, and 1 µg/ml. These well-mixed solutions were loaded into a syringe and produced as a nanofiber membrane by electrospinning method. The electrospinning parameters included a flow rate of 1.5 ml/h, a voltage of 15 kV to be applied, and a distance of 17 cm between the needle tip and the collector. These fabricated membranes were labelled as AY1-AY8.

2.3.3 Characterizations of Electrospun Membranes

The fiber orientation, fiber diameters and pore sizes of membranes were examined using SEM (Carl Zeiss EVO LS10, Germany) at magnifications of 1000X, 2000X, 3000X and 5000X. The ImageJ software (National Institutes of Health, Bethesda, MD) was utilized to calculate the fiber diameters from SEM images. The chemical structure of the membranes was analyzed via FTIR analysis with a wavelength range of 400-4000^{-1} cm, using ATR technique. The hydrophilic properties of membranes were investigated by determining contact angle value in Contact Angle-Sessile Drop (Biolin Scientific Attention Theta Lite) device. An *in vitro* weight loss study of PLGA/gelatin membrane containing hawthorn extract and VEGF was conducted in PBS at 37ºC for 28 days. At specific time intervals (days 7, 14, 21 and 28) the membranes were removed from PBS and subjected to dry weighing. The *in vitro* degradation percentages were calculated using the initial weights (Mi) and final weights (Mf) of the membranes with the following equation;

$$\text{Weight Loss (\%)} = 100 \text{ x } \frac{Mf - Mi}{Mi} \quad \textbf{(2.3)}$$

(Mi= dry weight of membranes, Mf= final weight of membranes)

2.3.4 Controlled Release Profiles of Membranes

The release profiles of the hawthorn extract from AY2, AY3, AY4 and AY5 were investigated for 28-day period. Membranes, cut to a minimum size of 1cm x 1cm, were incubated in 15 ml of PBS at 37°C for 28 days. During this interval, 1 ml of liquid was withdrawn from the release environment, and 1 ml of PBS was replenished. To generate a calibration curve for hawthorn extract, hawthorn was dissolved at concentrations ranging from 2,5 to 0,2 mg/ml in water and scanned between 200-700 nm using a fluorescence spectrophotometer (Varioskan, Thermo Scientific). A specific excitation value of 320 nm and emission value of 420 nm were chosen for hawthorn extract. The hawthorn extract release in the collected liquids were quantified by measuring fluorescence (λ_{ex}: 320 nm λ_{em}: 420 nm) with the spectrometer. The cumulative release graphs were generated using the following equation:

$$\text{Cumulative Release (\%)} = 100 \text{ x } \left[\frac{Vm \text{ x } C(n) + 1 \text{ ml x } \sum C(n-1)}{Wo} \right] \quad \textbf{(2.4)}$$

In this equation, Vm represents the volume of the release medium, C(n) denotes the amount of hawthorn extracted from the single release medium (mg/ml), C(n-1) represents the amount of hawthorn previously extracted from the environment, and W_0 (mg) is the initial amount of hawthorn loaded onto the membrane [147, 148]. The release profiles of VEGF from VEGF-containing membranes were investigated for 28 days. The membranes were incubated in PBS at 37°C for 28 days, and released samples were collected at the specified intervals (1, 2, 3, 4, 5, 6 and 12 hours and 7, 14, 21 and 28 days) and stored at -20°C. Released VEGF was quantified using an Eliza kit (MyBiosource, MBS2514274) at 450 nm. To construct a standard curve, 2000 pg/ml VEGF standard was diluted at ½ ratios according manufacturer's protocol. The release behaviour (%) of VEGF was calculated from the standard curve using the aforementioned equation.

2.3.5 *In vitro* Anticoagulant Efficacy of Membranes

The *in vitro* anti-coagulant effect of membranes containing hawthorn extract were assessed using the activated partial thromboplastin time (APTT) assay. Initially, approval was obtained from the Ethical Committee (Erciyes University Clinical Ethics Committee

Approval Decision no: 2022/267, 23.03.2022), and 20 ml of healthy human blood was collected, to which 109 mM sodium citrate (9:1 v/v) was added to prevent coagulation. Platelets were then isolated from the blood through centrifugation at 2000xg for 20 minutes at 4°C, yielding platelet-poor plasma (PPP). Subsequently, 100 µL of PPP and APTT were mixed and incubated with the membranes for 5 minutes at 37°C. Following this, 50 µL of 25 mM $CaCl_2$ solution was added, and the activated partial thromboplastin time (APTT) was measured [149].

2.3.6 Investigation of VEGF Bioactivity by Bioassay

The bioactivity of VEGF was evaluated using VEGF Bioassay (Promega GA2001). Following the manufacturer's protocol, 10% Fetal Bovine Serum (FBS) was incorporated into DMEM, and KDR/NFAT-RE HEK293 cells (Promega GA2001) were combined with 4 ml of DMEM/FBS. Subsequently, 25 ml of the cell-DMEM mixture was added to the white 96-well plate. Positive controls containing VEGF, membranes containing VEGF, and reference standards were added to the plate, followed by the addition of 25 ml DMEM to each well. The plate was incubated in a 37 °C incubator for 6 hours. Following incubation, 75 ml of Bio-Glo reagent (Promega GA2001) was added to each well, and luminescence was measured using a luminometer (Varioskan Plate Reader, Thermo Scientific) [150].

2.4 Preperation and Characterizations of the Final Bilayered Cardiac Patch

The first and second layers of the cardiac patch were integrated using tissue glue. Initially, the 25 µl of tissue adhesive was dispensed and uniformly distributed between the layers using a sterile syringe needle. To commence, the integration of layers underwent scrutiny via SEM, the cross-sectional profile of the bilayered cardiac patch was coated with 5 nm gold layer under vacuum conditions, and SEM images were acquired at a 5 kV acceleration voltage.

2.4.1 Lap-Shear Test

The adhesive strength of tissue glue was assessed through Lap-Shear Testing. The first and second layers, each measuring 40 mm in length and 20 mm in width, were affixed to a 20 mm x 20 mm gauge length. The tensile test was conducted at a rate of 3 mm/min using a device with a load capacity of 10 N (Shimadzu, AGS-X 10 kN).

2.4.2 Tensile Test

The mechanical characterization of the bilayered cardiac patch, first layer of the cardiac patch, the electrospun PLGA/gelatin membrane (AY1), and the second layer of the cardiac patch (AY8) were examined through a tensile test, following the parameters outlined in 2.1.2.4 as previously mentioned. In a succinct overview, the tensile test was conducted at a 5 mm/min strain rate using a device with a load capacity of 10 N (Shimadzu, AGS-X 10 kN). Tensile strength, elastic modulus, and elongation ratios were computed from the stress-strain curve based on ASTM 638D standard, and the findings were graphically presented [141, 143, 151].

2.4.3 Blood Compatibility

The 20 ml of fresh human blood was obtained from Erciyes University Hakan Çetinsaya Good Clinical Practices Centre, with the explicit permission of the ethics committee obtained within the study's framework (Erciyes University Clinical Ethics Committee Approval Decision no: 2022/267, 23.03.2022). To prevent the blood clotting prior to experimentation, 3.8% (v/v) sodium citrate was added, and this blood solution was utilized throughout the experimental procedures. A physiological saline solution (0.9% (w/v) NaCl) was prepared beforehand. For the cardiac patch-containing and negative reference groups, 4.9 ml physiological salt solution was used, and then the cardiac patch was introduced into the physiological saline solution. The 4.9 ml distilled water was utilized for the positive reference group. Following, the 100 µl of blood was added to each tube, resulting in a total volume of 5 ml. Subsequently, the tubes were incubated at 37ºC for 30 minutes and then centrifuged at 1000xg for 10 minutes. The absorbance of the supernatants were measured at 545 nm, and the hemolysis rate of the cardiac patch was determined using the following equation, where As represents the

absorbance value of the cardiac patch, and Ap and An represent the absorbance values of the positive and negative references, respectively.

$$\text{Hemolysis Rate \%} = \frac{(\text{As}-\text{An})}{(\text{Ap}-\text{An})} \text{x}100 \text{ [149]} \quad \textbf{(2.5)}$$

2.4.4 Cell Viability

All cell studies were conducted in a laminar cabin under aseptic sterile conditions. The rat cardiomyocyte cell line (H9c2, ATCC® CRL-1446TM) were seeded in a 75 cm^2 tissue culture plate containing low-glucose DMEM, comprising 10% (v/v) FBS and 1% (v/v) penicillin/streptomycin. The seeded cells were then incubated at 37 °C with 5% CO_2 and 95% humidity in a standard incubator. DMEM was refreshed in every two days, and cells were passaged and propagated when they reached 90% density. The cell viability (%) of the cardiac patch with cardiomyocyte cells was determined using the commercial MTS kit "CellTiter 96® AQueous One Solution Cell Proliferation Assay (Promega)". Before experiment, the cardiac patch was sterilized using UV exposure for 30-minutes on each side of membranes and placed in 96-well plates. The 200 µl cell suspension containing 10^4 cells and medium was added to each well. Following the kit procedure, empty wells containing 10^4 cells and medium without a cardiac patch were used as the control group. Subsequently, the plates were incubated at 37ºC in a humidified atmosphere with 5% CO_2 for 24, 48 and 72 hours. After the incubation period, the cardiac patches were removed from the wells with sterile forceps, and 20 µl of MTS solution was added to each well. Then samples were incubated for 2.5 hours in a humidified atmosphere with 5% CO_2 at 37ºC under the dark conditions. The absorbance values of the wells were measured at 490 nm using a plate reader (Varioscan, Thermo Fisher). The following equation was utilized to calculate the cell viability (%) values of the wells containing the cardiac patch.

$$\text{Cell Viability (\%)} = 100\ x\ \frac{\text{Mean OD (sample)}}{\text{Mean OD(control)}} \quad \textbf{(2.6)}$$

In this equation, $OD_{(\text{cardiac patch})}$ represents the absorbance value averaged across wells containing the cardiac patch, while $OD_{(\text{control})}$ refers to the absorbance value averaged across control wells [152].

2.4.5 Cell Adhesion Study

For the *in vitro* cell adhesion study on the cardiac patch, the samples were initially sterilized by exposure to UV light for 30 minutes on each side. Subsequently, they were carefully placed in a 96-well plate using sterile forceps. A 200 µl of cell suspension containing 10^4 cells and medium was added on the cardiac patch. The samples were incubated for 24, 48 and 72 hours at 37ºC in a humidified atmosphere with 5% CO_2. After the incubation period, samples were gently removed from the wells with sterile forceps and washed with PBS. Next, 200 µl of 2.5% glutaraldehyde was added to the cardiac patch to fix the adhering cells, and the samples were kept at 4ºC overnight. Afterward, the glutaraldehyde was taken from the well, and the cardiac patch samples were dried at 37ºC. To visualize the nuclei of the adhering cells on the cardiac patch under the microscope, 20 µl of DAPI (300 nM, Sigma D9542) dye was added, kept in the dark for 10 minutes, and microscope images were taken under a fluorescent microscope at 20X magnification [151]. Additionally, the adherent and spread cells were examined by SEM, the cell-seeded cardiac patch was coated with a 5 nm gold layer under vacuum conditions, and SEM images were taken under a 5 kV acceleration voltage.

2.5 *In vivo* Study of Cardiac Patch

The whole *in vivo* studies were carried out under the "Erciyes University Animal Experiments Local Ethics Committee (HADYEK)" ethical committee permission with the decision number of 23/242, *in vivo* operations were conducted at Erciyes University Experimental Animal Production and Application Laboratory (DEKAM). A power analysis was performed (G*Power, version 3.1.9.6) to determine the minimum number of animals per group, and according to the entered values (t tests, means: Wilcoxon-Mann-Whitney test, α err prob= 0.05, power (1-β err prob) = 0.95), 8 rats were determined per group to obtain statistically significant results. The study was planned with the minimum number of animals that would allow for statistically significant results. According to these results Sprague Dawley male rats, aged 8-12 weeks and weighing 300-350 grams, were used. These groups are as follows: Group 1; the negative control group consisting of healthy rats with no surgical procedure performed, Group 2; the positive control group with MI, Group 3; the bilayered cardiac patch implanted group after MI, and Group 4; the PLGA/gelatin implanted group after MI.

Tablo 2.1 Information of the determined *in vivo* groups.

Group No	Group Name	Group Information
Group 1	Negative Control	Healthy rats without any surgical procedure (n=8).
Group 2	Positive Control	Myocardial infarction (MI) group without treatment (n=8).
Group 3	Bilayered Cardiac Patch Group	Bilayered cardiac patch implanted group after MI (n=8).
Group 4	Polymeric Membrane Group	PLGA/gelatin membrane implanted group after MI (n=8).

2.5.1 Anesthesia and Preparations

The left anterior descending (LAD) coronary artery ligation model was selected to create myocardial defect in the rats' hearts. All surgical operations were performed under anaesthetic and sterile conditions. Ketamine (80 mg/kg) and xylazine (5-10 mg/kg) anaesthetic agents were applied by intraperitoneally method. After the applying of anaesthesia, the fur on the chest, submandibular, and back regions of the rats were shaved and sterilized with Batikon. Under sterile conditions, the rats were placed on the surgery table, and their arms were fixed to the table with tape [153]. The paediatric ECG electrodes were attached to the shaved back area of the rats and connected to the ECG device (Philips, Efficia CM120).

2.5.2 Tracheostomy

A tracheostomy was performed of rats to provide oxygen support as seen in Figure 2.2. The skin of the rats was gently cut with scissors, the muscles were separated. After reaching the trachea, a sterile 16G grey branule with a 1.75 mm cannula diameter was placed into the trachea. The branule was fixed to the trachea with the 1-0 sized silk suture (Doğsan). The grey branule was connected to the ventilator device (Hamilton Medical, GALILEO) via a triple stopcock, providing a cycle of 80 breaths per minute and a tidal volume of 1.2 mL per 100 g body weight [153]. During the operation, the rats' heart rate, temperature, and respiratory rate were controlled.

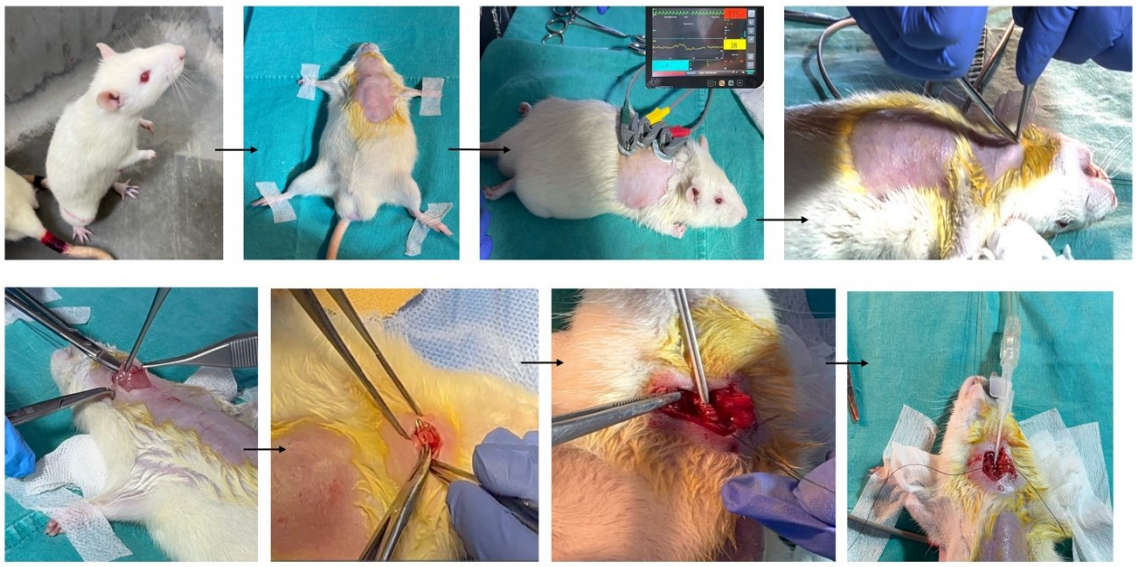

Figure 2.2 Representation of the operation photographs of rat' preparations and tracheostomy steps.

2.5.3 Opening the Chest and Induction of Myocardial Infarction (MI)

To induce myocardial infarction (MI) in the rat' hearts, the 3rd and 4th intercostal spaces were opened with a left thoracotomy. The skin and muscle tissues were retracted to the side with the help of a thoracic retractor to reach the heart (Figure 2.3). The pericardium was gently opened to reach the left anterior descending (LAD) coronary artery [153]. The LAD coronary artery was permanently ligated using 6-0 polypropylene sutures (Doğsan) to induce myocardial infarction (MI). An ECG was taken before and after MI, and the results were compared to confirm the induction of MI by observing ECG waves. Additionally, the formation of defect in the myocardium of the heart, close to the apex, was observed with cyanosis in the tissue within 15-20 minutes after MI. MI induction was applied to the three groups, including the positive control MI group (Group 2), the bilayered cardiac patch group (Group 3), and the PLGA/gelatin membrane group (Group 4).

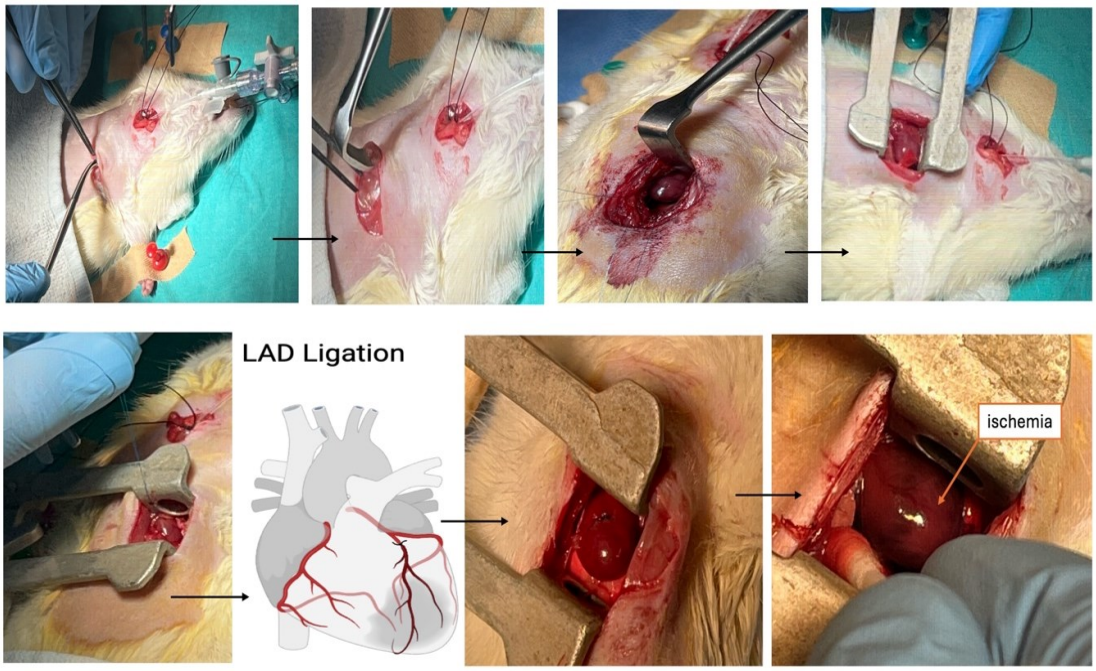

Figure 2.3 Representation of the operation photographs of opening chest, LAD ligation steps, induction of MI.

2.5.4 Cardiac Patch Implantation

For the patch implantation groups, cardiac patch samples were cut into a triangular shape and implanted (Figure 2.4) from three sides to the myocardium using 7-0 polypropylene sutures (Doğsan).

2.5.5 Closing the Chest

After the MI induction and patch implantation procedures, the muscles and skin layers in the chest cavity were closed using 4/0 silk sutures (Doğsan). Air, body fluids, and blood remaining in the chest cavity were removed with a 20G-pink branule.

2.5.6 Extubation

For the extubation process, the branule connected to the trachea was carefully removed, and the cartilage ring on the trachea where the branule was attached was closed with 4-0 silk sutures. Then, the muscle and skin tissues around the trachea were closed with sutures.

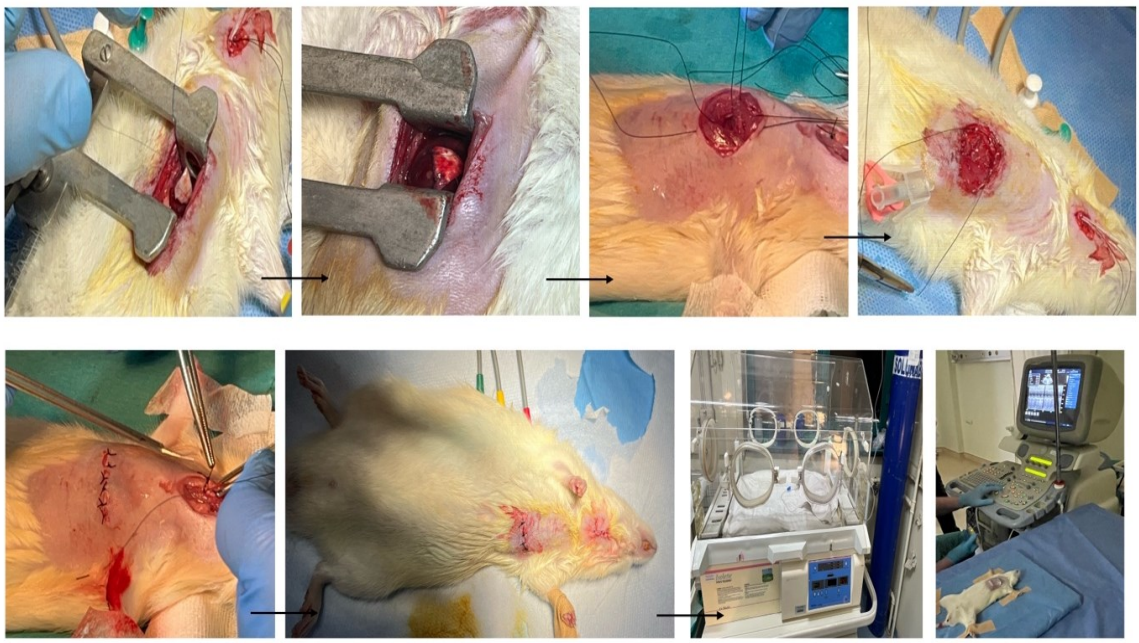

Figure 2.4 Representation of the operation photographs of patch implantation on myocardial defect area of rats, closing chest, extubation and post-op care steps.

2.5.7 Post-op Care

After the operation, Batikon was applied to the sutured areas to prevent adverse infection effect on wound cite. The rats were incubated for 45 minutes in an incubator providing oxygen and temperature support, then placed in their cages. All groups were implemented postoperative pain relief medication (Butomidor, Richter Pharma) and physiological saline (SF) supplementation, and their recovery processes were monitored.

2.5.8 Assessments of Cardiac Functions

Cardiac function was assessed using a paediatric transthoracic echocardiography (GE Healthcare, Vivid 7 Pro). In the echocardiography imaging system, M-mode images were obtained from the parasternal short-axis view at the mid-papillary muscle level [153]. The rats were anesthetized (ketamine/xylazine), and their fur was shaved from the chest, then gel was used to optimize the visibility of heart structures. The cardiac functions of the rats were measured before the operation and after the 4 weeks of operation. For cardiac function assessments, the left ventricular end-systolic and end-diastolic diameters (LVESd, LVEDd), ejection fraction (EF) and fractional shortening (FS) were measured from cardiac cycles.

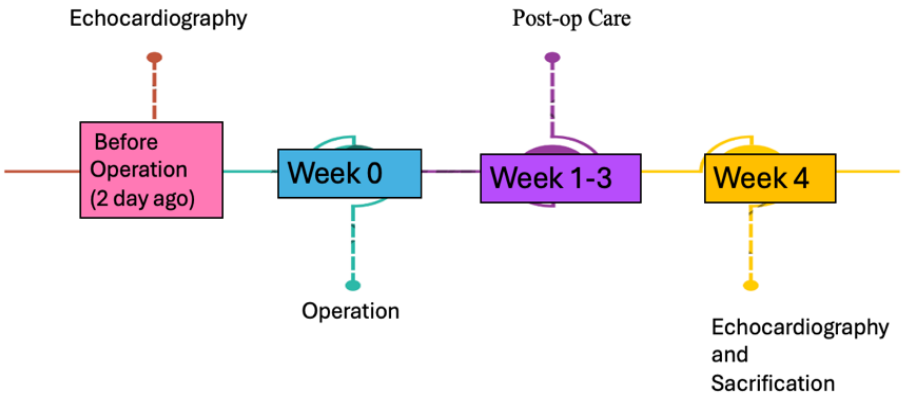

Figure 2.5 The timeline of the study from operation to sacrification of the rats.

2.5.9 Sacrification

After the 28 days of operation, the rats were sacrificed under anesthesia. The chest cavity of the rats was opened, and their hearts were carefully cut out with scissors and placed in a PBS solution containing 1 molar potassium chloride (KCl) for 1 minute. While the heart was still beating, the potassium ions in the KCl solution stopped the heart in systole. Then, blood residues were washed with PBS, and the heart was placed in a Formol (Formaldehyde: Ethanol, 10:90) fixative solution.

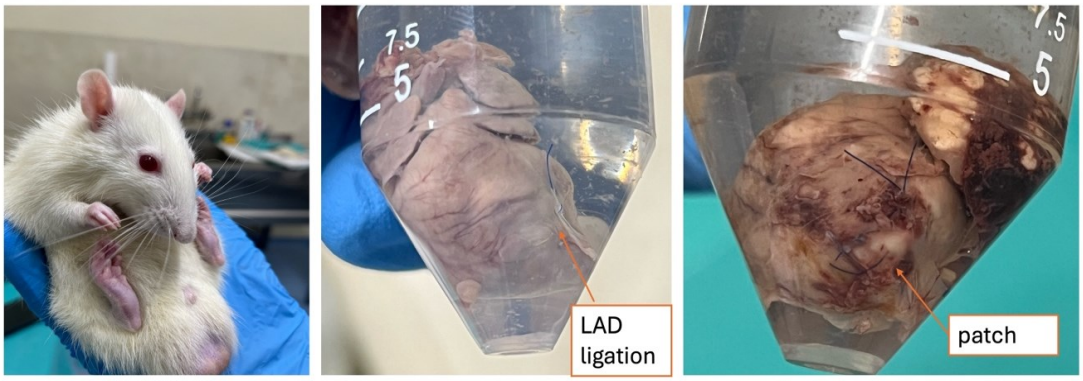

Figure 2.6 The photographs of sacrificed heart from rats.

2.5.10 Paraffine Embedding

The formol-fixed hearts were immersed in alcohol series as 96% alcohol, 100% alcohol I, II, and III for 1 hours, then immersed in methyl benzoate for 24h. Following,

the tissues were immersed in benzol series for 30 minutes, then incubated at 58ºC for 4h. The tissues were cut from the middle to separate the apex and base sections, then embedded in molten paraffine and stored at 4ºC. The 5 µm heart sections were taken in the microtome, then sections were located in water bath to collect with glass slide. The tissue adhered glass slides were dried at 37ºC for overnight.

2.5.11 Histological Evaluations

The dissected hearts were fixed in 10% formalin fixative solution and embedded in molten paraffin after dehydration. The embedded samples in paraffin were sectioned with a microtome at 5 µm thickness, then used for staining. Hematoxylin & Eosin (H&E) and Masson's trichrome staining procedures were performed by following the steps in Table 2.2 and 2.3. After the H&E staining procedure, the tissues were observed with a light microscope and images were taken. Masson's trichrome staining was used to observe the defected area of the heart. The left ventricular (LV) wall thickness was measured from H&E microscope images by ImageJ software program using the obtained microscope images [153].

Tablo 2.2 Hematoxylin-eosin (H&E) staining procedure steps.

1	Xylene I	5 min	**11**	Rinsing Tap Water	6 min
2	Xylene II	5 min	**12**	Acetic acid 2% (v/v)	1 min
3	Absolute Alcohol I	3 min	**13**	Rinsing Tap Water	6 min
4	Absolute Alcohol II	3 min	**14**	Eosin	30 sec
5	Alcohol %96	3 min	**15**	Rinsing Tap Water	30 sec
6	Alcohol %80	3 min	**16**	Alcohol %96	3 min
7	Alcohol %70	3 min	**17**	Absolute Alcohol I	3 min
8	Distilled Water	3 min	**18**	Absolute Alcohol II	3 min
9	Rinsing Tap Water	5 min	**19**	Xylene I	3 min
10	Hematoxylin	3 min	**20**	Xylene II	5 min

Tablo 2.3 Masson's Trichrome staining procedure steps.

1	Xylene I	5 min	**16**	Distilled Water	X 4
2	Xylene II	5 min	**17**	Phosphotungstic Acid I	7 min
3	Absolute Alcohol I	3 min	**18**	Phosphotungstic Acid II	7 min
4	Absolute Alcohol II	3 min	**19**	Distilled Water	7 min
5	Alcohol %96	3 min	**20**	Distilled Water	7 min
6	Alcohol %80	3 min	**21**	Anillin Blue	30 sec
7	Alcohol %70	3 min	**22**	Distilled Water	X 2
8	Distilled Water	3 min	**23**	Acetic acid 2% (v/v)	1 min
9	Rinsing Tap Water	5 min	**24**	Distilled Water	3 min
10	Weigert Hematoxylin	8 min	**25**	Alcohol %96	3 min
11	Rinsing Tap Water	5 min	**26**	Alcohol %96	3 min
12	Methyl Carbonate	1 min	**27**	Absolute Alcohol I	3 min
13	Rinsing Tap Water	5 min	**28**	Absolute Alcohol II	3 min
14	Distilled Water	3 min	**29**	Xylene I	5 min
15	Acid Fuchsin-dipping	X 20	**30**	Xylene II	5 min

2.5.12 Immunofluorescence Analysis

The immunofluorescence staining was conducted to investigate the formation of cardiomyocyte cells and neovascularization on infarcted hearts. GATA4 (Bioss, BS-1778R) was used to monitor the formation of cardiomyocyte cells, ∝SMA (Elabscience, e-ab34268) was used to examine actin of muscle cell, CD68 (Bioss, BS-0649R) was used to observe macrophages accumulating in the defected area, von Willebrand Factor (Bioss, BS-0586R) and CD31 (Bioss, BS-0468R), CD34 (Bioss, BS-0646R) markers were used to monitor neovascularization. Elab Fluor®647 (Elabscience, E-AB-1075) and Elab Fluor®488 (Elabscience, E-AB-1055) were used as secondary antibodies. All antibodies were diluted with antibody dilution solution (Thermo Fisher Scientific) at a ratio of 1:200 before use. Paraffin-embedded tissue sections were deparaffinized by passing through xylene and alcohol steps. Then, UV block hydrogen peroxide (Thermo Fisher Scientific) was applied to the preparations for 10 min and PBS was rinsed 5 minutes 2 times. Antigen retrieval was performed using 1X citrate buffer (pH 6.0) for 5 min x 4 times. After the blocking solution, primary antibodies were added and incubated at 4 °C for 18−22 hours. After the tissue sections were thoroughly washed 4 times with PBS, they were incubated

with secondary antibody in the dark for 3 hours at 4 °C. After the washing steps with PBS, DAPI stain was added, and the slides were covered with covering solution in the dark and left to dry. The dried preparations were examined under a fluorescence microscope [153].

2.5.13 Immunohistochemistry Analysis

Antibodies were diluted with antibody dilution solution (Thermo Fisher Scientific) at a ratio of 1:200 before use. Paraffin-embedded tissue sections were deparaffinized by going through xylene and alcohol steps. Then, UV block hydrogen peroxide (Thermo Fisher Scientific) was applied to the preparations for 10 min and PBS was rinsed 5 min x 2 times. Antigen retrieval was performed using 1X citrate buffer (pH 6.0) for 5 min x 4 times to reveal antigens. After the blocking solution, primary antibodies were added and incubated at 4 °C for 18−22 hours. After the tissue sections were thoroughly washed 4 times with PBS, they were kept in Biotinylated Goat Anti-Polyvalent (Thermo Fisher Scientific) solution for 12 minutes, washed 4 times with PBS and subjected to streptavidin peroxidase (Thermo Fisher Scientific) treatments. DAB Substrate kit (Thermo Fisher Scientific) was dropped and then stained with hematoxylin dye to perform the exit alcohol stages. The slide was covered with Entellam® and examined under a light microscope.

2.6 Statistical Analysis

In whole experiments were conducted with a minimum of three repetitions to ensure robustness and reliability. For statistical analysis the GraphPad Prism program was employed, utilizing both t-test and ANOVA. All data presented in the results include ± standard deviation values. Significance was determined with a threshold p-value less than 0.05, were values meeting this criterion were considered statistically significant. Error bars indicate standard deviation and **e**rror bars are invisible when they are smaller than the line thickness of these graphs.

Chapter 3

Results and Discussions

In this thesis, we developed a conductive, biocompatible, biodegradable and bioactive bilayered scaffold for cardiac patch applications. There is a huge challenge to replicate native heart ECM since its complex architecture and function. Because of that many researchers prefer to use decellularized tissue as a scaffold for cardiac applications [154]. Herein, we choose a bovine pericardium as an ECM scaffold due to its ECM structure abundant with collagen and elastin fibers, makes it mechanically strong and elastic. However, the native tissues can trigger the host immune responses and resulting tissue rejection by body. In order to solve this issue, we preferred the decellularization procedure to remove cellular and genetic residue of pericardium. The decellularization agents can be damaged to ECM structure, for that we optimized decellularization process to achieve high cell removal without damaging ECM structure. Furthermore, the heart contraction-relaxation function can be actualized by transmissions of electrical impulses through myocardium. To mimic that, we combined with decellularized pericardium with PANI nanoparticles, act as a conductive-biologic layer for cardiac patch. On the other hand, we designed a polymeric second layer to achieve suitable degradation rate and ensuring bioactivity by loaded bioactive molecules. The second layer was designed to fabricate from a PLGA/gelatin biocompatible polymer with suitable morphology by electrospinning which is mimicking native ECM fibers. There is a critical limitation in cardiac application, which is lack of vascularization [154]. In this study, VEGF and Hawthorn extract were selected as bioactive molecules to loaded into PLGA/gelatin. VEGF was selected to enhance angiogenesis and subsequently cardiac repair, while the hawthorn extract was chosen to prevent blood coagulation in myocardium. Also, PLGA or gelatin are highly preferable in the several studies for improve healing of tissues [86, 154, 155]. Both layers of scaffold were fabricated and characterized separately, then two layers were integrated by tissue glue as a bilayered cardiac patch. It was aimed to enhance mechanical strength of scaffold by integration two layers to each other. In this study, it was aimed to solve the current low biocompatibility, blood non-compatibility, weak

mechanical strength, lack of vascularization and tissue healing, conductivity, and coagulation problems by this proposed bilayered scaffold. The detailed characterizations and examinations for bilayered cardiac patch were represented in below sections. Following the *in vitro* characterizations of bilayered cardiac patch, its efficiency on myocardial defect was examined in rat MI model. Firstly, rat MI model was optimized, and cardiac patch samples were implanted on rat's heart. After the 28 days from implantation, the hearts were evaluated histologically. Also, cardiac functions of rats were determined by Echo measurements. The cardiac patch in vivo efficiency were represented in below sections with comparison the control groups.

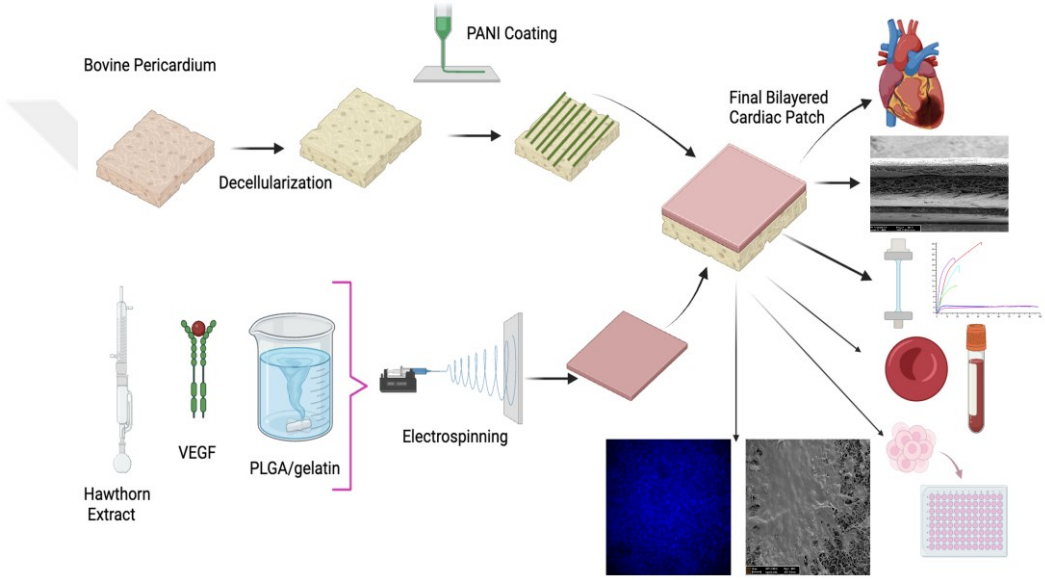

Figure 3.1 Graphical representation of bilayered cardiac patch fabrication and characterization parts.

3.1 First Layer of Cardiac Patch

3.1.1 Decellularization and Characterization of Pericardium

3.1.1.1 DNA Quantification

The decellularization efficiency of bovine pericardium was investigated quantitatively through a DNA assay, and the DNA content were graphically represented as µl/mg and ng/mg in Figure 3.2. Native pericardium exhibited 294.86±118.62 ng DNA in a 1 µl solution, while decellularized pericardium demonstrated 34.77±14.34 ng DNA in a 1 µl solution. Furthermore, native bovine pericardium demonstrated 982.88±395.42

ng/mg DNA, while decellularized pericardium demonstrated 115.9±47.8 ng/mg DNA. Based on these results, the decellularization process removed approximately %88.2 DNA from the pericardium. In a study by Heuschkel et al., the DNA amount in native pericardium was reduced from 846 ± 181 ng/mg to 198.7 ± 94.33 ng/mg through an SDS (0.1%), ethanol (70%), and NaCl (0.9%) decellularization protocol [157]. Another study by Wollman et al. found that the DNA amount in native and decellularized pericardium was 1591±726 ng/mg and 511.23±120.4 ng/mg, respectively [158]. In a study, decellularization utilizing 0.5% deoxycholic acid and DNase, resulted in a reduction of DNA content from 86.5 ng/mg to 48.24 ng/mg in porcine pericardium [159]. Additionally, a decellularization protocol involving 0.5% sodium deoxycholate/SDS demonstrated a decrease in DNA content from 72.14 ± 34.63 ng/mg to 11.59 ± 4.39 ng/mg [160]. In our study, the utilization of a combination of SDS, SDC, and TritonX-100 agents produced a synergistic effect, thereby enhancing the efficiency of the decellularization process [160, 161]. Upon comparing these results with data from the literature, it was inferred that the DNA content in native and decellularized pericardium tissue ranges approximately between 500-1500 ng/mg and 50-300 ng/mg, respectively [156, 162]. Our findings suggest that the decellularization process significantly eliminated cells and genetic materials, aligning with established literature standards.

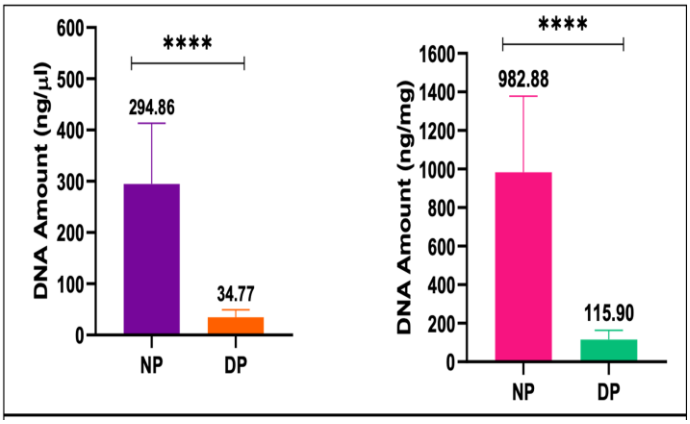

Figure 3.2 Graphical representations of the DNA amounts in native pericardium (NP) and decellularized pericardium (DP), illustrating values in ng/µl and ng/mg (n=27, p <0.0001: **** considered sginificant).

3.1.1.2 Histologic Staining of Pericardium

Furthermore, the qualitative assessment of decellularization was conducted through histological staining of the pericardium using DAPI and H&E. Figure 3.3 displays H&E

staining results, clearly demonstrating the presence of cells in the native pericardium, while no cell presence was observed in the decellularized pericardium. The DAPI staining results are depicted in Figure 3.3, where cell nuclei in native pericardium appear blue, contrasting with the lack of visible cell nuclei in the decellularized pericardium. These findings affirming the success of the decellularization process. In existing literature, analogous DAPI and H&E staining images can be observed, derived from the decellularization of pericardium employing Triton X-100, SDS and SDC [161]. Another study notes that although cells were entirely removed from the pericardium, the ECM components decreased due to decellularization process [158]. Heuschkel et al., achieved 77% decellularization of the pericardium without compromising ECM components, utilizing 0.1% SDS as decellularization agent [157]. According to Crapo et al., tissue can be deemed as decellularized when there is no visible nucleus in histological evaluation using H&E and DAPI staining methods [106]. In concordance with the histological staining data obtained, the pericardium in our study was completely decellularized, and the results obtained are consistent with existing literature data.

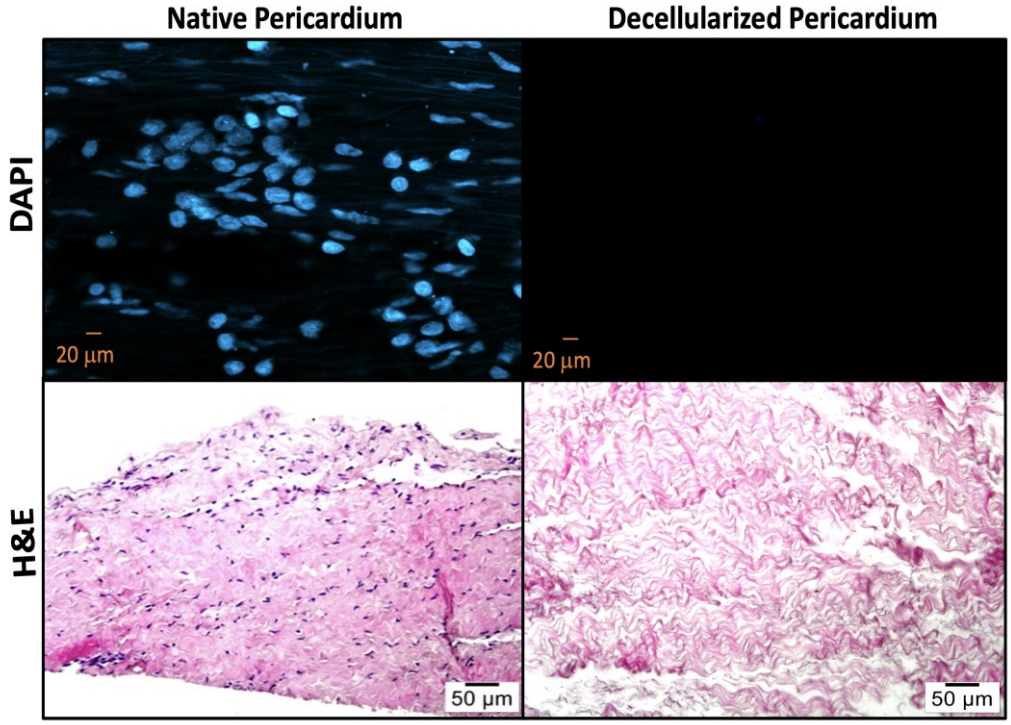

Figure 3.3 Optical microscope images of H&E stained native and decellularized pericardium, Confocal microscope images of DAPI stained native and decellularized pericardium at 20X magnification.

3.1.1.3 Collagen Analysis of Pericardium

The impact of decellularization on the collagen content in the pericardium was quantitatively investigated and graphically presented in Figure 3.4. One milligram of native pericardium contained 132.02±6.91 µg of collagen, while decellularized pericardium contained 145.72±15.2 µg of collagen. Similarly, one square centimeter of native pericardium contained 332.73±63.6 µg/cm^2 of collagen, whereas decellularized pericardium exhibited 216.81±34.24 µg/cm^2 of collagen. It can be comment that the decellularization process did not damaged completely to the collagen content in the decellularized pericardium. The observed increase in total collagen amount in 1 mg of tissue with decellularization aligns with findings in similar studies in the literature. For instance, Wollmann et al., demonstrated that the collagen amount in native pericardium increased from 126.9 ± 45.8 µg/mg to 138.3 ± 58.6 µg/mg following decellularization [158]. This augmentation can be attributed to the removal of protein and cellular structures, resulting in a decrease in the dry weight of the pericardium and subsequently reducing the ratio of these structures to the total dry weight. Similarly, in the study by Zouhair et al., the rise in collagen amount is elucidated by the dominance of the variation in collagen due to the removal of cells [163]. In another study, collagen content elevated from 100.5 ± 43.82 to 121.9 ± 50.85 after decellularization, with the loss of cells and soluble proteins outweighing the reduction in collagen content in the pericardium [164]. Contrary to the observed increase in collagen content, literature studies indicate a decrease in collagen amount when the decellularization process damages the collagen. For instance, collagen content in native pericardium decreased from 170 µg/mg to 150 µg /mg due to decellularization [161]. It is concluded that these results obtained in this study are consistent with the trends observed in the literature.

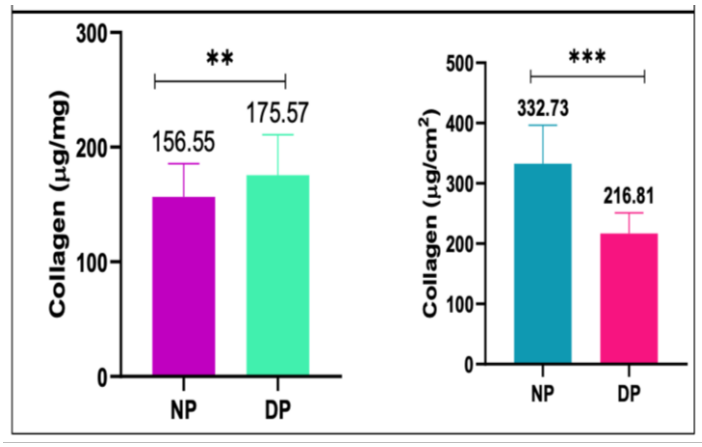

Figure 3.4 Graphical representation of the collagen content in native and decellularized pericardium, depicting values in µg/mg and µg/cm^2 (n=9). (p <0.01: **; p <0.001: ***; p <0.0001: **** considered significant).

3.1.1.4 Mechanical Characterizations of Pericardium

The impact of the decellularization process on the mechanical strength of the pericardium was investigated through a universal tensile test. According to the acquired data, the ultimate tensile strengths (UTS) of native and decellularized pericardium were 17.080±2.71 and 13.138±3.42 MPa, respectively. The native pericardium exhibited 21.46±2.84% elongation and a Young's Modulus of 3.049±0.87 MPa, whereas decellularized pericardium exhibited 20.489±1.65% elongation and a Young's Modulus of 2.84±1.12 MPa. Comparable findings are evident in the literature; for instance, the UTS of native pericardium decreased from 31.64 MPa to 26.11 MPa following decellularization with Triton X-100 [164]. In another study, pericardium decellularized with SDS/deoxycholic acid exhibited a decrease in Young's Modulus from 27 MPa to 12 MPa, along with a UTS of 7 MPa [165]. Additionally, both decellularized and native pericardium demonstrated very similar values, with a tensile strength of 4 MPa, an elastic modulus within the range of 20-30 MPa, and an elongation of 20% [158]. It is concluded that the obtained results align with the data reported in the existing literature.

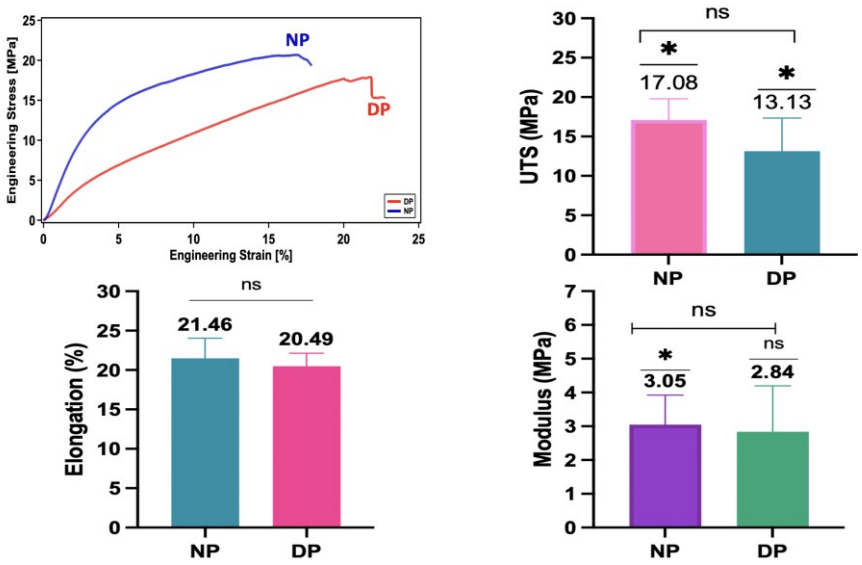

Figure 3.5 Mechanic test results of native (NP) and decellularized (DP) pericardium (ns: non-significant, p <0.05: *; significant).

3.1.1.5 Morphological Characterizations of Pericardium

The surface morphology of decellularized and native pericardium, as well as the impact of decellularization on extracellular matrix fibers, were investigated using SEM. Figures 4 depict the serosum and fibrosum layers of native and decellularized pericardium at 100X magnification. The acquired data elucidates that both native and decellularized pericardium exhibited comparable surface morphologies in both serous and fibrous layers. Microscopic analysis reveals the preservation of the smooth surface of the serosum layer following decellularization. Furthermore, the fibrous structure of the decellularized pericardium exhibited no discernible deformities or damages, and collagen elastin fibers of the ECM were distinctly observable in SEM images. Parallel SEM images portraying similar ECM fiber characteristics were documented in the study by Shchotkina et al [166]. In another study, the decellularization process induced the formation of 50 µm gaps between ECM fibers, underscoring its damaging effect [167]. In our study, it was concluded that decellularization process did not compromise the structural integrity of ECM.

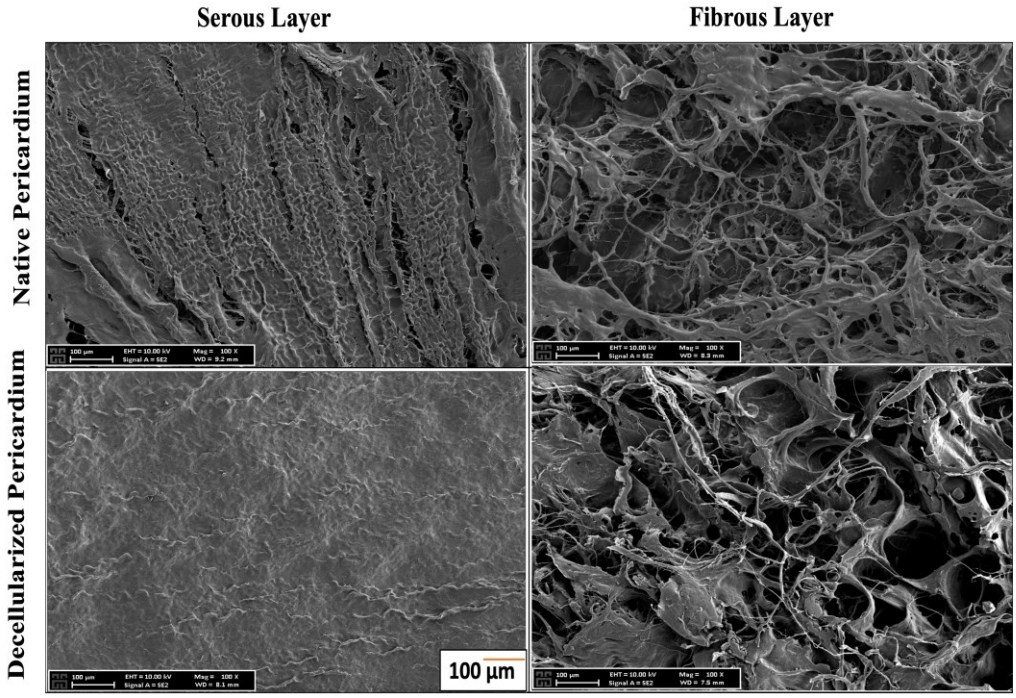

Figure 3.6 SEM images of the Serosum and Fibrosum layers of native and decellularized pericardium at 100X magnification.

3.1.2 Synthesis and Characterizations of PANI Nanoparticles

The polyaniline (PANI) nanoparticles were synthesized as ink form through oxidative polymerization [168]. This process involves the transformation of the emeraldine-base to emeraldine-salt form of aniline, which is conductive and exhibits a dark-green colour [169]. The particle-size of the PANI were examined through dynamic light scattering spectrometry (DLS), was measured as 104.94 ±13.7 nm (Figure 3.6A). In the literature, the particle size of PANI was reported as 82 nm, and it was indicated that particle size can vary within a range of 65 nm to 1000 nm with an increase in the amount of APS in the reaction medium. Additionally, it was reported that an elevated DBSA ratio stabilizes the reaction, preventing excessive growth of polymer chains and consequently leading to a reduction in particle size [168]. In another study, the incorporation of SDS as a surfactant in the reaction medium during PANI synthesis resulted in a noteworthy decrease in particle size from 713 nm to 212 nm [170]. The characteristic FTIR peaks of PANI was investigated, and revealed the characteristic peaks at 3344, 2969,2923, 2872, 1563,1454, 1044, 878 and 600-700 cm^{-1}. The peak at 3344 cm^{-1} is corresponds to the vibration of N-H bonds in the emeraldine, the peaks in the range of 2800-2900 cm^{-1} are

associated with aliphatic -CH_2 or -CH_3 stretching vibrational bonds. The peaks between 1563-1462 cm^{-1} represents the C=C bonds of the quinoid and benzenoid rings of the emeraldine. Additionally, the peak at around 800 cm^{-1} corresponds to C-H transplantations of 1,4-disubstituted aromatic rings [171]. A notable peak at 1044 cm^{-1} indicates successfully bonding through hydrogen bonding between $NH4^{+1}$ in the PANI structure and the SO^{-3} functional groups of DBSA. Furthermore, the presence of a peak at around 1100 cm^{-1} indicates the formation of an oxidized PANI block structure [172]. It can be concluded that the synthesized PANI nanoparticles size and chemicals structure are consistent with data reported in the literature.

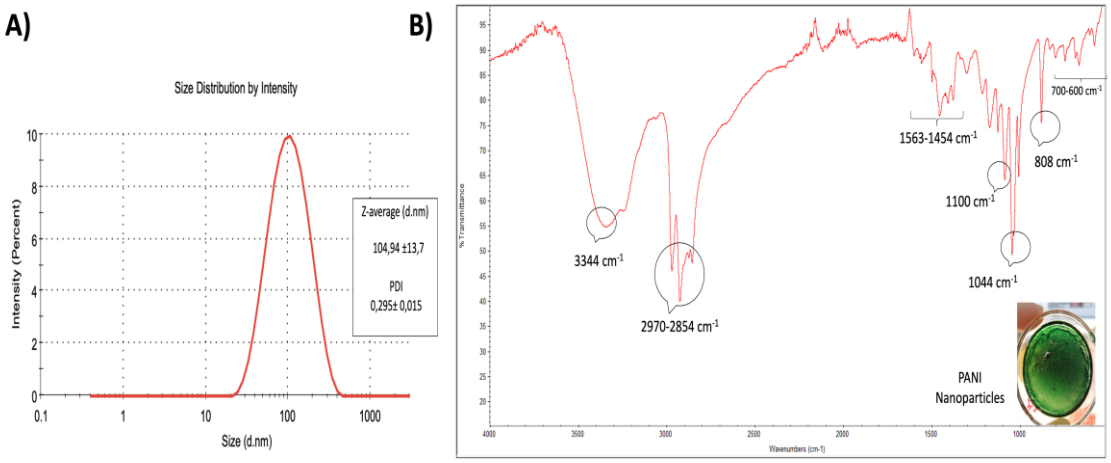

Figure 3.7 A) The average particle size of PANI nanoparticles through DLS analysis, B) FTIR spectrum of PANI nanoparticles.

3.1.3 PANI Coating of Decellularized Pericardium

The serosum surface of the decellularized pericardium was coated with PANI nanoparticle ink solution through a printing method as parallel lines to impart electrical conductivity to the pericardium. These parallel patterns can be change depending on the purpose of use and design of scaffolds. The PANI-coated pericardium serves as the first layer of final bilayered cardiac patch, and its SEM images were depicted in Figure 3.8.

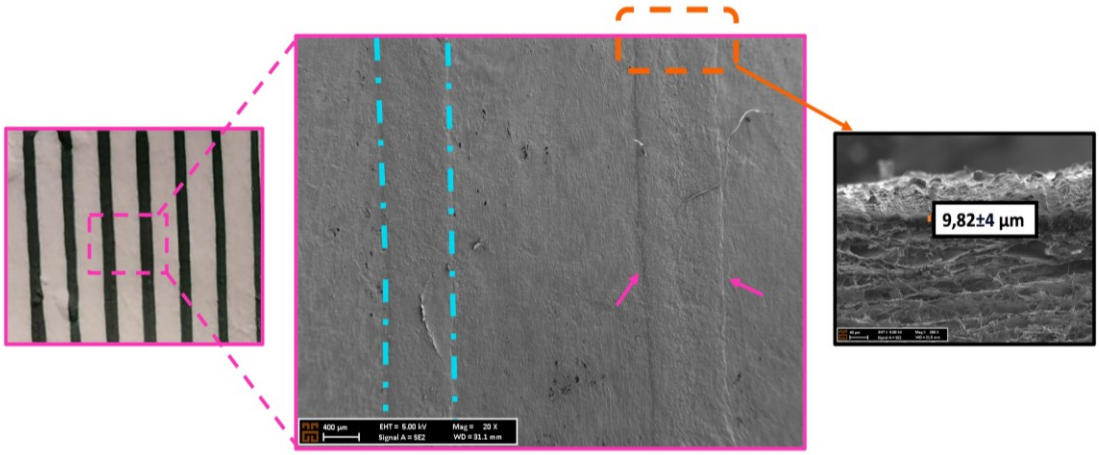

Figure 3.8 SEM microscope image of PANI-coated pericardium surface section and cross-sections.

The PANI-coated decellularized pericardium was subsequently crosslinked with genipin to stabilize PANI pattern on pericardium, and crosslinking was confirmed by FTIR analysis in Figure 3.9. A reduction in the intensity of the N-H bond vibration peak at around the 3300 cm^{-1} was observed after-crosslinking with genipin. Additionally, a decrease was noted in the peaks within the 2800-2900 cm^{-1} range, attributed to aliphatic -CH_2 or -CH_3 bonds stretching vibrations [172]. This decline in peaks is rationalized by the binding mechanism of genipin with amine (N-H) groups in both pericardium and PANI [173]. In the literature, genipin is favoured as a crosslinker due to its significantly lower toxicity, being at least 100 times less toxic than alternative crosslinkers [173], it was used to crosslink several materials such as pericardium, gelatin, collagen, and chitosan [168]. Therefore, we preferred to use genipin as a crosslinker agent without toxicity.

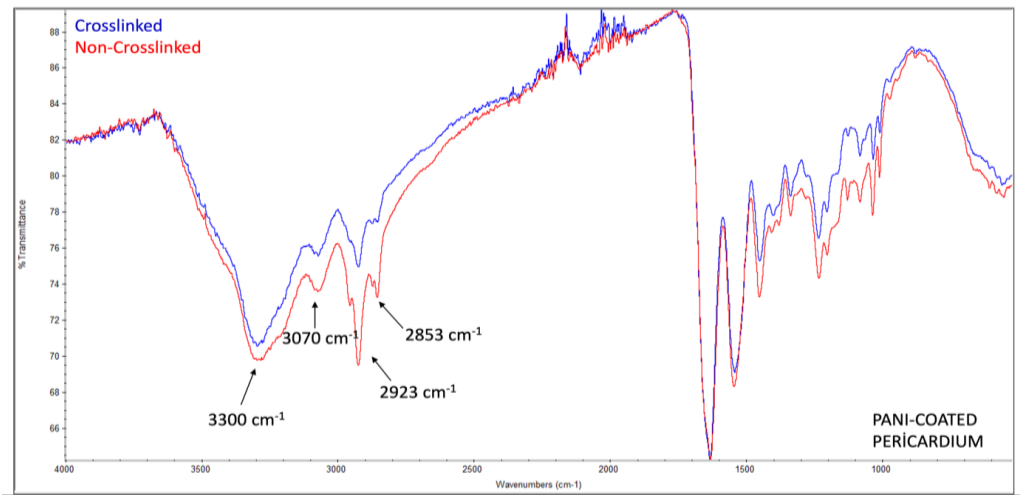

Figure 3.9 FTIR spectrum of PANI-coated pericardium before and after crosslinking with genipin.

The PANI-coated decellularized pericardium conductivity was determined using the 4-point probe technique [168], an average conductivity of 9.093±8.6x10^{-4} S/cm was achieved. The native myocardium conductivity is approximately 10^{-4} S/cm, the first layer of cardiac patch conductivity's matched with it [174]. Comparatively, literature reports indicate a range of electrical conductivity for PANI film layers, spanning from 8x10^{-4} S/cm to 324x10^{-4} S/cm [145]. In a study, a PANI film layer, when combined with PGS polymer, exhibited a conductivity of 0.018 S/cm. Additionally, another investigation reported a conductivity value of 10x10^{-4} S/cm for a PANI film layer [121]. As a conclusion, the obtained conductivity is suitable with native myocardium, therefore this PANI-coated decellularized pericardium can be used as a first layer of bilayered cardiac patch.

The preparation and characterization the first layer of the cardiac patch covered the first part of the thesis. Firstly, the decellularization process was optimized for completely decellularization of pericardium. Then, the success of decellularization was scrutinized by quantitative, histologic, morphologic and mechanic techniques. The targeted decellularization efficiency has been achieved. The PANI nanoparticles were synthesized and characterized chemically by FTIR. The PANI nanoparticle size was determined as 104.94±13.7 nm by DLS. In the last part, decellularized pericardium surface was coated with PANI nanoparticles by ink-printing method in order to complete first layer of cardiac patch. The first layer conductivity was measured as 9x10^{-4} S/cm by four-point probe method. The native myocardium has the conductivity level of 10^{-4} S/cm, therefore the first layer' conductivity ensures the myocardium conductivity.

3.2 Second Layer of Cardiac Patch

3.2.1 Characterization of the Hawthorn Extract

Hawthorn extract was obtained through Soxhlet extraction technique and subjected to characterization through FTIR and GC-MS. Hawthorn is known to predominantly contain phenolic and organic acids, flavonoids, terpenoids and sugar [175]. The phytochemicals such as quinic acid, furfural, 5-hydroxymethylfurfural, triethyl boron, galactitol and 2,3-dihydro-3,5-dihydroxy-6-methyl-4H-pyran-4 was identified in GC-MS spectra as represented in Figure 3.10. These phytochemicals were confirmed by

comparisons with existing literature [175, 176]. Quinic acid, a significant organic acid, and galactitol, a component of fruit sugars, were notably present in hawthorn [175]. Pyran derivatives, identified as monoterpene components, and furan compound derivatives, known for inhibiting blood platelet aggregation [176, 177]. Moreover, the hydroxymethylfurfural was identified in the hawthorn extract, acknowledged for its antiplatelet and anticoagulant properties in the literature [177, 178].

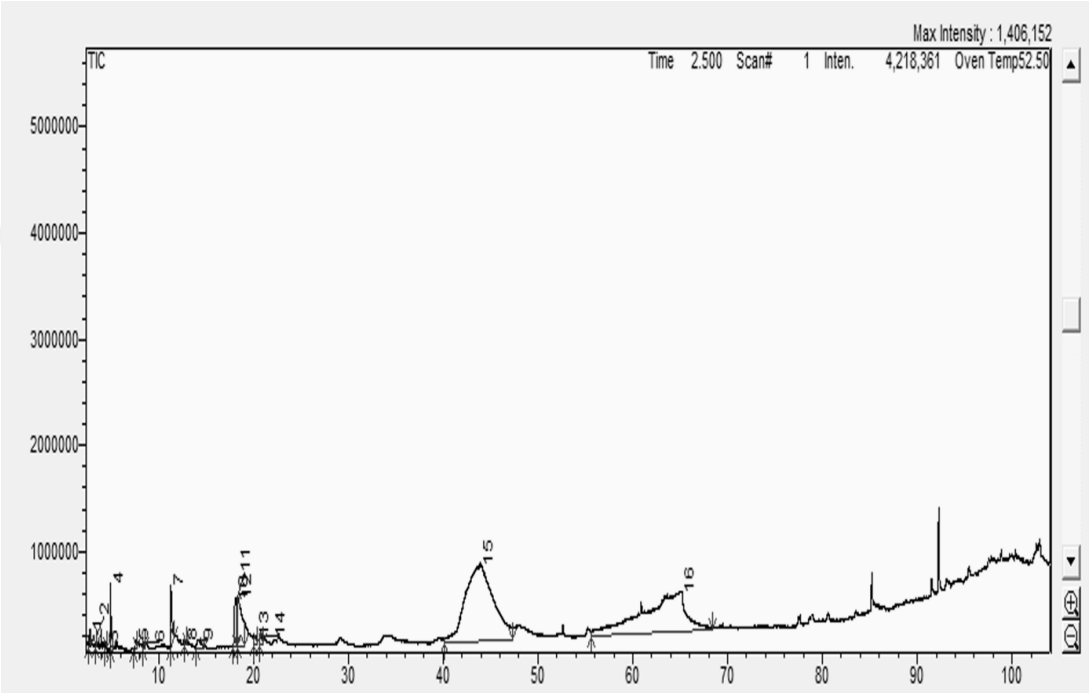

Peak#	Ret.Time	Start Tm	End Tm	m/z	Area	Area%	Height	Height%	A/H	Mark	Name
1	2.695	2.655	2.820	TIC	525204	0.17	147394	3.37	3.56		Acetic acid (CAS)
2	3.445	3.410	3.495	TIC	292271	0.09	106369	2.43	2.75	V	Glycerin
3	4.396	4.355	4.550	TIC	266853	0.09	56182	1.28	4.75		(2H) - furan - 3 - one
4	4.957	4.880	5.155	TIC	3339462	1.07	622523	14.22	5.36	V	2-Furancarboxaldehyde (CAS)
5	7.655	7.400	7.690	TIC	696629	0.22	80367	1.84	8.67	V	2(3H)-Furanone, 5-methyl- (CAS)
6	8.360	8.305	8.550	TIC	619038	0.20	56802	1.29	10.94	V	2,4-Dihydroxy-2,5-dimethyl-3(2H)-furan-3-one
7	11.306	11.225	11.695	TIC	6252404	2.00	560998	12.81	11.15		Borane, triethyl- (CAS)
8	12.791	12.770	13.010	TIC	330420	0.11	36150	0.83	9.14	V	Maltol
9	14.198	13.910	14.755	TIC	2484617	0.79	80708	1.84	30.79		4H-Pyran-4-one, 2,3-dihydro-3,5-dihydroxy-6-methyl-
10	18.097	17.895	18.185	TIC	5696557	1.82	441568	10.08	12.90	V	5-Hydroxymethylfurfural
11	18.347	18.295	18.385	TIC	2468528	0.79	470802	10.75	5.24	V	5-Hydroxymethyl-2-furaldehyde
12	18.405	18.385	19.025	TIC	12718188	4.06	453130	10.35	28.07	V	2-Furancarboxaldehyde, 5-(hydroxymethyl)- (CAS)
13	20.250	20.065	20.465	TIC	1608367	0.51	89870	2.05	17.90	V	5-(Hydroxymethyl)-2-(dimethoxymethyl)furan
14	20.856	20.695	20.985	TIC	1132834	0.36	76722	1.75	14.77	V	2-Methoxy-4-vinylphenol
15	43.968	40.125	47.335	TIC	149570053	47.73	726026	16.59	206.01	V	Quinic acid
16	65.092	55.630	68.380	TIC	125295743	39.99	373215	8.52	335.72	V	Galactitol

Figure 3.10 GC-MS spectrum of hawthorn extract.

The characteristic FTIR peaks of hawthorn were revealed at 3301, 2929, 1716, 1405, 1344, 1231 and 1027 cm^{-1} as represented in Figure 3.11. The peak at around 3300 cm^{-1} corresponds to the –OH groups of phenolic compounds within the extract, while the peak at 2929 cm^{-1} corresponds to the C–H stretching vibrations. Peaks within the range of 1700-1400 cm^{-1} are associated with aromatic vibrations of C=C. The aimed phytochemicals and characteristic FTIR peaks were achieved hawthorn extract, the findings are consistent with literature findings [180].

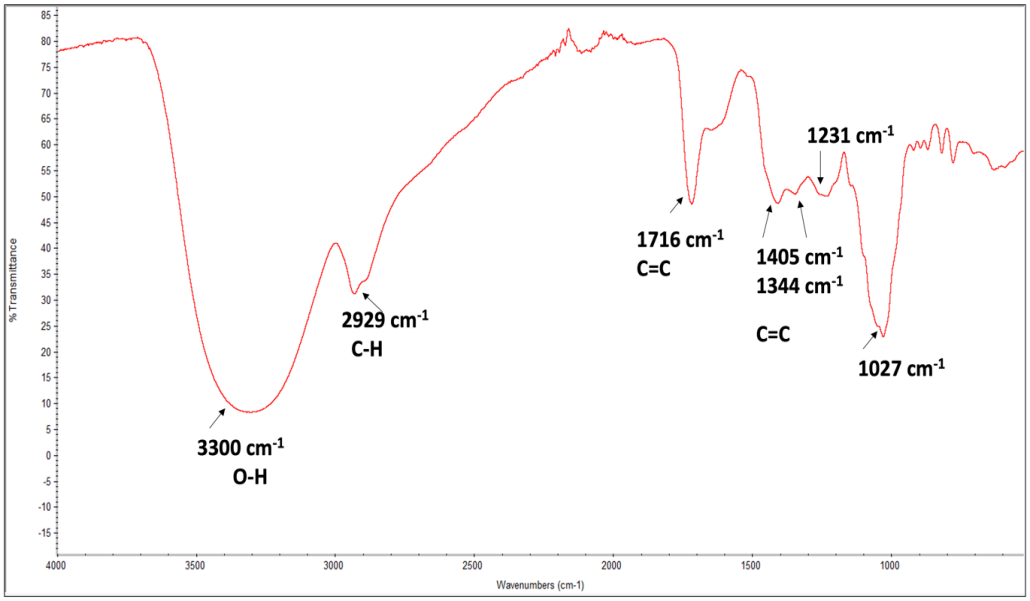

Figure 3.11 FTIR spectrum of hawthorn extract.

3.2.2 Fabrication and Characterization of Electrospun Membranes

Hawthorn and VEGF containing PLGA/gelatin (%15, w/v, with the ratio 9:1 (w/w)) membranes were fabricated via electrospinning, and membranes were labelled as outlined in Table 3.1. The neat PLGA/gelatin membrane was denoted as AY1, while hawthorn extract-containing membranes with the concentration of 1, 5, 10 and 15 wt.% (w/v) were labelled as AY2, AY3, AY4 and AY5, respectively. The concentration of 10 wt.% (w/v) hawthorn extract was selected as the optimum concentration and incorporated into the VEGF-containing membranes. VEGF at concentrations of 0.1 µg/ml, 0.5 µg/ml and 1 µg/ml was added to15 wt.% (w/v) PLGA/gelatin and 10 wt.% (w/v) hawthorn solution, resulting membranes labelled as AY6, AY7 and AY8, respectively.

Tablo 3.1 The combination and nomenclature of electrospun membranes

Sample	PLGA/gelatin (9:1) (%, w/v)	Hawthorn Extract Concentration (%, w/v)	VEGF Content (µg/ml)
AY1	15	-	-
AY2	15	1	-
AY3	15	5	-
AY4	15	10	-
AY5	15	15	-
AY6	15	10	0.1
AY7	15	10	0.5
AY8	15	10	1

3.2.2.1 Morphological Characterization of Membranes

The fiber morphology and pore structure of the fabricated electrospun membranes was examined through by SEM (Figure 3.12). The SEM images revealed that the membranes comprised uninterrupted, uniformly dispersed and bead-free fibers. Notably, AY3 and AY4 membranes, containing 5% and 10% hawthorn extract, exhibited more homogenous fiber structures. This enhanced homogeneity can be attributed to the synergistic effect of the hawthorn extract in conjunction with PLGA/gelatin polymers.

The average fiber diameters and pore sizes of membranes were determined using Image J program, the results are presented in Figures 3.12. The fiber diameters were measured as 1176.61± 860 nm, 855.11± 645 nm, 685.88± 377 nm, 935.71± 842 nm, 1197.85± 877 nm, 930.85±550 nm, 902.72±460 nm and 890.91±518 nm for AY1 to AY8, respectively. The neat PLGA/gelatin membrane (AY1) exhibited fibers with a diameter around 1 micrometer. A decrease in fiber diameters was observed with the addition of 1%, 5%, and 10% hawthorn extract, attributed to the extract reducing the viscosity of the PLGA/gelatin polymer solution. However, the membrane containing 15% extract showed an increase in fiber diameter, reaching 1197 nm. The addition of VEGF did not significantly alter the mean fiber diameters, which remained approximately 900 nm. Comparing with the literature data, the fiber diameters of PLGA/gelatin membranes typically fall between 1000-1200 nm [181]. For instance, PLGA/gelatin demonstrated a

fiber diameter of approximately 1085 nm [182]. When plant extract like *Hypercium* was added in PLGA/gelatin, the fiber diameter decreased from 1.83±1.02 µm to 0.49 ± 0.2 µm due to the decrease in viscosity of solution [183]. In another study, when *Aloe vera* extract was added to PLGA, fiber diameters decreased from 561 nm to 486 nm [184]. In conclusion, polymer concentration, conductivity, solution viscosity, polarity, surface tension and density of net charges in solution are main parameter that can affect the membranes fiber structure in electrospinning technique [185]. The average pore sizes of membranes were measured as 14.43±8.5 µm, 16.7±12.5 µm, 16.9±10.1 µm, 19.2±11.4 µm, 16.5±10.9 µm, 20.86 ±7.4 µm, 19.24±4.3 µm, and 20.002±5.4 µm for AY1 to AY8 respectively. The neat membrane had smaller pore size, while the addition of hawthorn extract and VEGF enlarged the pores up to 20 µm. This consistent with findings in Hu et al.'s study, where an average pore size of 17 µm was reported in PLGA membrane [182]. The scaffold's morphology and por structure have important impact on the controlled release of bioactive molecules and degradation of polymeric fibers [45]. Therefore, we preferred to electrospinning technique to fabricate biodegradable polymeric layer, the obtained SEM results suggested that the hawthorn and VEGF containing membranes are good candidate for cardiac patch applications.

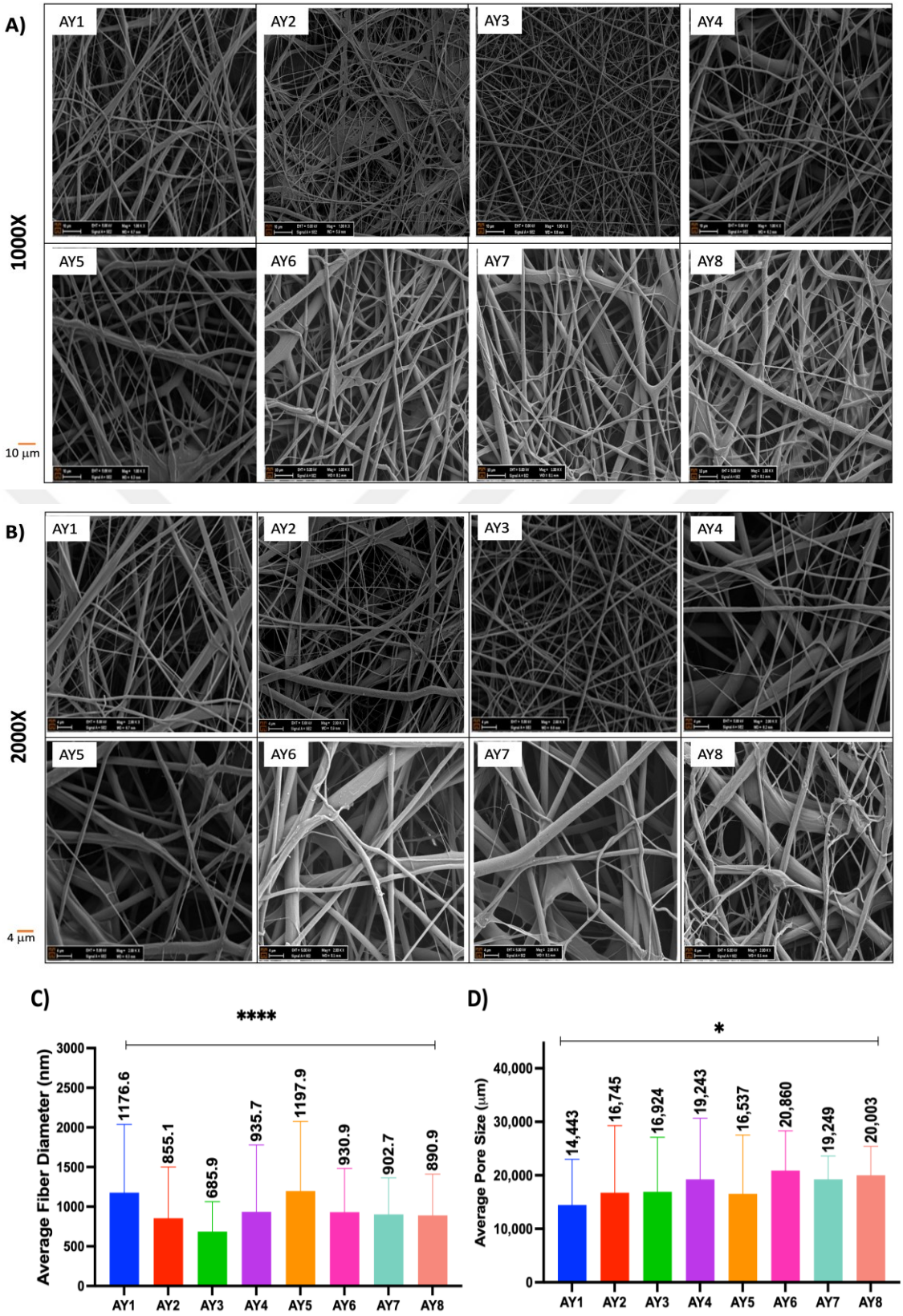

Figure 3.12 SEM images of electrospun membranes with A) 1000X magnification, and B) 2000X magnification. C) Graphically representations of the average fiber diameters membranes, and D) pore sizes of membranes (n=100, $p < 0.05$: *; $p < 0.0001$: ****).

3.2.2.2 Chemical Characterization of Membranes

The incorporation of hawthorn extract and VEGF into PLGA/gelatin membranes were scrutinized through FTIR analysis, as depicted in Figure 3.13. The FTIR spectrum revealed characteristic peaks corresponding to PLGA and gelatin components. Specifically, the peaks include C-O, C-O-C and C-H stretching peaks at 1129-1752 cm^{-1}, 1752 cm^{-1} and 1182 cm^{-1}, respectively. The presence of gelatin was affirmed by peaks at 1646 cm^{-1} and 1540 cm^{-1}, originating from the amide structure [186]. Upon the addition of hawthorn extract to the membranes, a peak density increased at 3301 cm^{-1} proportionally with the amount of extract increased due to the intermolecular hydrogen bond interactions of the phenolic and flavonoid components present in the hawthorn extract [143, 147, 148]. The chemical structure of AY6, AY7, and AY8 membranes containing hawthorn extract and VEGF was examined, an increase in peak intensity around the 3301 cm^{-1} wavelength was observed with the increase in the amount of VEGF in the membrane. This increase is due to the N-H stretching of the amino groups present in the structure of growth factors [187]. This finding indicates that VEGF has successfully incorporated into the membrane, and an increase in the amount of VEGF within the membrane results in an increase in peak intensity. The FTIR spectrum confirm the successful incorporation of hawthorn extract and VEGF into the PLGA/gelatin membranes, validating the FTIR analysis.

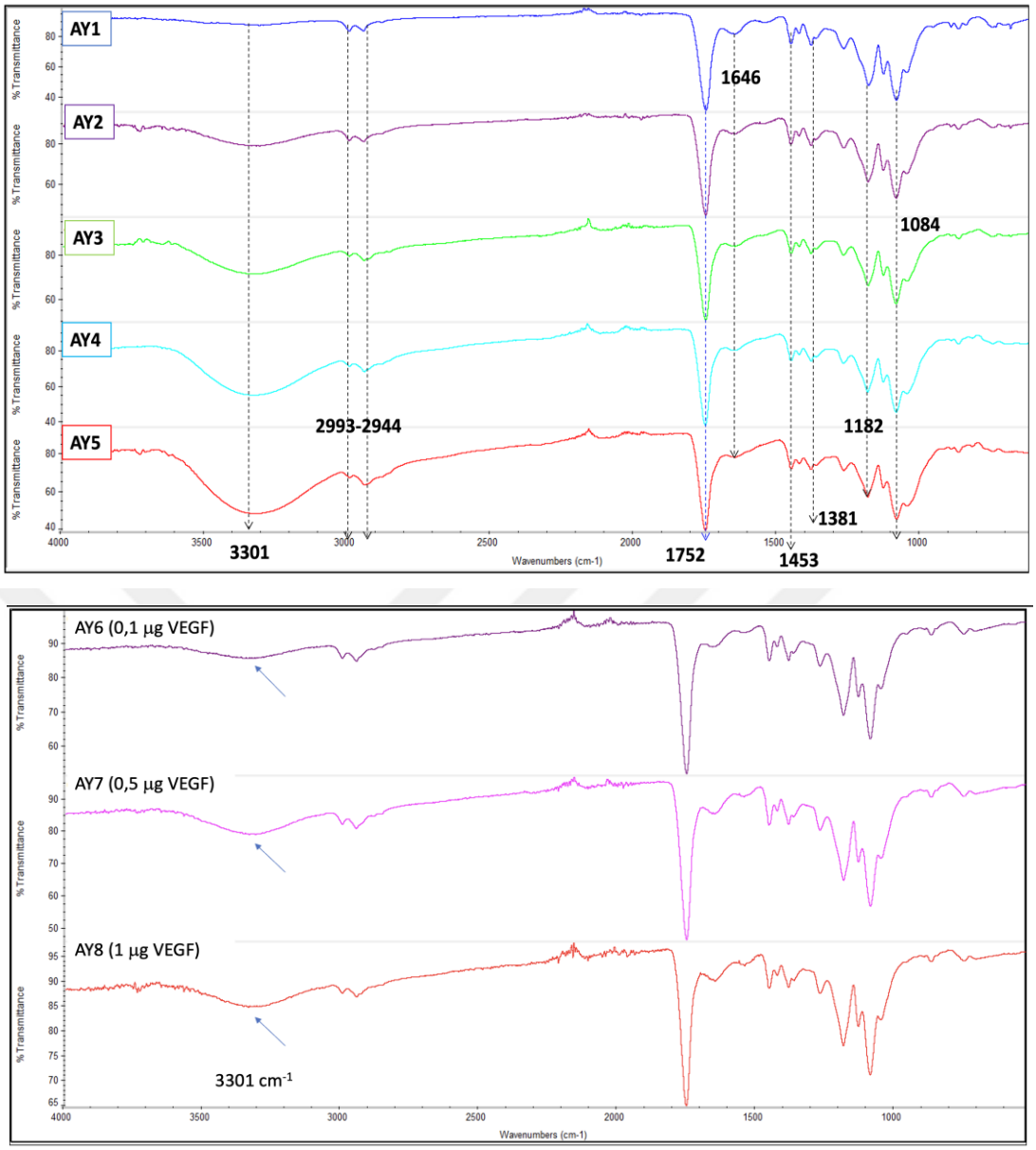

Figure 3.13 FTIR spectrum of membranes.

3.2.2.3 Physical Characterizations of Membranes

The wettability and hydrophilic properties of the membranes were assessed through Sesile Drop-Contact Angle analysis, and results are illustrated in Figure 3.14. The contact angle of the PLGA/gelatin membrane was recorded as 109.58º. In contrast, the contact angle values of the hawthorn extract-containing membranes decreased significantly with the increasing extract concentration, measuring 71.82º, 53.91º, 39.79º and 27.01º, for AY2-AY5, respectively. Similarly, VEGF-containing membranes exhibited contact angle values of 39.11º, 37.765º, and 34.525º for AY6-AY8, respectively. The reduction in contact angle values increasing hawthorn extract content indicates a substantial

improvement in the hydrophilic and wettability properties of the PLGA/gelatin membrane. This effect can be attributed to the hydrophilic side groups present in the phenolic compounds in hawthorn extract, a characteristic supported by the presence of N-H and O-H in the FTIR spectrum of membranes containing hawthorn extract. Comparing with the literature, similar trends were observed. In studies where *Ajwa-Dates* or *Hypercium* extracts were added to membranes, a decrease in contact angle was reported, indicating enhanced hydrophilicity [182, 187]. Additionally, the addition of VEGF was found to further increase the hydrophilicity of the membranes from 39.79º to 34.525º. In the literature, a study by Kai et al., reported changes in contact angles from 35.2±2.7° to 21.7±1.3° and 31.4±2.5° values when 10 mg VEGF was loaded in the electrospun PCL/gelatin membrane, suggesting that VEGF has the potential to increase membrane hydrophilicity [189]. Additionally, it has been reported in the literature that the addition of heparin and VEGF to the electrospun PCL membrane increases hydrophilicity due to the presence of hydrophilic proteins [190]. Another study reported in the literature stated that the addition of growth factors to the electrospun PVA membrane leads to an increase in membrane hydrophilicity [187]. Evaluating these finding, it can be concluded that the obtained results in our study are consistent with the literature data's.

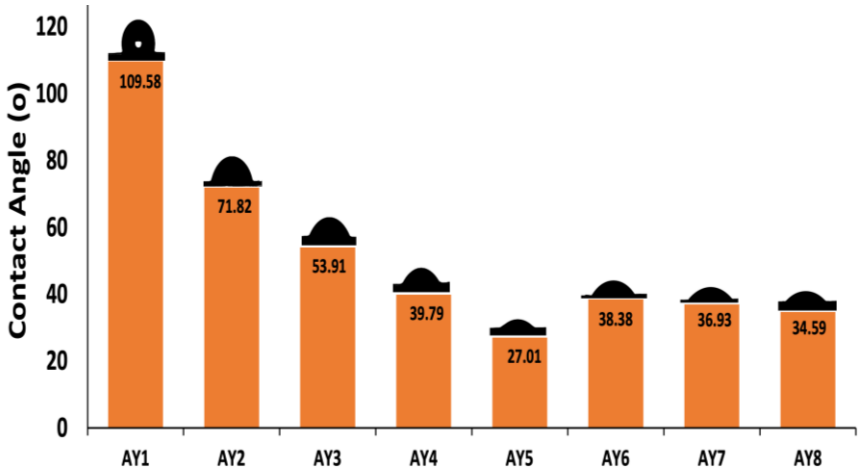

Figure 3.14 Contact angle values of the membranes.

The *in vitro* weight loss behavior of the membranes was assessed over a 4-week period in PBS, and the results are graphically depicted in Figure 3.15. The neat PLGA/gelatin membrane (AY1) exhibited a weight loss of approximately 14.6±1.41% over 28 days. In contrast, the membranes containing hawthorn extract (AY2, AY3, AY4

and AY5) displayed increasing weight loss, with values of %26.99±2.8, %38.47 ±1.27, %44.38±2.03, and %49.6 ±1.62, respectively, within the same frame. Similarly, VEGF-containing membranes (AY6, AY7 and AY8) demonstrated weight loss of %39.67±0.17, %38.28±0.1, and %40.37±2.7 over 28 days. These results align with observations from studies in the literature, where membranes containing extracts or bioactive compounds showed greater weight loss compared to neat membranes. For instance, a PLGA membrane exhibited a weight loss of 13% in 1 week, while the extract-containing membrane showed a higher weight loss of 30% [183]. Additionally, membranes containing green tea extract demonstrated greater weight loss than neat membrane [191]. Therefore, the weight loss behaviours observed in the electrospun membranes containing extract in this study are consistent with the existing literature data.

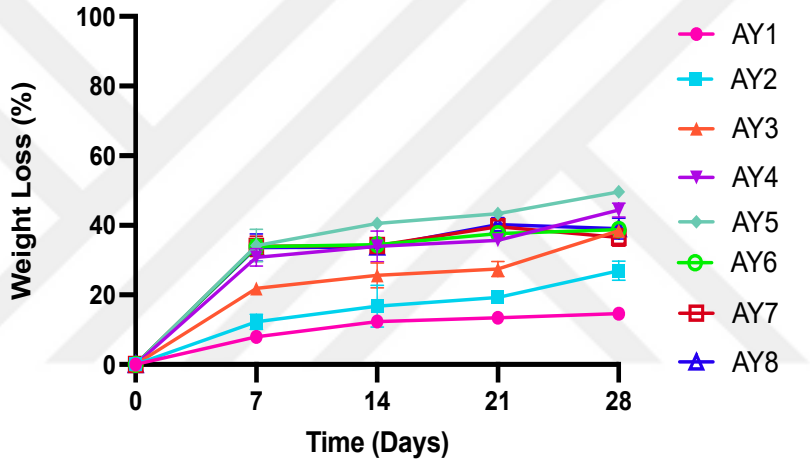

Figure 3.15 The weight loss (%) studies of membranes.

3.2.2.4 Controlled Release Profiles of Membranes

The release profiles of hawthorn extract and VEGF from the membranes were examined over a 28-day period, and the results are presented graphically in Figure 3.16. For hawthorn extract, membranes AY2, AY3, AY4 and AY5 exhibited initial releases of 70.8% ± 1.5%, 79.44 ±1.2%, 86.6% ±6.4, and 88.6±4.4%, respectively, in the first week. This initial burst release effect is a common phenomenon in the first week [183]. Subsequently, the release of hawthorn extract from AY2, AY3, AY4 and AY5 reached %92±0.6, 94.4±1.38%, 98.9±0.3%, and 95.6±4.1% within the third week, respectively. The data suggest that the entire hawthorn extract was released from membranes within 4 weeks. In comparison, a membrane containing green tea extract released 60% of the extract in the first 10 days [191]. Another study reported the release of approximately

89% of a drug in the first 168 hours [192], while another study on curcumin extract observed 40% release within the first hours and 85% release by the end of the 10th day [193]. For VEGF, membranes AY6, AY7 and AY8 exhibited release of 74%, 76%, and 68% within the first 6 hours, respectively. By the end of 7 days, VEGF release reached up to 85%, continuing to release up to 90% in the second week. Almost all of the VEGF was released within 3-4 weeks. In literature studies, VEGF release from electrospun membranes was reported to be completed within 28 days [194]. Other studies reported 55-70% VEGF release on the first day, with 60% and 90% release rates reached within 28 days [195]. In another study, around 70% of VEGF was released within the first 24 hours, and 90% was released within 120 hours [196]. PLGA/gelatin membrane containing VEGF showed a release behavior of around 90% within 25 days [197], and in another study VEGF release reached 72% at 168 hours [198]. It can be concluded that the release behavior of VEGF and Hawthorn extract from the membranes are suitable for cardiac patch applications since the most of them released between 2 to 4 weeks. In the literature, generally release behaviour investigates for 4 weeks period, it may be an optimum time for myocardium repair because most *in vivo* studies focus on 4 weeks implantation of cardiac patches [198, 199].

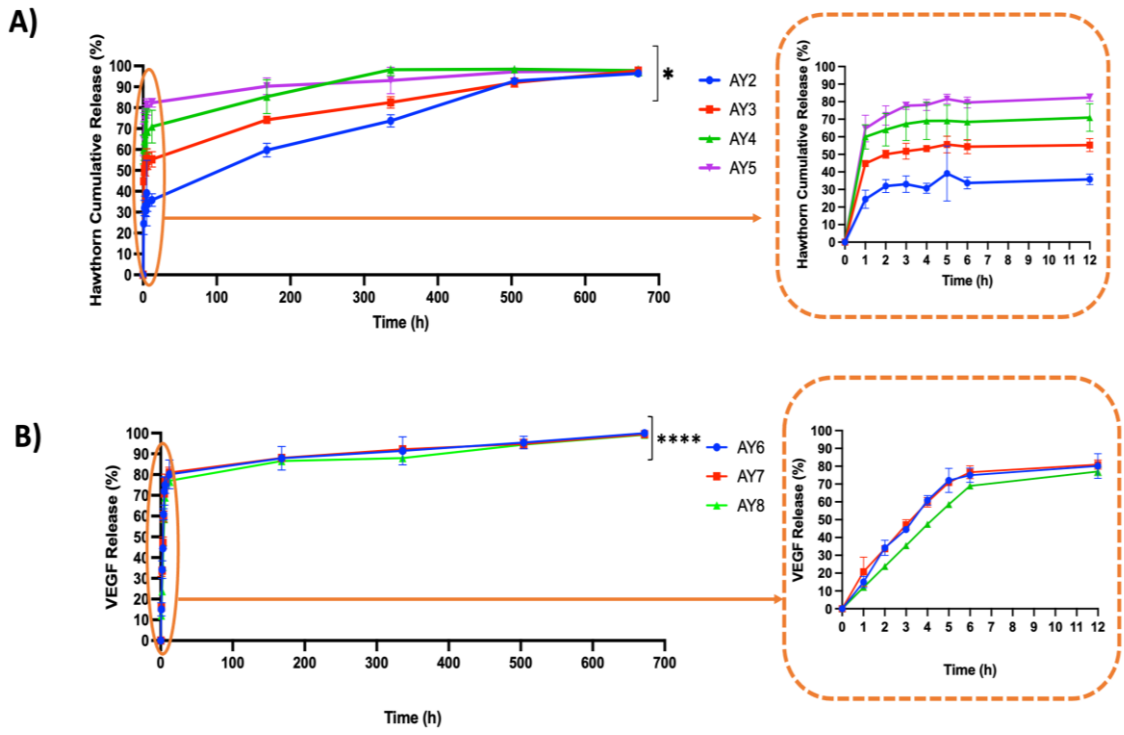

Figure 3.16 A) Cumulative Release (%) behaviour of hawthorn extract from membranes ($p < 0.05$: *). B) Cumulative Release (%) behaviour of VEGF from membranes ($p < 0.0001$: ****).

3.2.2.5 *In vitro* Anti-coagulant Efficacy of Membranes

The *in vitro* anti-coagulant properties of the membranes were assessed through activated partial thromboplastin time (APTT), as illustrated in Figure 3.17. The study included the following groups: the blank group, a group containing 0.5 IU/ml Heparin, and membrane groups labelled as AY1, AY2, AY3, AY4, and AY5. The coagulation times for these groups were recorded as 43.3±2.5 seconds, 114.33±20.2 seconds, 45±4.35 seconds, 97.33±8.02, 168±29.10, 331±65.1, and 425±9.53 seconds, respectively. In a study, the APTT test revealed that the addition of 4 mg/ml of hawthorn extract extended the coagulation time to 104.0±5.2. Notably, it was shown that the coagulation time was longer than heparin with the purification of the components in the hawthorn extract [200]. Literature reports highlighted the efficiency of hawthorn extract in preventing platelets in rabbits [177], and inhibiting platelet functions in Wistar albino rats even at low doses [134]. The study also suggested that polyphenol-polysaccharide structures within hawthorn extract could protract coagulation times, even at minimal concentrations such as 31.25 µg/ml [175]. This effect is attributed to the interaction of functional groups in hawthorn extract with antithrombin, preventing thrombin accumulation. A study supporting this hypothesis revealed that heparin, with functional groups like -SO3, -COO, -NHSO3 and -OH, exhibited anti-coagulant effects [201]. In conclusion, membranes containing hawthorn extract demonstrated anticoagulant properties as evidenced by APTT results, aligning with findings reported in the literature.

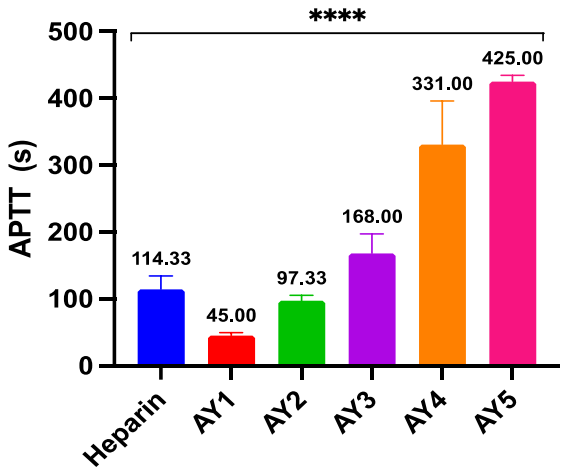

Figure 3.17 Graphical representation of APTT times of hawthorn containing membranes ($p < 0.0001$: ****).

3.2.2.6 VEGF Bioactivity

The VEGF is already known as a protein having ability to improve the angiogenesis, in the literature reports [126, 194, 195, 202, 203]. Therefore, herein we just investigated the bioactivity of VEGF in the membranes to avoid just in case the electrospinning negative effect to VEGF. The commercial VEGF Bioassay kit's results were represented in Figure 3.18. Luminescent values obtained were 117,063.33 RLU for AY6, 129,942.0 RLU for AY7, 139,646.0 RLU for AY8, and the 367.86 RLU for blank. VEGF-containing membranes significantly increased the luminescence signal, reaching levels at least 300 times higher than the blank group. This indicates the bioactivity of VEGF within the entire membranes. Moreover, an escalation in the amount of VEGF in the membranes correlated with an increase in luminescence signals. Comparing these results with literature data, where a 10 ng/ml VEGF-containing sample demonstrated approximately 100,000 RLU and a 100 ng/ml VEGF-containing sample demonstrated approximately 300,000 RLU [204]. In another study, an 18 ng/ml VEGF sample produced a luminescence signal of 60,000 RLU [205]. Thus, it can be inferred that the bioactivity of VEGF in the membranes is compatible with findings reported in the literature.

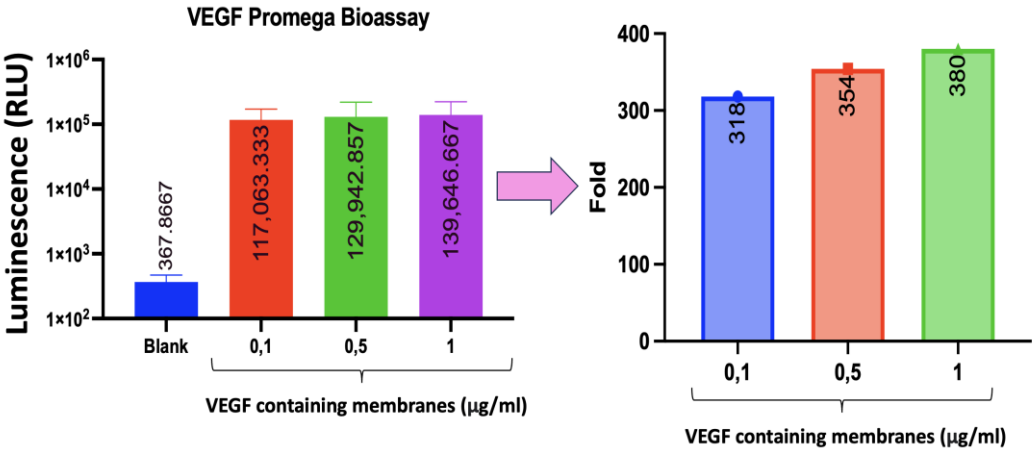

Figure 3.18 VEGF Bioactivity Assay of VEGF containing membranes (AY6, AY7, and AY8) with Luminescence (RLU) values and Fold values.

3.3 Preperation and Characterizations of the Final Bilayered Cardiac Patch

The integration of the first layer, derived from decellularized bovine pericardium and coated with PANI nanoparticles, with the second layer, a 15% (w/v) PLGA/gelatin electrospun membrane containing VEGF (1 µg/ml) and 10% (w/v) hawthorn extract, was achieved through a tissue glue. SEM analysis, as depicted in Figure 3.19, revealed the successful integration of two layers without morphological damage and discernible gaps between them. This conclusive SEM evidence attests to the seamless integration of the bilayered cardiac patch. Similar SEM images in the literature showcase the integration of bilayered scaffold structures, such as porous silk fibroin combined with electrospun silk fibroin layers [206] and -N-(2-Hydroxypropyl) meth acrylamide cryogel paired with an electrospun poly(4-vinylpyridine) membrane [207]. Additionally, comparable SEM images highlighted the successful integration of porous chitosan layer containing nano hydroxyapatite particles with electrospun POSS layer containing Zein protein [208]. Drawing parallels from these established scaffold integrations in the literature, the SEM images affirm the successful integration of the two layers in cardiac patch.

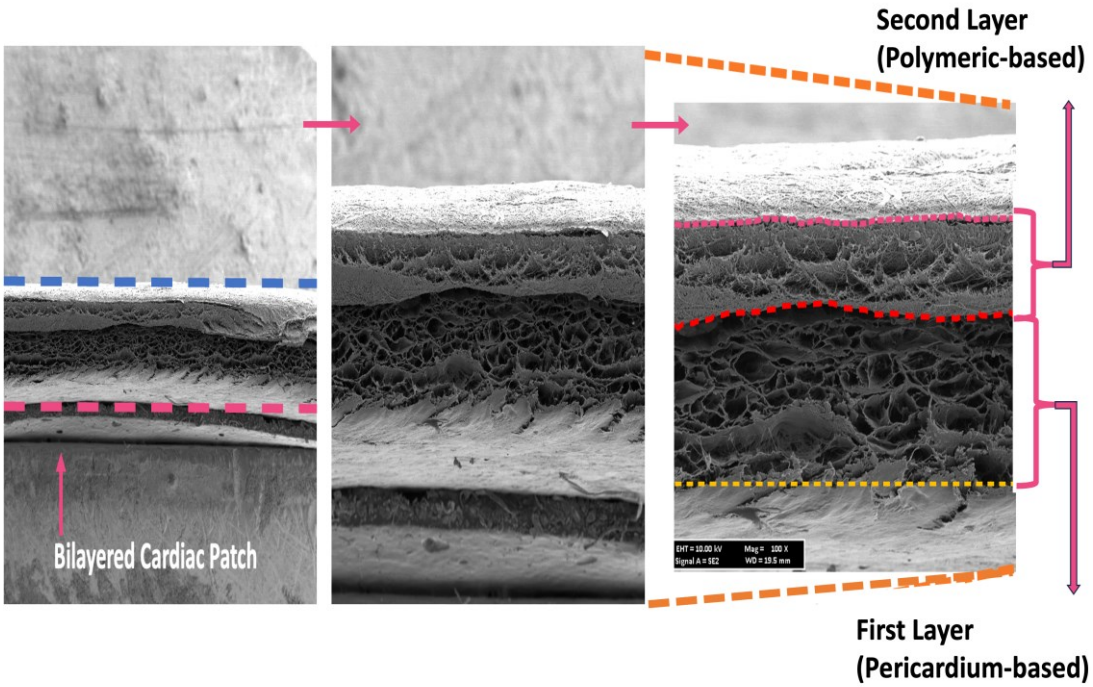

Figure 3.19 Cross-sectional SEM images of integrated final bilayered cardiac patch.

The adhesive strength of the bilayered cardiac patch was meticulously assessed through Lap-Shear test. The cardiac patch exhibited notable mechanical properties, showcasing a maximum tensile strength of 533±70 kPa, an elongation of 16.62±5.07%, and a Young's Modulus of 466±210 kPa. Comparative insights from the literature reveal Lap-Shear test results ranging between 11.76 kPa and 22.26 kPa [209]. Moreover, another study reported adhesion strength values spanning from 21 kPa to 220.20 kPa, attributing the increase in adhesion strength to heightened covalent bonding between the polymer and the tissue [210]. In another study, adhesion modulus values were examined for heart, lung, liver, and intestinal tissues. The intestinal tissue had an adhesion modulus of approximately 724 kPa, while heart tissue showed an adhesion modulus of 296 kPa, liver tissue 431 kPa and lung tissue 72 kPa. It is explained that the increase in the adhesion modulus obtained in different tissues is due to the difference in the amount of aldehyde groups in the tissues [211]. In conclusion, the adhesion strength exhibited by the cardiac patch align with reported data in the literature.

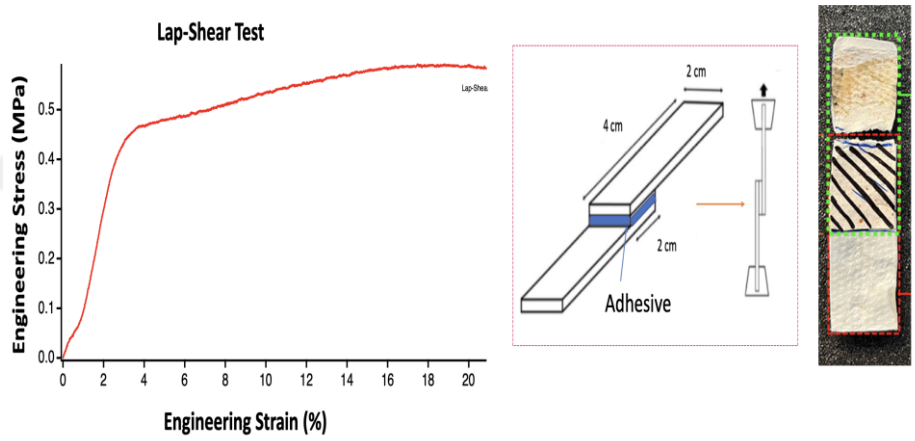

Figure 3.20 Lap-Shear test's Stress- Strain Curve of bilayered cardiac patch.

3.3.1 Mechanical Evaluations of Bilayered Cardiac Patch

The mechanical properties of the final bilayered cardiac patch, native pericardium, first layer, second layer and PLGA/gelatin membrane (AY1) were compressively assessed through tensile test, the Stress-Strain Curve of samples were represented graphically. The electrospun PLGA/gelatin membrane (AY1) exhibited an ultimate tensile strength of 2.22±0.42 MPa, an elongation of 80.25±25.22%, and a Young's Modulus of 2.97±0.87 MPa. In comparison, the PLGA/gelatin membrane incorporating 10% (w/v) hawthorn extract and 1 µg/ml VEGF PLGA/gelatin membrane (AY8, second

layer of cardiac patch) demonstrated an ultimate tensile strength of 2.32±2.24 MPa, an elongation of 92.19±10.75%, and a Young's Modulus of 3.36±1.5 MPa. On the other hand, the native pericardium exhibited an ultimate tensile strength of 17.08±2.71 MPa, an elongation of 21.46±2.84%, and a Young's Modulus of 3.04±0.87 MPa. Following the decellularization process, the ultimate tensile strength slightly decreased to 13.13±3.42 MPa, accompanied by a 20.48±1.65% elongation and a 2.84±1.35 MPa Young's Modulus. The PANI-coated decellularized pericardium, serving as first layer of cardiac patch, displayed an ultimate tensile strength of 10.38±0.28 MPa, an elongation of 14.93±4.54%, and a Young's Modulus of 1.71±0.8 MPa. Remarkably, the final bilayered cardiac patch demonstrated enhanced mechanical characteristics, with an ultimate tensile strength of 22.70±6.33 MPa, an elongation of 53.58±10.63%, and a Young's Modulus of 0.67±0.10 MPa. While the polymeric electrospun membranes such as AY1 and AY8 demonstrated a ductile response in the mechanic test, pericardium-based samples such as native pericardium and first layer demonstrated a brittle response. Despite polymeric membranes withstanding an ultimate tensile strength of approximately 2 MPa, they exhibited an elongation of at least 80%. In contrast, pericardium-based samples demonstrated an ultimate tensile strength exceeding 10 MPa with an elongation of approximately 20%. The combination of pericardium-based and polymeric-based layers in the bilayered cardiac patch created a synergistic effect on mechanical strength, increasing not only the ultimate tensile strength but also elongation ratio of the cardiac patch. A cardiac patch should mimic the mechanical properties of native myocardium, the stiffness of a myocardium ranges from 10-20 kPa in diastole to 200-300 kPa in systole [212]. It is suggested that a cardiac patch should possess higher mechanical strength than a normal myocardium to withstand the stress during contraction and relaxation [212, 213]. The bilayered cardiac patch's mechanical strength aligns well with these requirements. In comparison with the literature, a collagen cardiac patch demonstrated a Young's Modulus of 120 kPa, which increased to 1100 kPa with the addition of 800 µg/ml graphene oxide [214]. Additionally, poly(glycerol-sebacate) cardiac patches mimicked the mechanical strength of myocardium, ranging from 0.05 MPa to 1.2 MPa Young's Modulus [212]. In another study, it was emphasized that having a Young's Modulus of the cardiac patch between 100 kPa and a few MPa could reduce the stress of the heart wall [214]. In the literature, the native pericardium was crosslinked with genipin, genipin crosslinked pericardium demonstrated that at around 12 MPa tensile strength and the increasing genipin concentration decreased the pericardium elongation from %35 to %28

[215]. In another study, decellularization and genipin crosslinking decreased the tensile strength of pericardium from 17.53 MPa to 14.51 MPa [216]. In Yao et al.'s study, porous polyurethane cardiac patch demonstrated 727 kPa Young's Modulus [217]. The obtained bilayered cardiac patch demonstrated compatibility with the literature in terms of mechanical strength, providing a promising material for cardiac patch applications.

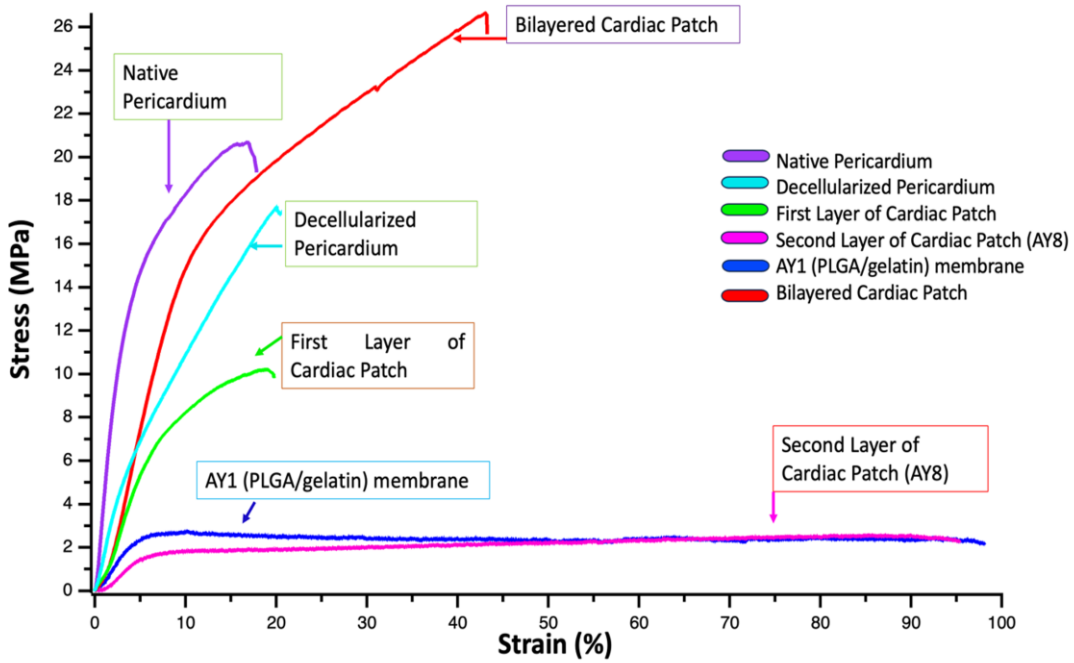

	UTS (MPa)	Elongation(%)	Young's Modulus (MPa)
AY1(PLGA/gelatin)	2,22±0,42	80,25±25,22	2,97±0,87
AY8-Second Layer of CP	2,32±2,24	92,19±10,75	3,36±1,5
Native Pericardium	17,08±2,71	21,46±2,84	3,04±0,87
Decellularized Pericardium	13,13±3,42	20,48±1,65	2,84±1,35
First Layer of CP	10,38±0,28	14,93±4,54	1,71±0,8
Bilayered Cardiac Patch	22,70±6,33	53,58±10,63	0,67±0,10

Figure 3.21 Stress-Strain Curve, UTS, Elongation and Young's Modulus values of PLGA/gelatin membrane (AY1), Native Pericardium, Decellularized Pericardium, First Layer, Second Layer, and Bilayered Cardiac Patch (CP: Cardiac Patch).

3.3.2 Blood Compatibility of Bilayered Cardiac Patch

Blood compatibility stands as a pivotal criterion for materials in direct contact with blood, as those lacking compatibility may induce hemolysis through membrane disruption, influencing cell and protein binding due to the surface tension of the materials.

The hemolysis rate (%) serves as a crucial indicator of blood compatibility. According to ISO 10993.4:2002 standards, a material is deemed safe for medical use if its hemolysis rate is below 5%. The bilayered cardiac patch exhibited a notably low hemolysis rate of 0.421±0.191%, well below the acceptable threshold, confirming its blood compatibility. In a study conducted in the literature, the hemolysis rate of an electrospun silk scaffold was initially 0.850%, but with incorporation of hydroxyapatite, this rate decreased to 0.765%, showcasing an improvement in blood compatibility [218]. In another study, scaffolds composed of polyurethane and fibrin exhibited hemolysis rates below 1.5% [219]. In a study involving a scaffold of poly (lactic acid) and poly (glycerol sebacate), the hemolysis rates was recorded at 1.67%, falling with the range (0-2%) associated with materials considered non-hemolytic [220]. Further advancements in blood compatibility were achieved through surface modification with heparin-fibronectin, reducing the hemolysis rate from 1.5% to 0.5% in a titanium-containing material [221]. Conversely, the hemolysis rate of a double-layer patch consisting of chitosan and poly (vinyl alcohol) exhibited a hemolysis rate of 1.2%, which increased to 3.8% with the addition of graphene oxide and copper oxide [221]. In conclusion, the final bilayered cardiac patch, aligning with established safety standards.

3.3.3 Cell Viability

The heart myocardium includes the cardiomyocyte, vascular smooth muscle, fibroblast, endothelial and immune cell types [33]. Therefore, we investigated the cell viability of bilayered cardiac patch with cardiomyocyte and fibroblast cell lines by MTS assay. The bilayered cardiac patch demonstrated the cell viability over the %90 at 24, 48, and 72 hours with cardiomyocytes and fibroblast cell lines. It can be explained by the PLGA is biocompatible, FDA approved copolymer for clinical applications, and hawthorn species are known with antioxidant effect in the literature reports [134, 222]. This synergistic effect provided the high cell viability to the bilayered cardiac patch without any toxic effect on these cell lines. Comparatively, in existing literature, a cardiac patch compromising silk fibroin and carbon nanotube demonstrated 80% cell viability over a 2-day period [223]. In another study, decellularized heart tissue exhibited cell viability of 94%, and 92% at the end of 3 and 4 weeks, respectively [224]. A chitosan scaffold containing graphene oxide and gold nanosheets exhibited cell viability close to that of the control group [225]. Furthermore, a TiONts/PEG scaffold demonstrated over

90% cardiomyocyte cell viability, and a concentration of 5µg/mL TiONts/PEG was deemed non-cytotoxic for 24h incubation [226]. In another study, a microneedle cardiac patch, a live-dead assay revealed almost 100% cell viability after 1, 3 and 7 days [227]. In the literature, the 80% cell viability was observed on the 0.08% PANI containing cardiac patch while the 1.34% PANI containing cardiac patch showed approximately 60% cell viability. The reduction in the cell viability was attributed to potential stress exposure, resulting in a corresponding decrease [228]. In conclusion, bilayered cardiac patch is biocompatible with these cell lines.

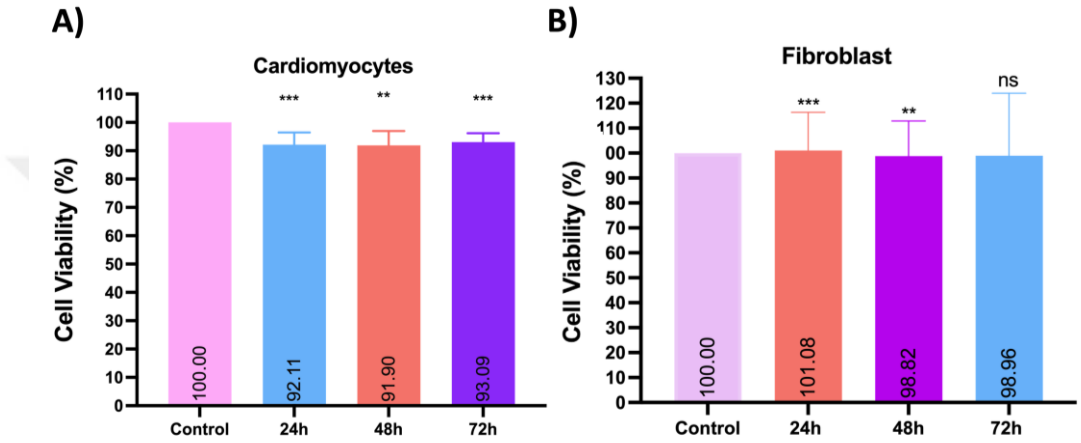

Figure 3.22 Graphical representation of *in vitro* cell viability (%) of bilayered cardiac patch with cardiomyocyte and fibroblast cell lines ($p < 0.01$: **; $p < 0.001$: *** considered significant).

3.3.4 Cell Adhesion Study

Figures 3.23 and 3.24 illustrate the cardiomyocyte cells adhesion on the bilayered cardiac patch. DAPI staining in Figure 3.23 reveals cardiomyocyte cell nuclei as blue under a fluorescent microscope image for 24, 48 and 72 hours. The images show that cardiomyocyte cells adhered to the surface of bilayered cardiac patch within the first 24 hours. Subsequently, the density of adhered cells increased at the 48th hour, and by the end of 72 hours, adhered cells proliferated to reach a certain density.

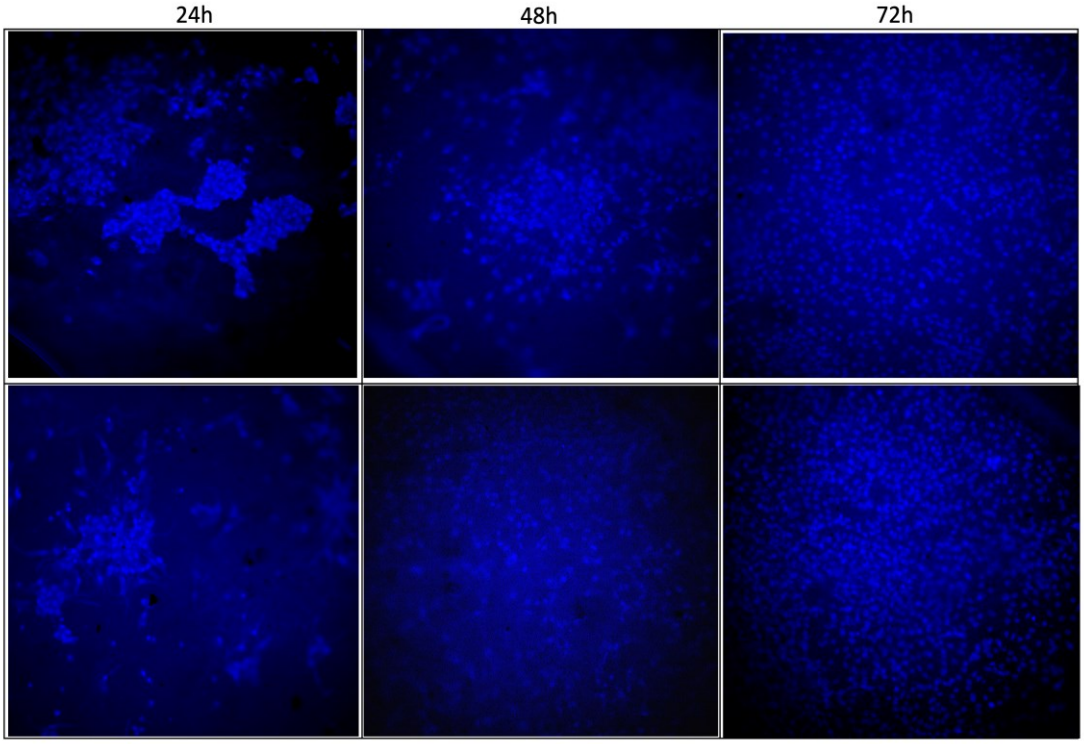

Figure 3.23 DAPI Staining and of the cardiomyocytes cells on bilayered cardiac patch for 24h, 48h and 72h by fluorescence microscopy at 20X magnification.

SEM images in Figure 3.24, following DAPI staining, further confirm that the cell adhered and proliferated on the bilayered cardiac patch within 3 days. Considering both DAPI staining and SEM images, it can be concluded that the bilayered cardiac patch is a suitable material for adhesion and proliferation of cardiomyocyte cells. In the literature, the PANI-containing cardiac patches exhibited similar microscope images with cardiomyocyte cells [229]. Cardiomyocyte cells seeded on decellularized heart tissue covered the tissue surface within 2 weeks [224]. In the Saravanan et al.'s study, cardiomyocyte cells completely covered on the gold nanostructures and graphene oxide containing chitosan scaffold [225]. In the literature, it is emphasized that the cardiomyocyte cell adhesion on the PLGA scaffold was achieved 60% for 12h and 80% for 24h [230]. Another study showcased cardiomyocyte cells adhesion on the collagen/chitosan scaffold was showed through fluorescence microscope images [231]. In conclusion, the bilayered cardiac patch is suitable material for cardiomyocyte cell adhesion and proliferation, hawthorn extract and VEGF containing PLGA/gelatin layer of bilayered cardiac patch have positive effect on cell adhesion.

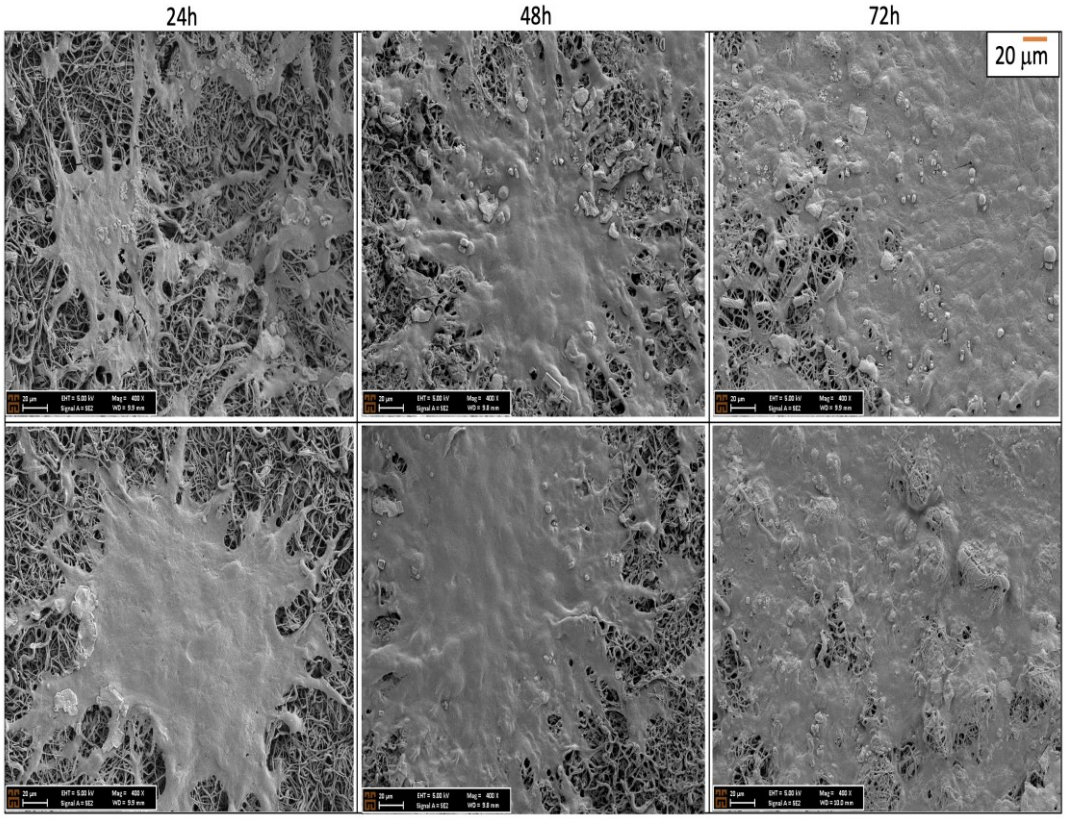

Figure 3.24 SEM images of cardiomyocyte cell seeded bilayered cardiac patch after 24h, 48h and 72h.

3.4 *In vivo* Study of Cardiac Patch

The left coronary artery (LAD) ligation method was used to create a myocardial defect model in rats. After the LAD ligation resulting myocardial defect was observed with cyanosis in the left ventricle of heart within 15-20 minutes. The heart rhythm was monitored via the ECG device throughout the operation. The induction of MI sign was confirmed by ECG waves of before and after the MI as seen Figure 3.25

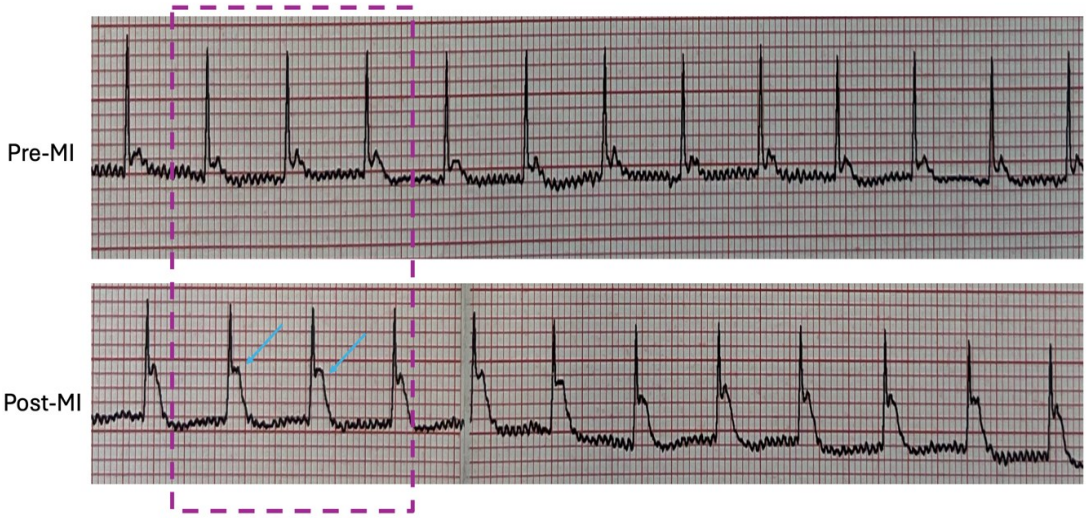

Figure 3.25 ECG waves before and after MI.

3.4.1 Assessments of Cardiac Functions

The transthoracic echocardiograph was used to assess the improvement of cardiac functions, echocardiography results were represented in Figure 3.26. As shown in ultrasonic images in Figure 3.26, the left ventricle of control group demonstrated the normal contraction amplitude, while a weak contraction amplitude was obtained in the MI group. When compared with the MI group, the bilayered cardiac patch implanted group demonstrated better contraction amplitude than MI and PLGA/gelatin implanted groups. Also, we investigated the quantitative cardiac functions, the healthy rats demonstrated the 0.51 cm LVEDd and 0.23 cm LVESd, while the MI group demonstrated the 0.62 cm LVEDd and 0.33 cm LVESd. The bilayered cardiac patch and PLGA/gelatin implanted groups showed the 0.61 cm and 0.65 cm LVEDd and 0.30 cm and 0.35 cm

LVESd, respectively. The increase of left ventricle systole and diastole diameters in MI and patch implanted groups can be explained by the ventricular dilatation after MI [232].

Fractional shortening (FS) is a change in the percentage of ventricular inner diameter of the heart between systole and diastole, briefly providing information about the contractile function of the heart. According to the obtained data, control group showed 55.43±7.9 FS (%), while MI group demonstrated the 44.35±3.9 FS (%) after 28 days of operation. The FS (%) was improved up to 50.46±4.5 and 47.19±9.7 in the bilayered patch and PLGA/gelatin groups after the 28 days of patch implantation, respectively.

The Ejection Fraction (EF%) is a parameter that shows how much of the blood in the heart is pumped to the body. A low EF can be an indication that the heart is not functioning properly such as heart failure. The control group showed the 89.11±6.7 EF (%), while MI group demonstrated the 80.73±3.68 EF (%). The bilayered patch implantation improved the EF (%) up to 87.99±2, but the PLGA/gelatin group showed a slight increase in EF (%) as 82.58±9.6. It is expected that being a weakness in heart functions after the MI, but there is a significant increase of cardiac functions in bilayered cardiac patch implanted group. It can be concluded that the bilayered cardiac patch improved the cardiac functions by providing mechanically support and healing to the heart. In a study, PTFE-based commercial patch was used in an 8-week study for comparison with the polymeric PEUU patch. According to the echocardiography results obtained, the fractional change of the heart undergoing MI was 18% at the end of 8 weeks, while the value was 19% in the group to which the PTFE patch was applied, with a 1% improvement [233]. In another study, a GORE-TEX® brand commercial PTFE-based cardiac patch was implanted into the hearts of rats and compared with the synthesized P(CL-DLLA) cardiac patch over a long period of 48 weeks. According to the obtained data, it was mentioned that the PTFE-based patch was too stiff for the contraction-relaxation function of the heart [234]. In another study, the Cor-Matrix® commercial patch was examined in a 16-week study on myocardial defect in rats in comparison with the MI group and Cor-Matrix with growth factor. In cardiac function evaluations, while the EF value of the MI group was around 35%, the EF value of the Cor-Matrix® group showed similar values to the MI group at the end of 16 weeks, while the EF value increased to approximately 50% in the group to which growth factor was added. When no growth factor was added to the commercial patch, cardiac function values were

obtained at values close to the MI group [235]. When the PCL/gelatin polymeric cardiac patch produced by Kai et al. was examined in an *in vivo* rat model, it was reported that it improved the EF value from 16% to 35% and improved the FS value from 8.9% to 20.06% [236]. When we compare the cardiac function values of the bilayered cardiac patch with the polymeric patches and commercial patches reported in the literature, results are compatible with the literature data. The targeted improvement in cardiac functions of bilayered cardiac patch implanted group was achieved successfully.

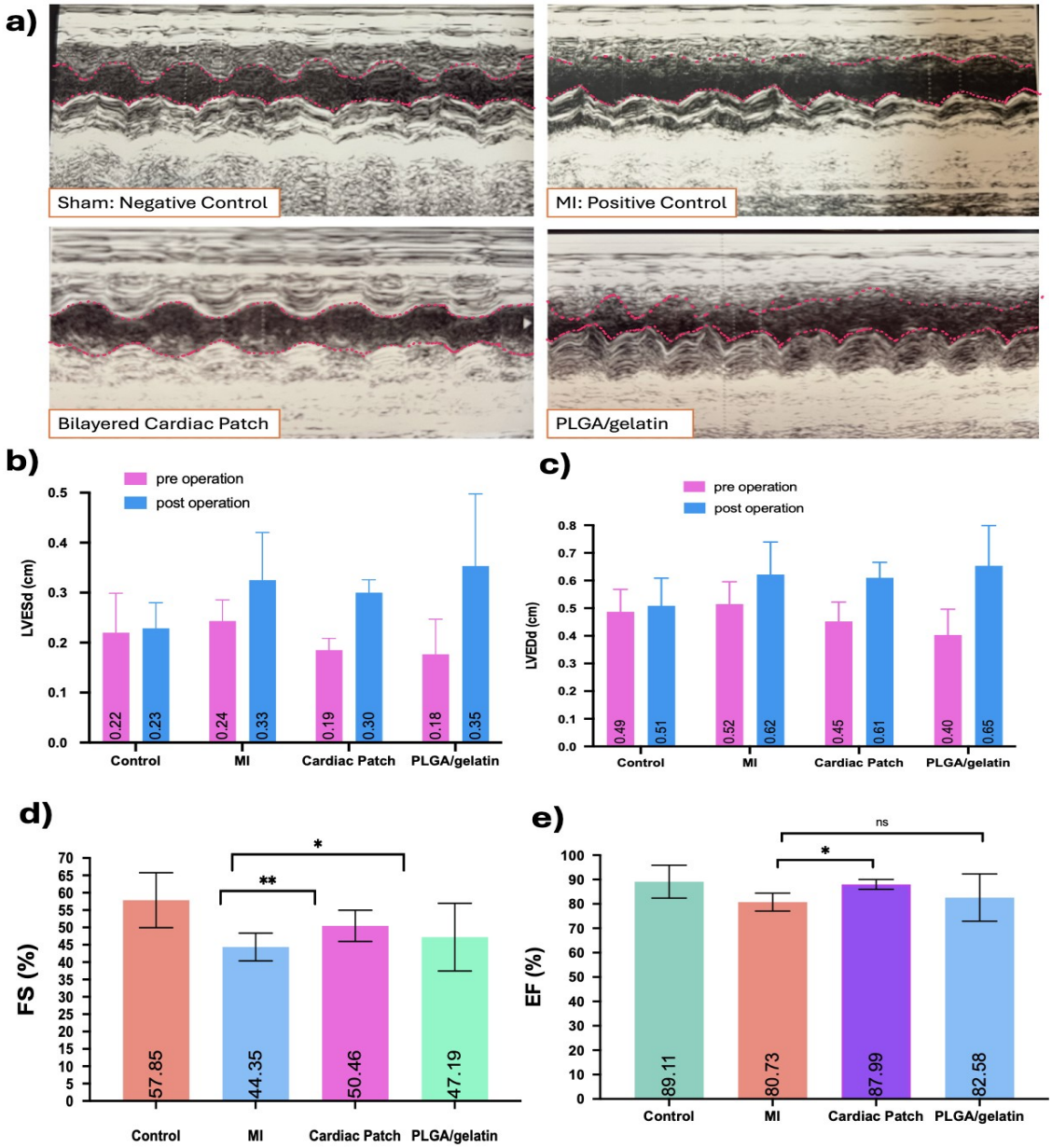

Figure 3.26 a) The ultrasonic images of cardiac cycles, b) LVEDd, c) LVESd, d) FS (%), and e) EF (%) results of groups. (ANOVA test, $p < 0.05$: *; $p < 0.01$: **; $p < 0.001$: ***; $p < 0.0001$: **** were considered significant, ns: non-significant. Error bars indicate standard deviation and error bars are invisible when they are smaller than the line thickness of these graphs.

4.2.2 Hematoxylin & Eosin staining

Hematoxylin & Eosin staining was applied to heart sections, the cell nuclei is coloured as blue-purple by hematoxylin, while cytoplasm and extracellular structures are coloured as pink by eosin. H&E staining images represented in Figure 3.27 for all groups. According to these images; the heart' cells can be seen as homogenously distributed through the myocardium in the control group. In the MI group, the clusters of cells can be observed in some regions within the myocardium due to the thinning of the ventricular wall. In the bilayered patch implanted group, intense cell migration into the patch is observed, along with areas dense with round-red erythrocytes. It has been determined that the regions with clustered erythrocytes represent the presence of blood vessels. In the PLGA/gelatin applied group, the cell nuclei can be seen from figures.

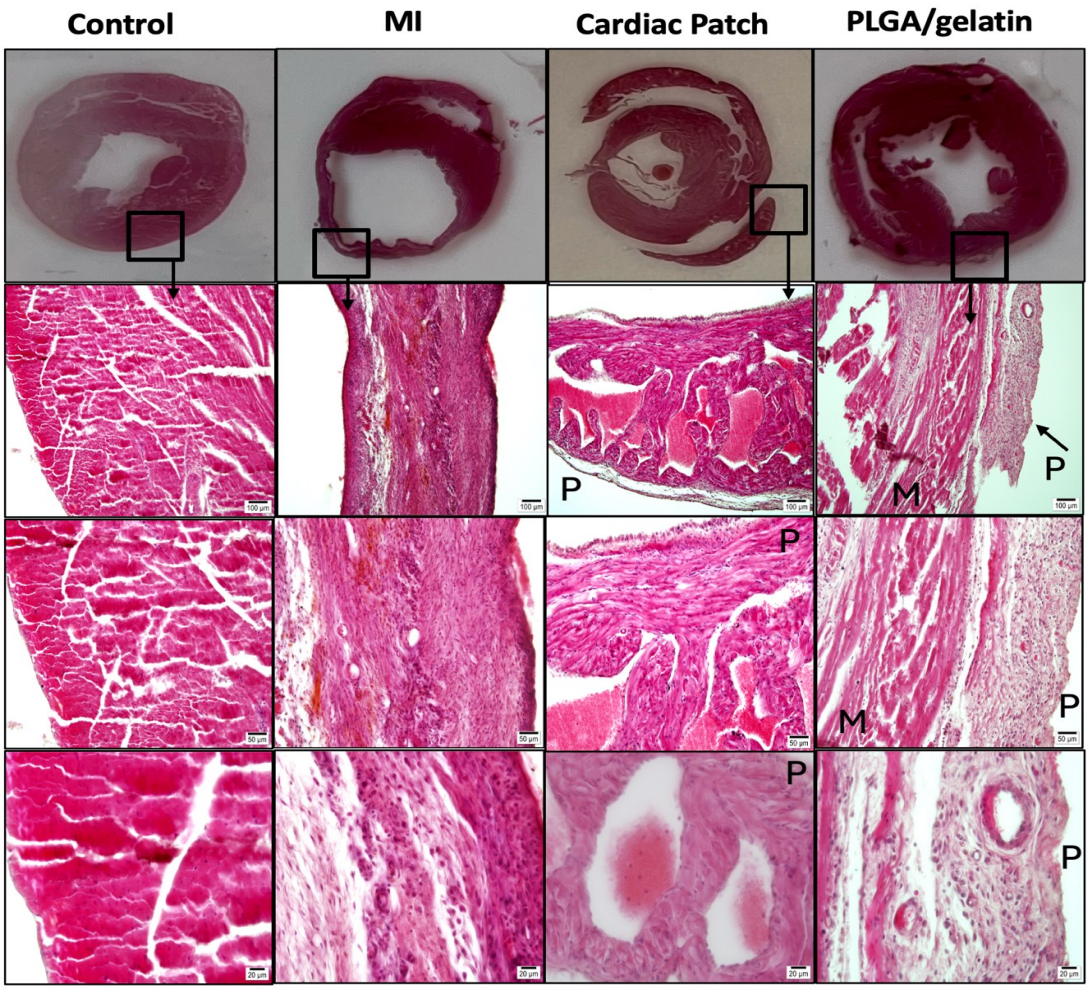

Figure 3.27 Comparative representation of Hematoxylin & Eosin stained microscope images of heart tissues at 10X, 20X, and 40X magnifications. (P: applied patch material, M: myocardium).

Following the Hematoxylin & Eosin staining, left ventricular (LV) wall thicknesses were calculated from microscope images using ImageJ program and are presented graphically in Figure 3.28. LV wall thickness was obtained as 2981±116 μm for the control group, 910±159 μm for the MI group, 3054±257 μm for the bilayered patch implanted group and 2271±244 μm for the PLGA/gelatin implanted group. Septum thicknesses of the groups were obtained as 2544.69±309 μm, 2118.27±131 μm, 3461.89±232 μm, 3222.66±52 μm, respectively. The thickness of the scar in the myocardium were obtained as 1048.85±348 μm for the MI group, 448.36±147 μm for the cardiac patch group and 544.87±301 μm for the PLGA/gelatin group. After the induction of MI in the myocardial tissue, due to the decrease or complete cessation of blood flow, nutrients and oxygen cannot reach the cells. Accordingly, the cells in the myocardial tissue begin to die and then neutrophil and macrophage cells migrate to this region. Then, phagocytosis occurs, and the necrotic tissue was replaced with granulation tissue by immune cells. Collagen accumulation begins in the defected area, and the thickness of the ventricular wall decreases due to the weakening of the heart muscle. Since the self-renewal feature of the heart cells cannot be provided sufficiently in the defected area of the heart, it is devoid of healthy cells, and for this reason, electrical conductivity in the tissue is disrupted, mechanical dysfunction and structural integrity are disrupted. This condition is also called dilated cardiomyopathy [237]. In this regard, cardiac patch applications are of great importance in order to limit the growth of the defec so that the heart does not lose its function. As seen in the figures, the application of cardiac patch materials 4 weeks after MI prevented the expansion of cardiomyopathy and the decrease in ventricular thickness was limited. While it was observed that the LV wall thickness was significantly thinned at the end of 4 weeks in the MI group, the decrease in wall thickness was limited in the cardiac patch and PLGA/gelatin groups, and the deterioration of the tissue structure was prevented. Ventricular dilatation was not observed in these groups because the applied bilayered patch and PLGA/gelatin membrane acted as a mechanical barrier preventing the expansion of the left ventricular wall [236]. The ventricular wall thickness of the bilayered cardiac patch group was significantly greater than that of the PLGA/gelatin group, which can be explained by the mechanical strength of the bilayered patch is better than the PLGA/gelatin membrane and is close to the mechanical properties of the native myocardium. According to the data obtained from *in vitro* mechanical tensile test results within the scope of the project, the bilayered cardiac patch has a tensile strength of 22.70±6.33 MPa, an elongation ratio of 53.58±10.63% and

an Elastic Modulus of 0.67±0.10 MPa, while the PLGA/gelatin membrane has a tensile strength of 2.22±0.42 MPa, an elongation ratio of 80.25±25.22% and an Elastic Modulus of 2.97±0.87 MPa. It is known that the elastic modulus of a healthy heart tissue is 10-20 kPa in diastole, 200-300 kPa in systole and the elongation rates are 10% in diastole and 15-22% in systole [212]. The applied bilayered cardiac patch was compatible with the mechanical properties of the native myocardial tissue, thus acting as a mechanical barrier, ventricular contraction was limited, and deterioration of the tissue structure was successfully prevented.

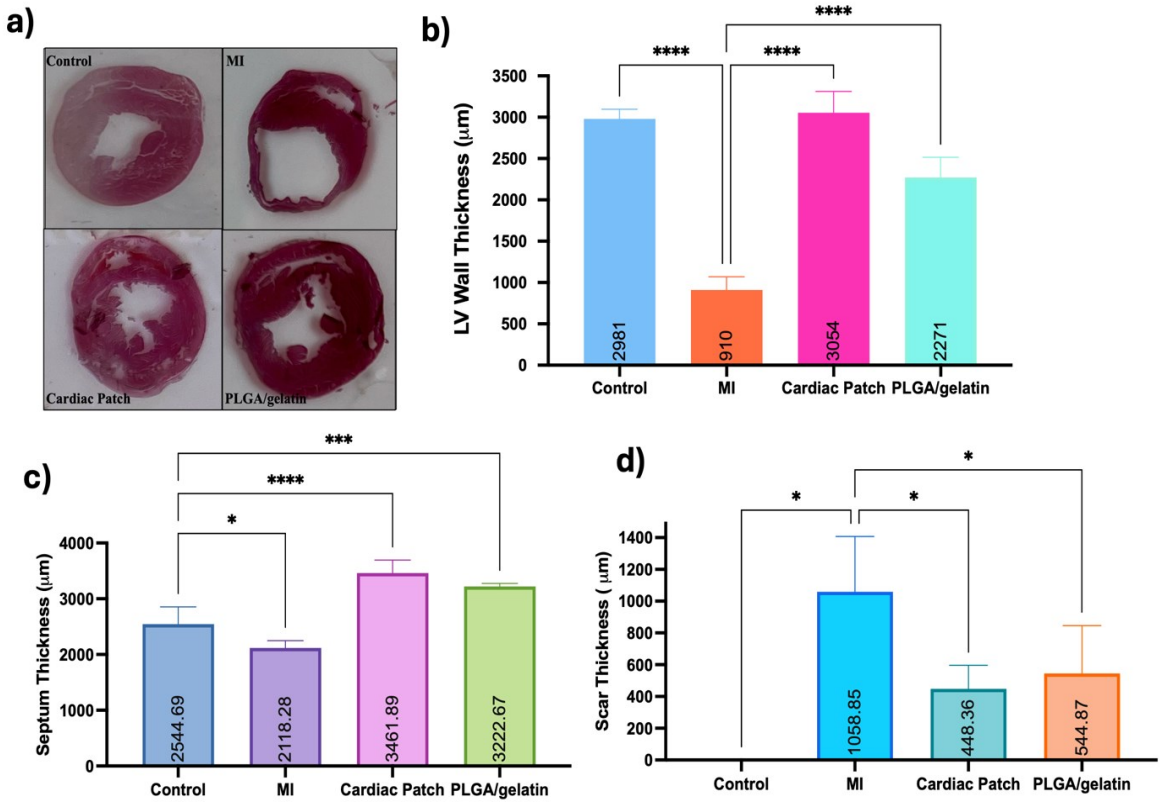

Figure 3.28 Graphical representation of the left ventricular wall thickness, septum thickness, and scar thickness of heart tissues. (ANOVA $p < 0.05$: *; $p < 0.01$: **; $p < 0.001$: ***; $p < 0.0001$: **** were considered significant. Error bars indicate standard deviation and error bars are invisible when they are smaller than the line thickness of these graphs.

4.2.3 Masson's Trichrome staining

Masson's trichrome staining was applied to investigate fibrous scar and heart muscles. Masson's trichrome staining is based on the principle of staining cells in blue-black, cytoplasm in red, muscle tissue in purple and collagen in blue. According to result in Figure 3.29, the heart muscles of control group can be seen in purple colour and no

defect was observed in the myocardium. On the other hand, the scar was highlighted as blue in the MI group, and scar covered the large portion of the left ventricular wall within 28 days. In the bilayered cardiac patch implanted group, the scar was significantly reduced compared to the MI group, that is a sign the healing of myocardium within 28 days. The bilayered cardiac patch can be seen as blue due to it composed of decellularized bovine pericardium. Similarly, a reduction in the scar area was observed in the PLGA/gelatin implanted group. It was concluded that the groups treated with patches showed significant improvement in myocardial scar after MI within four weeks, while in the untreated group, the scar expanded within four weeks. Blood vessels and cell migration were found in the defected myocardium in all MI induced groups. In the cardiac patch and PLGA/gelatin group, images showed that the material fused and integrated with the myocardium within four weeks. The integration of the implanted patch was similarly observed within 1 to 4 weeks in decellularized myocardium patches in the literature. Additionally, similar to our results, intense cell migration and vascular structures in the ischemic area were observed [153]. Similar Masson's trichrome staining images were also observed in studies in the literature, with a reduction in defect in the groups treated with PCL and PCL/gelatin cardiac patches compared to the MI group, and similar cell migration and vascular structures were detected [236].

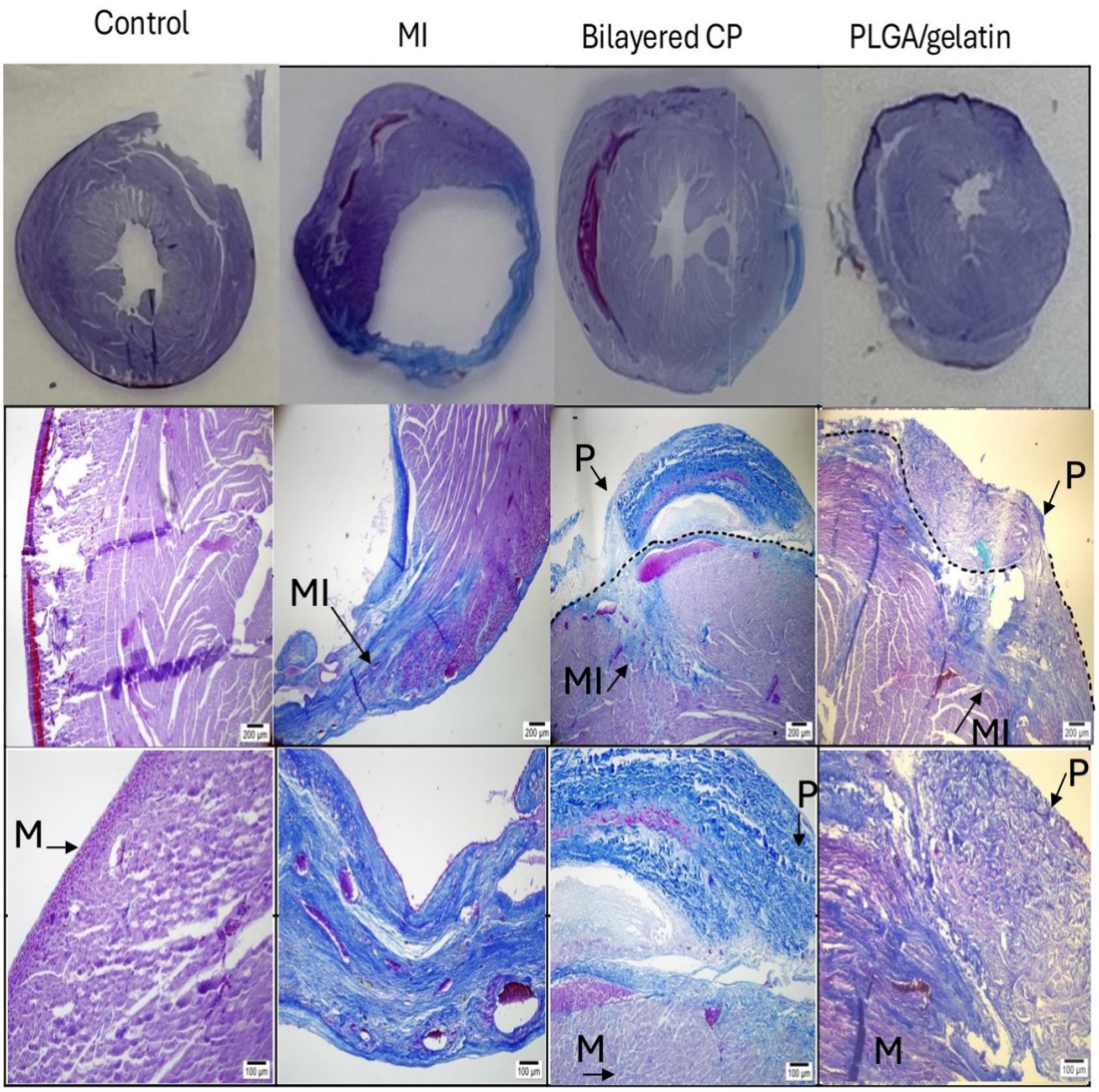

Figure 3.29 Examination of heart tissues with Masson's trichrome staining. (P: represents the applied patch material, M: myocardium of the heart).

In the Figure 3.30, heart muscle cells can be seen embedded within the heart muscle in the control group, with red blood cells appearing as red-purple, round nuclei. In the MI group, cell migration is observed in the scar area; these cells are thought to include heart muscle cells, immune cells, and erythrocytes. Large blood vessels within the scar area appear as clusters of blood cells. Additionally, blood vessel density was observed to be higher in the bilayered cardiac patch group than in the MI group. Blood vessels are also visible in the scar area of the PLGA/gelatin group. This increased blood vessel formation may be attributed to the release and effectiveness of the growth factor VEGF in the cardiac patch.

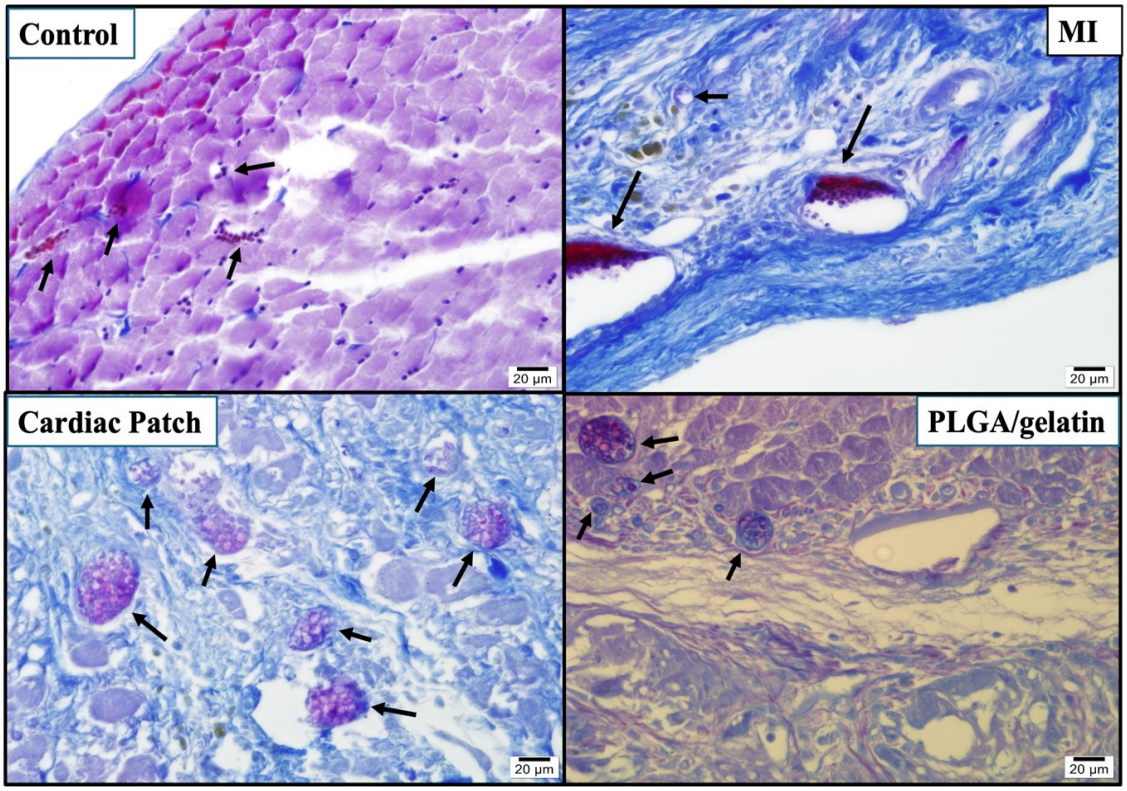

Figure 3.30 Examination of heart tissues with Masson's trichrome staining at 40X magnification, arrows represent vessels in the scar area. Scale bar represents 20 µm.

4.2.4 Immunofluorescence staining

Formation of new vessels is one of the most important criteria and one of the difficulties encountered in order to ensure healing in defected heart tissue. New vessel formations were examined with immunofluorescence staining methods using anti-von Willebrand Factor (vwf), anti-αSMA, anti-CD31 primary antibodies. While cell nuclei in heart tissues were stained with DAPI as blue lights, detection of the antibodies used was observed with red lights by binding with the "Goat Anti-Rabbit IgG (H+L) Elab Fluor®647 conjugated" secondary antibody. Blue and red images were combined in the ImageJ-Fiji program and presented comparatively. The immunofluorescence examination results of the anti-vwf primary antibody were presented in Figure 3.31. The anti-vwf primary antibody binds to a glycoprotein that allows the detection of the blood vessel wall and the erythrocytes inside it. According to the data obtained, vwf markers appeared with red light throughout the myocardium in the control group, reflecting normal blood flow in the heart. In the MI group, vwf markers were absent in the scar area due to reduced blood flow in the defected myocardium. They only labelled cells in the large vessels within the defected myocardium, which are thought to be the tissue's own

vessels. In the bilayered cardiac patch-implanted group, significant vwf markers were observed throughout most of the myocardium, including within the patch itself. In the PLGA/gelatin group, a similar reduction in vwf markers was seen in the scar area. vwf markers were also present in the applied PLGA/gelatin, though with less intensity than in the bilayered patch.

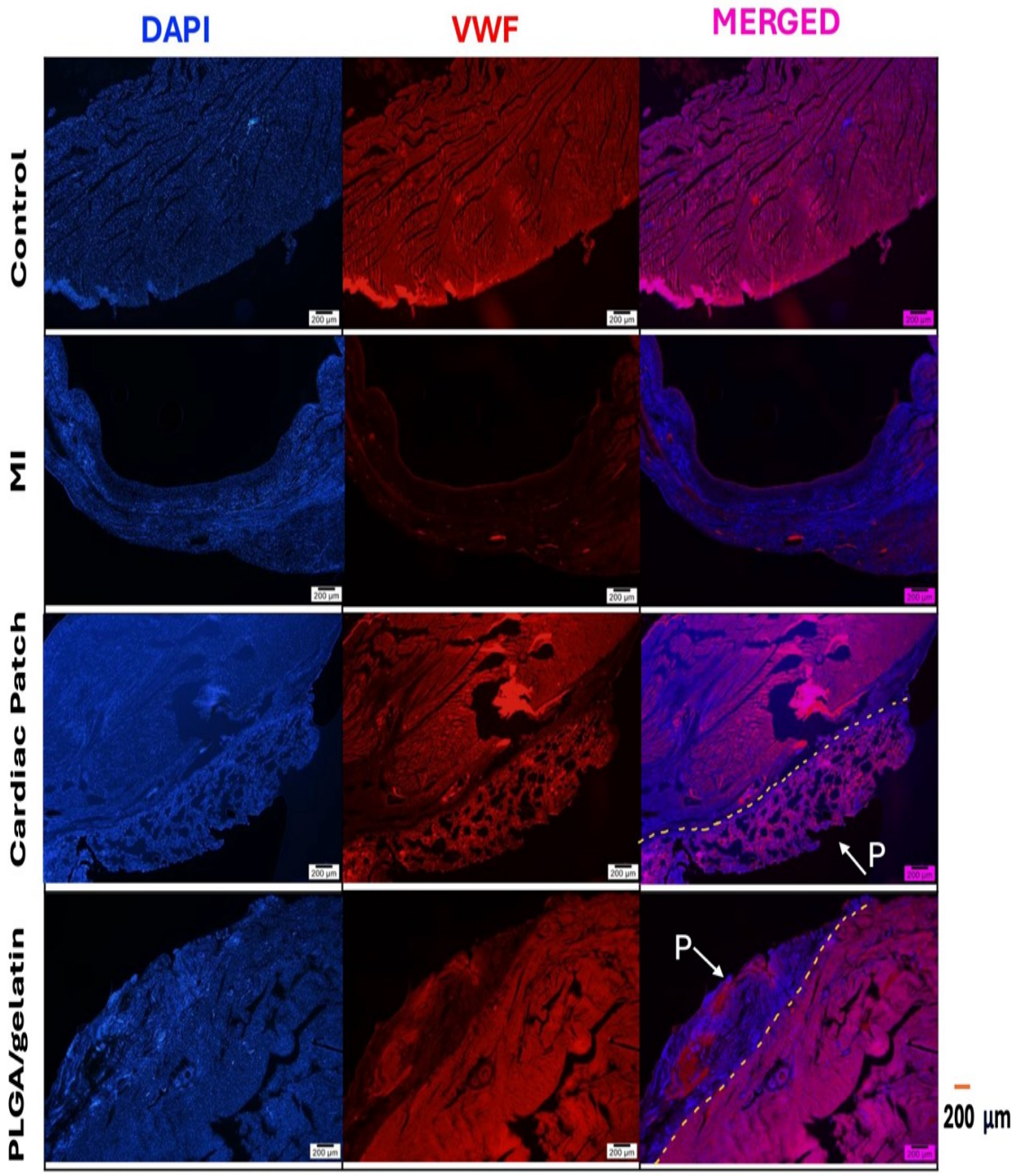

Figure 3.31 Examination of heart tissues with immunofluorescence staining techniques using anti-vwf. The scale bar represents 200 µm.

Another marker for vascularization is the anti-CD31 primary antibody, which indicates cell adhesion molecules expressed in vascular endothelial cells. According to

Figure 3.32, the CD31 antibody yielded similar results to those with the anti-vwf primary antibody. This alignment was interpreted as mutual support between the two markers, adding significance to the findings. The CD31 markers, present in high amounts in the control group, decreased significantly in the MI group. In the bilayered cardiac patch group, CD31 marker density closely resembled that of the control group, with vascularization markers also observed within the patch itself. In the PLGA/gelatin group, CD31 markers were less abundant than vwf markers, appearing at the outermost edge of the PLGA/gelatin. Cell nuclei within the PLGA/gelatin membrane were also considerably fewer than in the bilayered patch. Overall, the controlled release of the VEGF growth factor, which influences vascularization, from the applied bilayered patch to the defected area significantly increased vascularization both in the scar region and within the patch. This indicates that the cardiac patch developed within the scope of this thesis has effectively fulfilled its purpose.

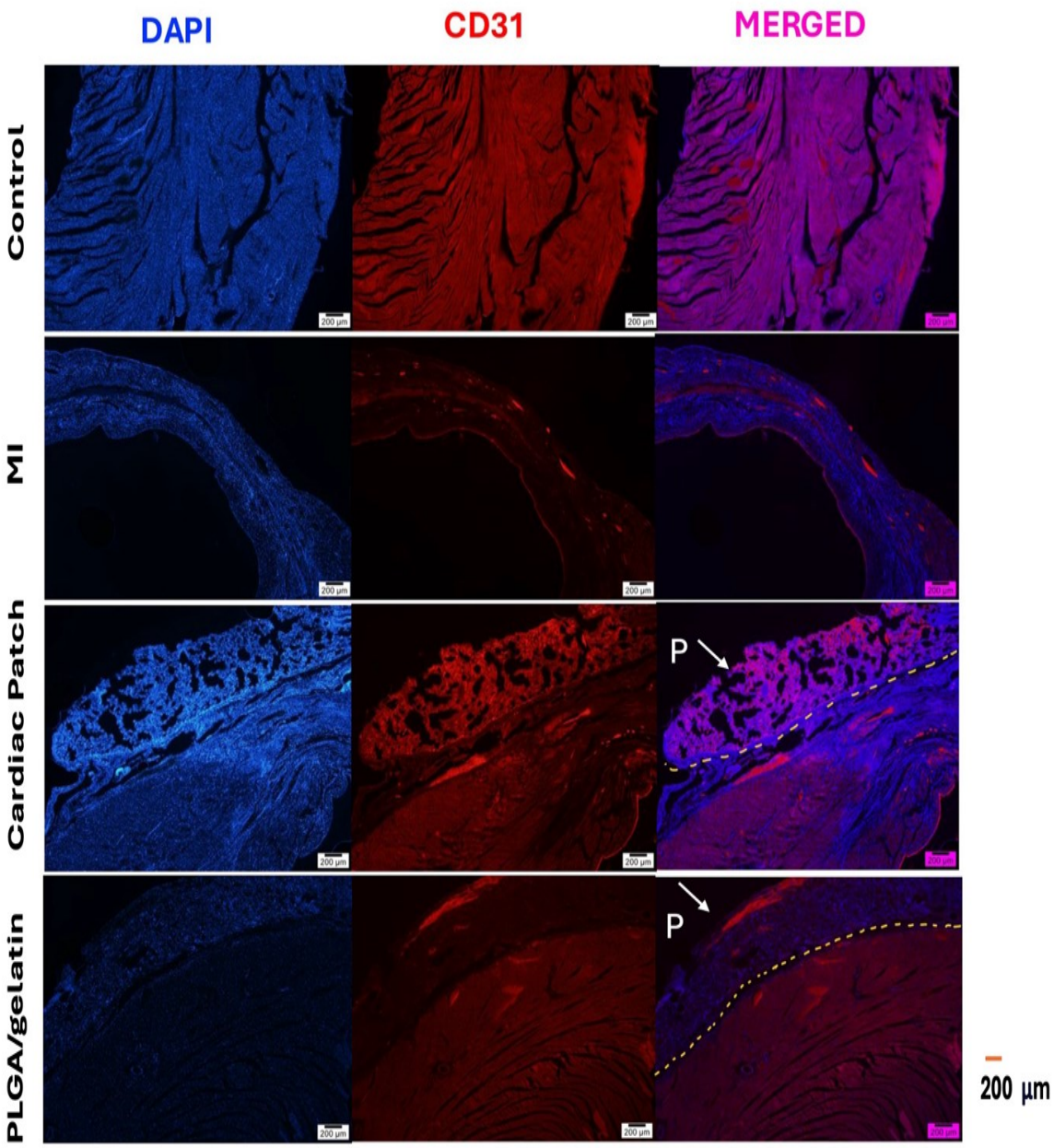

Figure 3.32 Examination of heart tissues with immunofluorescence staining techniques using anti-CD31. The scale bar represents 200 µm.

Another primary antibody, anti-αSMA, binds to the actin filaments of smooth muscle cells, which contribute to the contractile properties of cells, and also marks smooth muscle cells around blood vessels. In Figure 3.33, smooth muscle cells in the myocardium of control group were densely labelled with αSMA markers. In the MI group, a decrease in markers was observed in the scar area due to cell death, while markers were still present in the healthy myocardial region. In the myocardium of the bilayered cardiac patch group, αSMA markers were observed in high density, similar to the healthy group, and were also prominent within the applied patch itself. In the PLGA/gelatin group, markers appear as

thin lines along the outer edge of the membrane, with lower marker density in the myocardium compared to the bilayered patch.

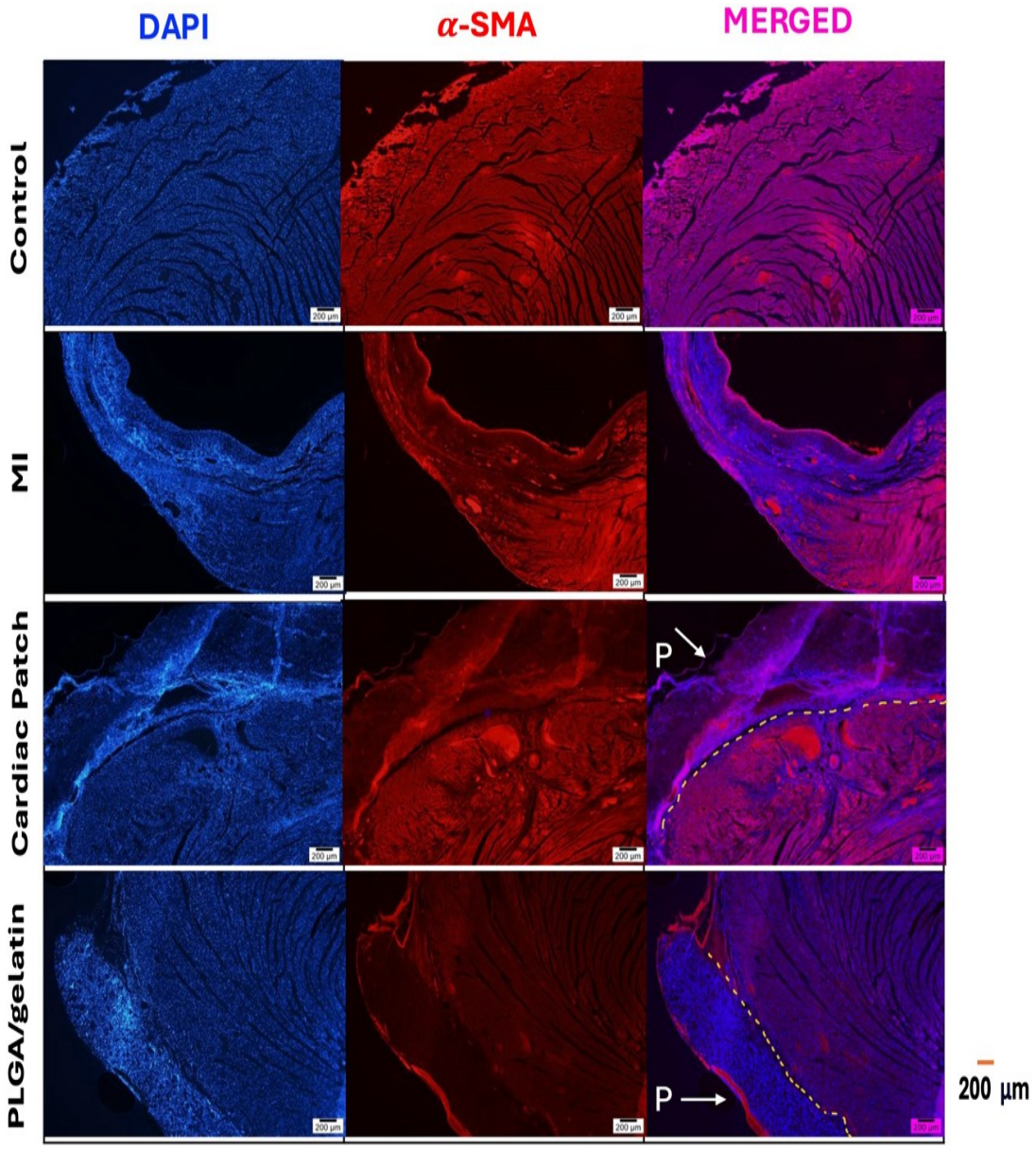

Figure 3.33 Examination of heart tissues with immunofluorescence staining techniques using anti-αSMA. The scale bar represents 200 µm.

GATA4 is a protein that plays an important role in heart development and heart regeneration, therefore cardiac markers were examined with anti-GATA4 primary antibody. While cell nuclei in heart tissues were stained with DAPI as blue lights, detection of the antibodies used was observed with green lights by binding with the "Goat Anti-Rabbit IgG (H+L) Elab Fluor®488 conjugated" secondary antibody. In Figure 3.34, while GATA4 markers were seen intensely in the control group, they were seen around the vascular structures in the defected area of the MI group. In the bilayered patch implanted group, they were seen intensely in the myocardium and the defected area. Some

GATA4 markers were also found inside the applied patch. In the PLGA/gelatin group, GATA4 markers were seen in the area close to the defected area in the myocardium, and the markers were seen sparsely in the form of green glows in the PLGA/gelatin. The intensity of cardiac markers in the bilayered patch group indicates that heart regeneration has started to occur in the defected area. In a study in the literature, decellularized myocardial scaffold was produced as a cardiac patch and examined in a MI rat model. According to the reported results, it was stated that GATA4 markers were not found in the patch-containing groups [153].

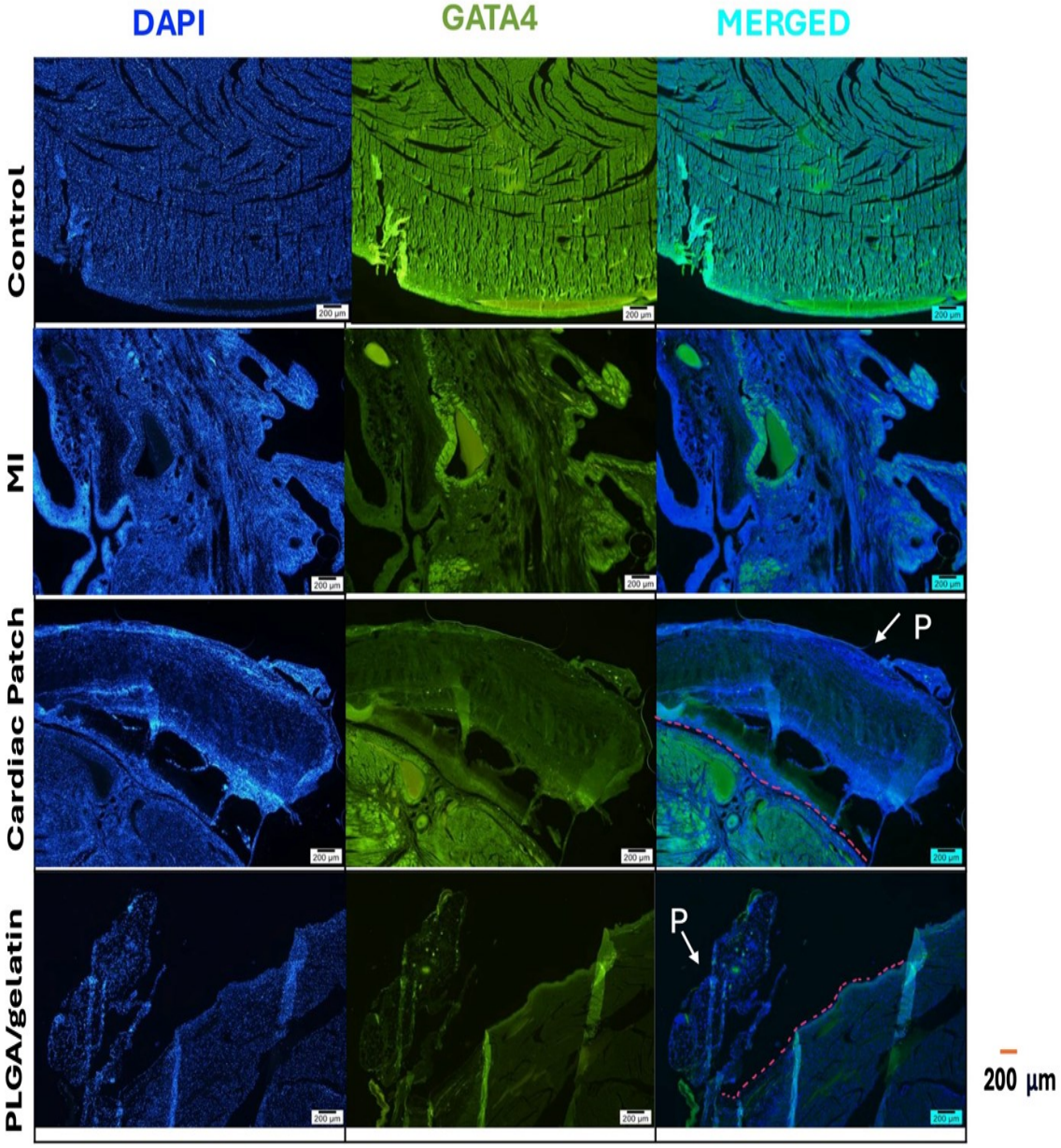

Figure 3.34 Examination of heart tissues with immunofluorescence staining techniques using anti-GATA4. The scale bar represents 200 µm.

The anti-CD34 primary antibody is used to mark intercellular adhesion molecules and endothelial cells in vascularization. As seen in Figure 3.35, CD34 markers in the MI group were significantly reduced compared to the healthy group. In the bilayered patch group, markers were detected in the areas where blood vessels are located. In the PLGA/gelatin group, it was seen on the outside of the membrane.

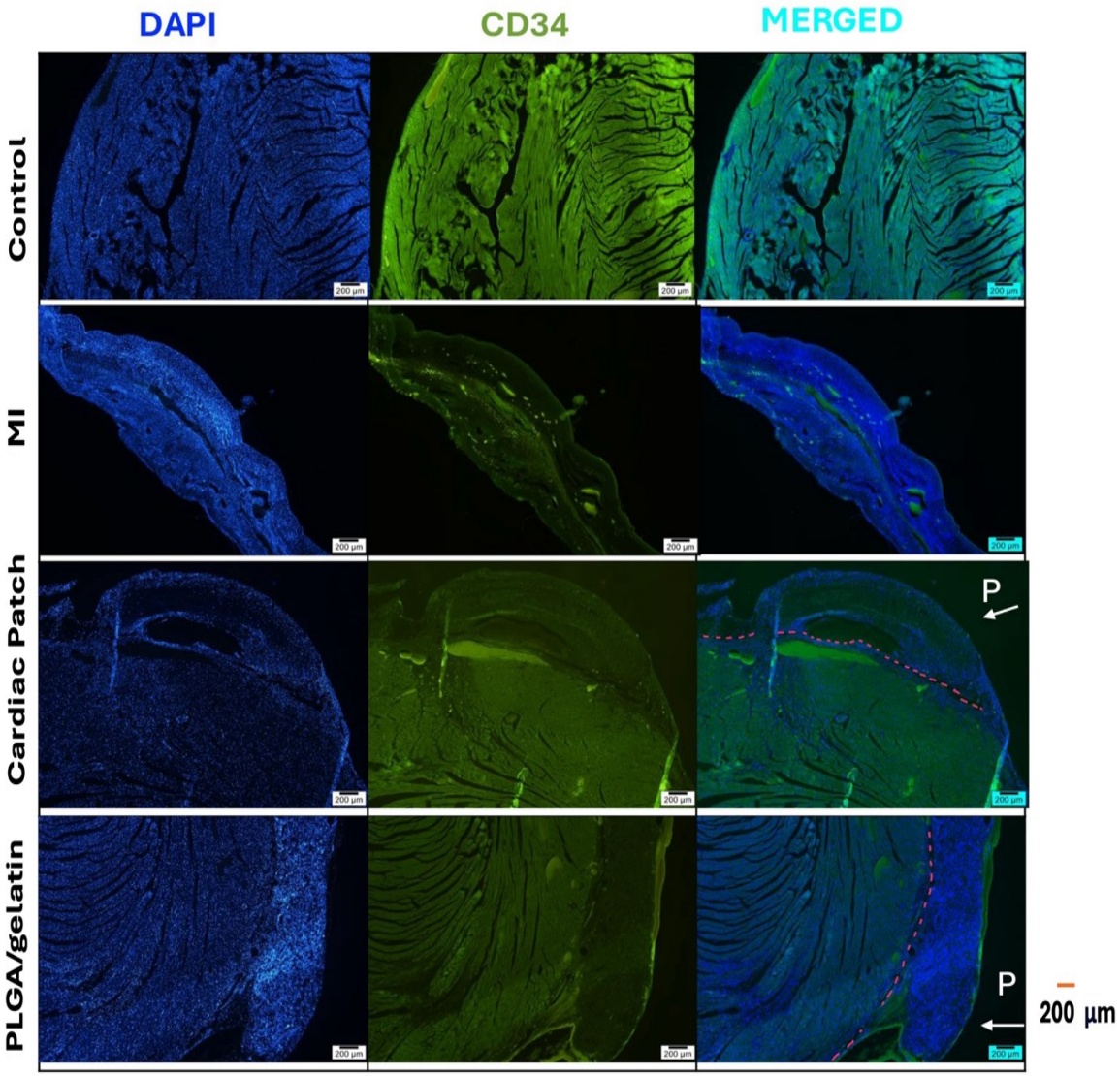

Figure 3.35 Examination of heart tissues with immunofluorescence staining techniques and anti-CD34. The scale bar represents 200 µm.

The presence of macrophages was examined with the anti-CD68 primary antibody and was presented comparatively in Figure 3.36. Macrophages were detected as green glows in the defected area of the MI group. In the healthy group, no significant macrophage markers were found. In the bilayered patch group, markers were seen in the patch, but no markers were found in the myocardium. In the PLGA/gelatin applied group, markers were detected both in the membrane and in the myocardium.

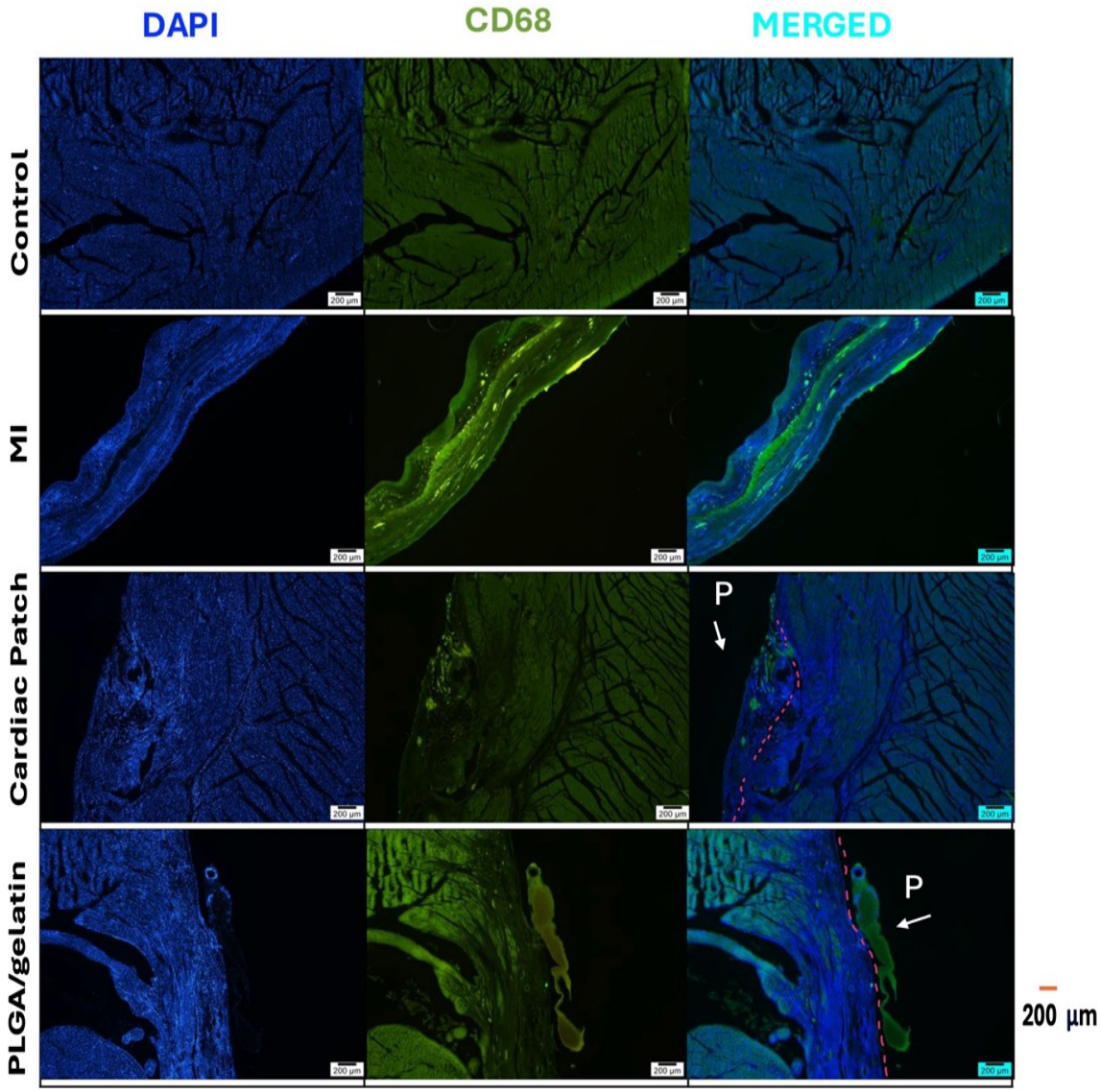

Figure 3.36 Examination of heart tissues with immunofluorescence staining techniques and anti-CD68. The scale bar represents 200 µm.

4.2.5 Immunohistochemistry

Heart tissues were also examined with immunohistochemistry staining with ABC method and data regarding vwf, CD31 and αSMA markers were presented in Figure 3.37. In the bilayered patch implanted group, vwf and CD31 markers and vascular structures were seen to be more compared to the other groups. αSMA markers were seen densely in the bilayered patch, indicating that cardiac cells migrated and integrated into the patch. Immunohistochemistry staining results were evaluated to be consistent with the Immunofluorescence staining results.

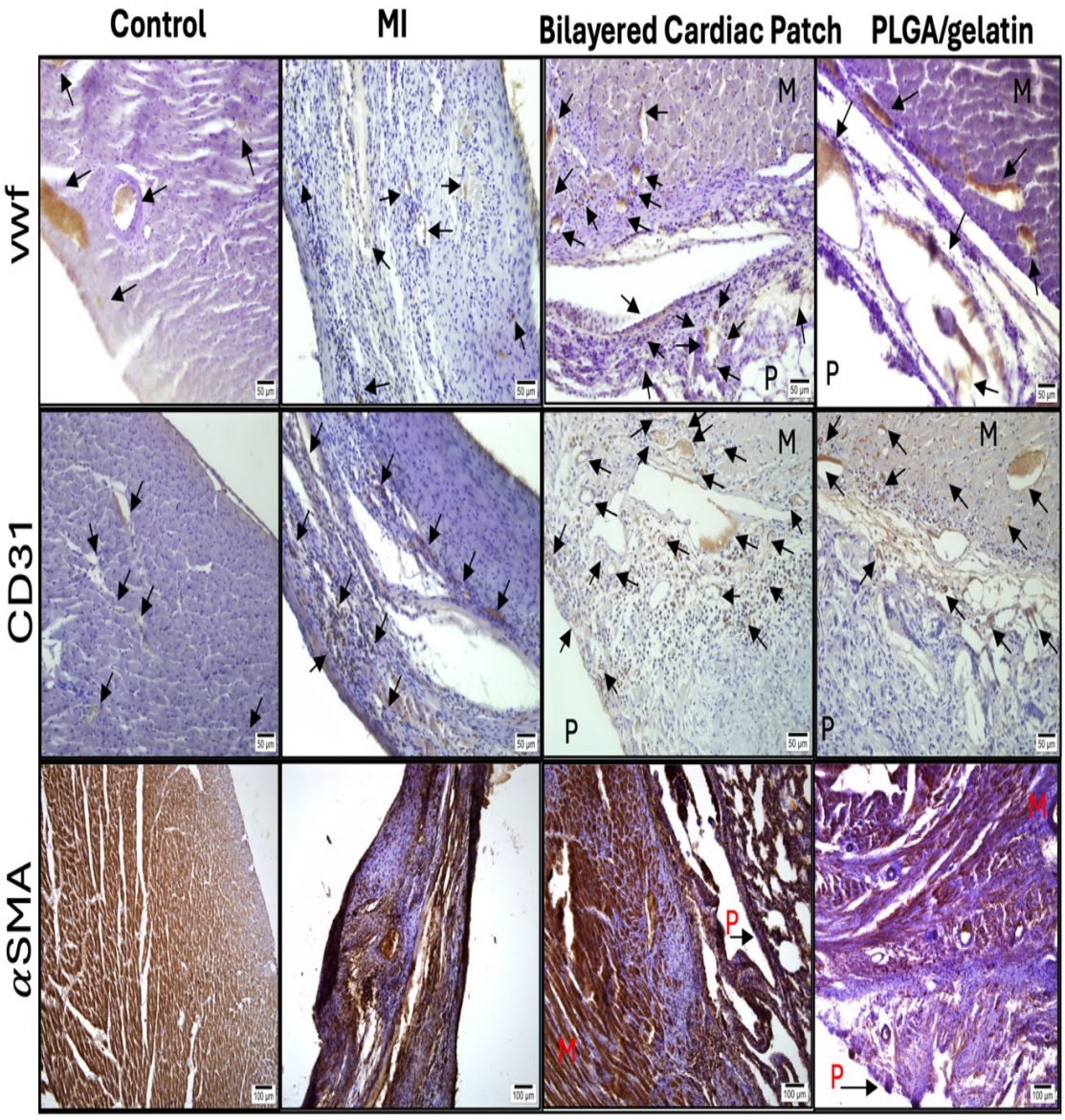

Figure 3.37 Immunohistochemical staining methods of heart tissues to show anti-vwf, anti-CD31 and anti-αSMA markers. (P: applied patch material, M: myocardium of the heart. Scale bar represents 50 μm for vwf and CD31, 100 μm for αSMA).

According to *in vivo* study results, cell deaths and scar lead to ventricular wall thinning and a decline in cardiac functions over a 4-week period in the MI group. However, patch or PLGA/gelatin implanted groups demonstrated that the improvement in cardiac functions and histological examinations. These applied materials provided mechanical support, preventing left ventricular expansion and thinning of the wall. In the bilayered cardiac patch group, patch not only offered mechanical support to the defected area but also significantly reduced the scar size due to the bioactive components. The hawthorn extract and VEGF inside patch created synergistic effect on cell migration, formation of vessels, healing of scar, and integration of patch material within 4 weeks.

Chapter 4

Conclusions and Future Prospects

4.1 Conclusions

This thesis aimed to develop a next-generation, bilayered cardiac patch, perform its *in vitro* characterizations, and assess its efficacy in an *in vivo* myocardial defect rat model. The resulting cardiac patch is expected to make a significant contribution to the treatment of myocardial defects caused by cardiovascular diseases, one of the leading causes of death worldwide. Additionally, by developing a domestic and nationally produced cardiac patch, this project will reduce foreign dependency and contribute to our country's economic growth. This thesis not only introduces a substantial advancement to the literature but also pioneers the development of a new-generation cardiac patch in our country. The first part of the thesis project involved the separate production of the bilayered cardiac patch's first and second layers, followed by detailed characterizations of each layer. For the first layer, the decellularization procedure of the pericardium was optimized to completely remove from cells. The decellularization of the pericardium was examined with histological staining techniques and H&E and DAPI staining, and it was shown that the cells were completely removed from the tissue. The amounts of DNA and collagen in the tissue were examined via commercial kits. While the pericardium was completely freed from cells, the tissue integrity was preserved, and it was proven that the structural integrity was preserved with mechanical testing and morphological examinations compared to the native pericardium. PANI nanoparticles were synthesized with a size of 104 nm to provide conductivity to the pericardium and chemical characterization was completed with FTIR, and size measurement was completed with DLS. Decellularized pericardium was coated with PANI nanoparticles and a $9x10^{-4}$ S/cm conductivity of was achieved, thus reaching the targeted 10^{-4} S/cm conductivity value of native myocardium.

To obtain the second layer of the cardiac patch, hawthorn extract was obtained using the refluxed method and chemical characterizations were completed with FTIR and GC-

MS analyses. For the production of the second layer, PLGA/gelatin polymers were produced with hawthorn extract and VEGF by electrospinning technique. At this stage, both electrospinning parameters and concentration optimizations of extract and VEGF were performed. 15% (w/v) PLGA/gelatin was used to fabricate membranes with 1, 5, 10 and 15 % (w/v) hawthorn extract. The hawthorn extract containing membranes were fabricated and 10 % (w/v) hawthorn was selected to produce 0.1, 5 and 1 μg/ml VEGF containing membranes. These fabricated membranes' morphological structure, fiber diameter, homogeneous fiber distributions, pore sizes, release behaviours, hydrophilic properties, weight loss behaviours were examined comparatively with each other, and then optimum hawthorn extract and VEGF values were determined. The second layer to be used in obtaining the cardiac patch was determined as 15% (w/v) PLGA/gelatin membrane containing 10% (w/v) hawthorn extract and 1 μg/ml VEGF. It was observed that the second layer released almost all of the hawthorn extract and VEGF within 3-4 weeks with an average fiber diameter of 890.91 nm and an average pore size of 19.2 μm. The anticoagulant effect of the hawthorn extract was examined by APTT clotting time test, and it was observed that the second layer had an APTT time of 331±65.1 seconds, which was much better than our targeted value. The bioactivity of VEGF in the second layer was confirmed with an *in vitro* commercial kit. Thus, when the second layer is applied to the defected myocardium as a biodegradable polymeric bioactive layer, it has been proven to have cardio-protective properties that can degrade within 3-4 weeks and provide controlled release of hawthorn extract and VEGF to the defected area, provide vascularization and prevent unwanted coagulation.

In the third part of the thesis, integration of the two layers of the bilayered cardiac patch was successfully achieved using a biocompatible tissue adhesive, confirmed by SEM imaging. The adhesive strength of layer integration was assessed through the Lap-Shear test, yielding results consistent with the literature. The mechanical properties of the bilayered cardiac patch were evaluated with a tensile test, demonstrating that the bilayered design significantly enhanced mechanical strength compared to native pericardium, decellularized pericardium, an electrospun PLGA/gelatin membrane, and each individual layers. The Young's modulus of the bilayered cardiac patch was approximately 675 kPa, exceeding the target minimum of 200 kPa, aligning with the modulus of native myocardium. Based on literature reports and the characteristics of defected heart tissue, the cardiac patch was deemed to possess mechanical properties compatible with native cardiac tissue. The cell viability of the bilayered cardiac patch was assessed using

cardiomyocyte cells, showing over 90% viability across 24, 48, and 72-hour assessments. Blood compatibility was also evaluated, achieving the target criterion of a hemolysis rate below 5% with a result of 0.421±0.191%, confirming the patch's blood compatibility and biocompatibility.

In the final and most challenging phase of the project, the efficacy of the cardiac patch was tested in an *in vivo* rat myocardial defect model. The left coronary artery ligation model was optimized to induce myocardial defect in rats, requiring intensive work and resulting in higher-than-expected mortality due to the method's high risk. After myocardial infarction, the bilayered cardiac patch was implanted on the rats' hearts, with positive and negative control groups established for comparison. Four weeks post-operation, the rats were sacrificed, and their heart tissues were subjected to histological examination. Echocardiographic evaluations during the 4-week period indicated significant improvements in cardiac function within the bilayered cardiac patch group, with cardiac function values recorded at 87.99% ejection fraction (EF) and 50.46% fractional shortening (FS), exceeding the targeted values. Histological evaluations were performed using H&E and Masson’s Trichrome stains to assess heart tissue defect, left ventricular wall thickness, and the applied patch. These evaluations revealed a decrease in tissue defect, an increase in vessel formation within the defected area, and a higher cell count in the bilayered patch applied group compared to other groups. It was also noted that the patched groups provided mechanical support, preventing left ventricular expansion, stopping ventricular wall thinning, and decreasing tissue death relative to the unpatched group. Immunofluorescence examinations on heart tissues were conducted using three different antibody markers to assess new vascular structure formation. In the bilayered cardiac patch group, a greater presence of vascular structures was observed both in the defected area and within the patch itself compared to other groups. The presence of more cardiac cells and cardiac muscle proteins in the cardiac patch groups was indicated by GATA4 and αSMA markers. The CD68 marker was used to detect immune cells, and no significant macrophage presence was observed within any groups during the 4-week period. Upon completion of heart tissue evaluations in the bilayered cardiac patch group, findings indicated greater tissue improvement in the defected area, as well as an increase in vascular structures and cells compared to the other groups.

In line with the results obtained in thesis project, the bilayered patch appears to be a promising candidate for the treatment of myocardial defect. The hypothesis stated in the project proposal has been successfully realized, with outcomes surpassing initial

expectations. It is expected that this will make a significant contribution to the literature in the future and be applied to many patients with heart disease, helping to prevent heart failure.

4.2 Societal Impact and Contribution to Global Sustainability

The bilayered cardiac patch developed in this thesis project holds significant potential for societal impact and contribution to global sustainability by addressing one of the most pressing health challenges worldwide—heart disease. Globally, cardiovascular diseases (CVDs) continue to be the major cause of death, claiming over 17 million lives annually. This novel cardiac patch aims to directly impact patient outcomes by providing an innovative treatment for myocardial defects, one of the most severe consequences of CVDs. Unlike traditional treatment options, which are often limited to medications or heart transplantation, our bilayered patch offers an affordable, easily accessible, and simple-to-apply solution. This patch promotes natural tissue repair, which could substantially improve patients' quality of life, reduce hospital readmissions, and decrease overall healthcare costs.

The integration of sustainable and locally sourced materials in the patch's design also contributes to its environmental and economic sustainability. By incorporating natural plants, such as hawthorn, into the patch's composition, we minimize the need for synthetic drugs, which often have a high environmental footprint during their manufacturing and disposal stages. Additionally, the use of electrospinning to develop the patch allows for efficient material utilization, reducing waste in production and ensuring a sustainable manufacturing process. As a locally developed and produced solution, this cardiac patch reduces dependency on imported biomedical devices, supporting economic self-sufficiency and fostering growth in the domestic medical technology sector.

On a broader scale, this project aligns with several United Nations Sustainable Development Goals (SDGs), particularly SDG 3 (Good Health and Well-Being) and SDG 9 (Industry, Innovation, and Infrastructure). By contributing a pioneering solution for CVD treatment, we advance medical innovation and support healthier lives, creating the

foundation for a more sustainable healthcare system. In summary, the bilayered cardiac patch not only promises to enhance cardiovascular treatment but also embodies principles of sustainability, local innovation, and accessibility, making it a valuable advancement with far-reaching implications for global health and sustainable development.

4.3 Future Prospects

The future prospects of the bilayered cardiac patch are highly promising, with the potential to significantly transform the treatment of cardiovascular diseases and contribute to advancements in regenerative medicine. As heart disease continues to be a leading cause of death globally, the demand for effective and sustainable treatments remains critical. This innovative cardiac patch has the potential to reduce the need for invasive surgeries, minimize complications, and provide long-term healing solutions for patients with myocardial defects.

In the near future, the patch can be optimized for broader clinical applications, including treatment for various types of heart defect, such as ischemic heart disease, heart failure, and congenital heart defects. With further research and development, the material properties of the bilayered patch, such as its mechanical strength, biodegradability, and drug delivery capabilities, can be fine-tuned to enhance its effectiveness in different patient populations.

In addition, the widespread use of this technology could lead to a reduction in healthcare costs by offering an affordable, easily accessible, and minimally invasive alternative to traditional therapies. As more data is collected from clinical trials and long-term studies, the patch could become an integral part of treatment protocols in hospitals worldwide, especially in regions with limited access to advanced cardiac care.

Moreover, the integration of this patch with emerging technologies, such as tissue engineering and stem cell therapy, could pave the way for next-generation treatments that promote the regeneration of heart tissue. This would not only benefit patients but also reduce the global burden of heart disease, contributing to the achievement of sustainable development goals related to health and well-being.

Ultimately, the success of the bilayered cardiac patch in clinical settings will be a key milestone in the advancement of cardiovascular medicine, potentially revolutionizing how heart disease is treated and managed in the future.

BIBLIOGRAPHY

[1] A. J. Weinhaus and K. P. Roberts, "Anatomy of the Human Heart," in *Handbook of Cardiac Anatomy, Physiology, and Devices*, Totowa, NJ: Humana Press, 2009, pp. 59–85. doi: 10.1007/978-1-60327-372-5_5.

[2] A. Varela and C. H. Davos, "Cardiovascular Anatomy and Physiology: Basic Principles and Challenges," 2019, pp. 3–11. doi: 10.1007/978-981-10-5092-3_1.

[3] J. G Betts, Desaix, P., Johnson, E., Johnson, J. E., Korol, O., Kruse, D., ... & Young, K. A. (2013). "Anatomy and Physiology," in *Anatomy and Physiology 2e*, OpenStax. Rice University: Houston, TX, USA, 13., 2013.

[4] M. Litviňuková *et al.*, "Cells of the adult human heart," *Nature*, vol. 588, no. 7838, pp. 466–472, Dec. 2020, doi: 10.1038/s41586-020-2797-4.

[5] Barbara Feldman, "Human Heart," https://www.surfnetkids.com/resources/human-heart/, 2024.

[6] Gaea Marelle Miranda, "Structure and Function of Heart," https://www.news-medical.net/health/Structure-and-Function-of-the-Heart.aspx.

[7] "Heart," https://my.clevelandclinic.org/health/body/21704-heart, 2024.

[8] R. M. Anderson, "Chapter 1:Normal Criculation ," in *The Gross Physiology of the Cardiovascular System*, Second Edition., RacquetPress, 1993.

[9] J. G. Betts, "The Cardiovascular System: The Heart," in *Anatomy and Physiology* , OpenStax. Rice University Houston, Texas: OpenStax, 2022, ch. 19.

[10] A. Shah, S. Seydafkan, and D. Sheps, "Introduction to Cardiac Anatomy, Physiology, and Pathophysiology," in *Handbook of Cardiovascular Behavioral Medicine*, New York, NY: Springer New York, 2022, pp. 23–44. doi: 10.1007/978-0-387-85960-6_2.

[11] Jennifer Lange, "Pericardial Membranes and Layers of the Heart Wall.," https://openstax.org/books/anatomy-and-physiology-2e/pages/19-1-heart-anatomy, OpenStax, 2024.

[12] Sam Kneller, "heart-myocardium-figure-8," https://theexplanation.com/muscles-inside-skin-hair-nails-outside-key-body-parts/heart-myocardium-figure-8/, 2024.

[13] B. D. Hoit, "Anatomy and Physiology of the Pericardium," *W.B. Saunders*. Nov. 01, 2017, doi: 10.1016/j.ccl.2017.07.002.

[14] Dr. S. Venkatesan, "What is the mechanism of pericardial rub?," https://drsvenkatesan.com/2008/09/28/what-is-the-mechanism-of-pericardial-rub/pericardium/, 2024.

[15] A. Kennedy, D. D. Finlay, D. Guldenring, R. Bond, K. Moran, and J. McLaughlin, "The Cardiac Conduction System: Generation and Conduction of the Cardiac Impulse," *W.B. Saunders*. Sep. 01, 2016, doi: 10.1016/j.cnc.2016.04.001.

[16] R. E. Ahmed, T. Tokuyama, T. Anzai, N. Chanthra, and H. Uosaki, "Sarcomere maturation: function acquisition, molecular mechanism, and interplay with other organelles," *Philosophical Transactions of the Royal Society B: Biological Sciences*, vol. 377, no. 1864, Nov. 2022, doi: 10.1098/rstb.2021.0325.

[17] A. Wei *et al.*, "*In Vivo* -Like Morphology of Intercalated Discs Achieved in a Neonatal Cardiomyocyte Culture Model," *Tissue Eng Part A*, vol. 26, no. 21–22, pp. 1209–1221, Nov. 2020, doi: 10.1089/ten.tea.2020.0068.

[18] Ren-Ke Li and Richard D. Weisel, *Cardiac regeneration and repair: Biomaterials and tissue engineering*. Elsevier, 2014.

[19] T. Solomon, M. Rajendran, T. Rostovtseva, and L. Hool, "How cytoskeletal proteins regulate mitochondrial energetics in cell physiology and diseases," *Philosophical*

Transactions of the Royal Society B: Biological Sciences, vol. 377, no. 1864, Nov. 2022, doi: 10.1098/rstb.2021.0324.
[20] Xingyu Wei; Sandesh Yohannan; John R. Richards., "Physiology, Cardiac Repolarization Dispersion and Reserve," https://www.ncbi.nlm.nih.gov/books/NBK537194/, 2024.
[21] Aykan Çelik, "Aksiyon Potansiyeli," http://www.aritmirehberi.com/aksiyon-potansiyeli/#:~:text=Aksiyon%20potansiyeli%20tek%20bir%20kalp,b%C3%B6lgenin%20toplam%20aksiyon%20potansiyelini%20g%C3%B6sterir, 2024.
[22] Dr Joshua Loh, "What Does An Abnormal ECG Mean?," https://www.capitalheart.sg/what-does-an-abnormal-ecg-mean/, 2024.
[23] "Heart Rate Graphics," https://www.shutterstock.com/search/normal-ecg, 2024.
[24] O. A. Bolonduro, B. M. Duffy, A. A. Rao, L. D. Black, and B. P. Timko, "From biomimicry to bioelectronics: Smart materials for cardiac tissue engineering," May 01, 2020, *Tsinghua University Press*. doi: 10.1007/s12274-020-2682-3.
[25] M. Vaduganathan, G. A. Mensah, J. V. Turco, V. Fuster, and G. A. Roth, "The Global Burden of Cardiovascular Diseases and Risk," *J Am Coll Cardiol*, vol. 80, no. 25, pp. 2361–2371, Dec. 2022, doi: 10.1016/j.jacc.2022.11.005.
[26] C. W. Tsao *et al.*, "Heart Disease and Stroke Statistics—2022 Update: A Report From the American Heart Association," *Circulation*, vol. 145, no. 8, Feb. 2022, doi: 10.1161/CIR.0000000000001052.
[27] World Heart Federation, " World Heart Report 2023: Confronting the World's Number One Killer.," Geneva, Switzerland. , 2023.
[28] World Health Organization, "The top 10 causes of death". https://www.who.int/news-room/fact-sheets/detail/the-top-10-causes-of-death, 2024.
[29] Türkiye İstatistik Kurumu (TUİK), https://www.tuik.gov.tr/, 2024.
[30] "CARDIOVASCULAR DISEASE INFOGRAPHIC," https://world-heart-federation.org/resource/cardiovascular-disease-infographic/, 2024.
[31] M. James Beckerman, "Cardiovascular Diseases", https://www.webmd.com/bio/beckerman-james?pg=15, 2024.
[32] "Cardiac Disease", https://www.creative-diagnostics.com/Cardiac-Disease.htm, 2024.
[33] D. Li, J. Sun, and T. P. Zhong, "Wnt Signaling in Heart Development and Regeneration," Oct. 01, 2022, *Springer*. doi: 10.1007/s11886-022-01756-8.
[34] "Anatomy and Function of the Coronary Arteries," https://www.hopkinsmedicine.org/health/conditions-and-diseases/anatomy-and-function-of-the-coronary-arteries, 2024.
[35] E. Tampakakis and C. Kwon, "Heart generation and regeneration," *Semin Cell Dev Biol*, vol. 118, pp. 92–93, Oct. 2021, doi: 10.1016/j.semcdb.2021.07.014.
[36] Y. Zhao, G. Eng, B. W. Lee, M. Radisic, and G. Vunjak-Novakovic, "Cardiac tissue engineering," in *Principles of Tissue Engineering*, Elsevier, 2020, pp. 593–616. doi: 10.1016/B978-0-12-818422-6.00033-2.
[37] Mayo Clinic Staff, "Heart attack," https://www.mayoclinic.org/diseases-conditions/heart-attack/symptoms-causes/syc-20373106, 2024.
[38] L. Lu, M. Liu, R. R. Sun, Y. Zheng, and P. Zhang, "Myocardial Infarction: Symptoms and Treatments," *Cell Biochem Biophys*, vol. 72, no. 3, pp. 865–867, Jul. 2015, doi: 10.1007/s12013-015-0553-4.
[39] Ranya N. Sweis and Arif Jivan, "Acute Myocardial Infarction (MI)," https://www.msdmanuals.com/en-nz/professional/cardiovascular-disorders/coronary-artery-disease/acute-myocardial-infarction-mi, 2024.
[40] M. A. Moreno-Palanco, P. Ibáñez-Sanz, C. Ciria-de Pablo, A. Pizarro-Portillo, F. Rodríguez-Salvanés, and C. Suárez-Fernández, "Impact of Comprehensive and Intensive Treatment of Risk Factors Concerning Cardiovascular Mortality in Secondary

Prevention: MIRVAS Study," *Revista Española de Cardiología (English Edition)*, vol. 64, no. 3, pp. 179–185, Mar. 2011, doi: 10.1016/j.rec.2010.07.002.
[41] M. C. Bahit, A. Kochar, and C. B. Granger, "Post-Myocardial Infarction Heart Failure," Mar. 01, 2018, *Elsevier Inc.* doi: 10.1016/j.jchf.2017.09.015.
[42] T. A. Marciniak and V. Serebruany, "Ranolazine, ACE Inhibitors, and Angiotensin Receptor Blockers," *American Journal of Medicine*, vol. 132, no. 12, pp. e844–e845, Dec. 2019, doi: 10.1016/j.amjmed.2019.02.032.
[43] R. Amezcua, A. Shirolkar, C. Fraze, and D. A. Stout, "Nanomaterials for cardiac myocyte tissue engineering," Jul. 19, 2016, *MDPI AG*. doi: 10.3390/nano6070133.
[44] L. E. Rodriguez, E. E. Suarez, M. Loebe, and B. A. Bruckner, "Ventricular Assist Devices (VAD) Therapy: New Technology, New Hope?", *Methodist DeBakey cardiovascular journal*, 9(1), 32., 2013.
[45] L. A. Reis, L. L. Y. Chiu, N. Feric, L. Fu, and M. Radisic, "Biomaterials in myocardial tissue engineering," *J Tissue Eng Regen Med*, vol. 10, no. 1, pp. 11–28, Jan. 2016, doi: 10.1002/term.1944.
[46] 2024 Mayo Foundation for Medical Education and Research (MFMER)., "Ventricular assist device (VAD)," https://middlesexhealth.org/learning-center/tests-and-procedures/ventricular-assist-device-vad, 2024.
[47] H. Jawad, N. N. Ali, A. R. Lyon, Q. Z. Chen, S. E. Harding, and A. R. Boccaccini, "Myocardial tissue engineering: A review," 2007, *John Wiley and Sons Ltd*. doi: 10.1002/term.46.
[48] C. B. Lombello, A. O. Masson, F. N. Ambrosio, D. C. Ferraraz, and M. H. M. do Nascimento, "Principles of Tissue Engineering and Regenerative Medicine," in *Current Trends in Biomedical Engineering*, Cham: Springer International Publishing, 2023, pp. 127–148. doi: 10.1007/978-3-031-38743-2_8.
[49] K. N. Alagarsamy, W. Yan, A. Srivastava, V. Desiderio, and S. Dhingra, "Application of injectable hydrogels for cardiac stem cell therapy and tissue engineering," *Rev Cardiovasc Med*, vol. 20, no. 4, pp. 221–230, 2019, doi: 10.31083/J.RCM.2019.04.534.
[50] M. A. Laflamme and C. E. Murry, "Regenerating the heart," *Nat Biotechnol*, vol. 23, no. 7, pp. 845–856, 2005, doi: 10.1038/nbt1117.
[51] R.-K. Li *et al.*, "Cardiomyocyte Transplantation Improves Heart Function," *Ann Thorac Surg*, vol. 62, no. 3, pp. 654–661, Aug. 1996, doi: 10.1016/S0003-4975(96)00389-X.
[52] Y. Zhao, G. Eng, B. W. Lee, M. Radisic, and G. Vunjak-Novakovic, "Cardiac tissue engineering," in *Principles of Tissue Engineering*, Elsevier, 2020, pp. 593–616. doi: 10.1016/B978-0-12-818422-6.00033-2.
[53] M. R. Afzal *et al.*, "Adult bone marrow cell therapy for ischemic heart disease: Evidence and insights from randomized controlled trials," *Circ Res*, vol. 117, no. 6, pp. 558–575, Aug. 2015, doi: 10.1161/CIRCRESAHA.114.304792.
[54] K. N. Alagarsamy, W. Yan, A. Srivastava, V. Desiderio, and S. Dhingra, "Application of injectable hydrogels for cardiac stem cell therapy and tissue engineering," 2019, *IMR Press Limited*. doi: 10.31083/J.RCM.2019.04.534.
[55] S. Di Franco, C. Amarelli, A. Montalto, A. Loforte, and F. Musumeci, "Biomaterials and heart recovery: Cardiac repair, regeneration and healing in the MCS era: A state of the 'heart,'" Jul. 01, 2018, *AME Publishing Company*. doi: 10.21037/jtd.2018.01.85.
[56] O. Okay, "General Properties of Hydrogels," 2009, pp. 1–14. doi: 10.1007/978-3-540-75645-3_1.
[57] B. Peña *et al.*, "Injectable Hydrogels for Cardiac Tissue Engineering," Jun. 01, 2018, *Wiley-VCH Verlag*. doi: 10.1002/mabi.201800079.

[58] N. J. R. Blackburn *et al.*, “Timing underpins the benefits associated with injectable collagen biomaterial therapy for the treatment of myocardial infarction,” *Biomaterials*, vol. 39, pp. 182–192, Jan. 2015, doi: 10.1016/j.biomaterials.2014.11.004.
[59] A. Chow *et al.*, “Human Induced Pluripotent Stem Cell-Derived Cardiomyocyte Encapsulating Bioactive Hydrogels Improve Rat Heart Function Post Myocardial Infarction,” *Stem Cell Reports*, vol. 9, no. 5, pp. 1415–1422, Nov. 2017, doi: 10.1016/j.stemcr.2017.09.003.
[60] S. McMahan, A. Taylor, K. M. Copeland, Z. Pan, J. Liao, and Y. Hong, “Current advances in biodegradable synthetic polymer based cardiac patches,” Apr. 01, 2020, *John Wiley and Sons Inc.* doi: 10.1002/jbm.a.36874.
[61] M. Muñoz *et al.*, “Nanoengineered Sprayable Therapy for Treating Myocardial Infarction,” *ACS Nano*, vol. 16, no. 3, pp. 3522–3537, Mar. 2022, doi: 10.1021/acsnano.1c08890.
[62] D. Bejleri and M. E. Davis, “Decellularized Extracellular Matrix Materials for Cardiac Repair and Regeneration,” Mar. 07, 2019, *Wiley-VCH Verlag*. doi: 10.1002/adhm.201801217.
[63] A. K. Capulli, L. A. MacQueen, S. P. Sheehy, and K. K. Parker, “Fibrous scaffolds for building hearts and heart parts,” Jan. 15, 2016, *Elsevier B.V.* doi: 10.1016/j.addr.2015.11.020.
[64] J. L. Olson, A. Atala, and J. J. Yoo, “Tissue Engineering: Current Strategies and Future Directions,” *Chonnam Med J*, vol. 47, no. 1, p. 1, 2011, doi: 10.4068/cmj.2011.47.1.1.
[65] B. Guo and P. X. Ma, “Conducting Polymers for Tissue Engineering,” *Biomacromolecules*, vol. 19, no. 6, pp. 1764–1782, Jun. 2018, doi: 10.1021/acs.biomac.8b00276.
[66] A. Hasan *et al.*, “Engineered Biomaterials to Enhance Stem Cell-Based Cardiac Tissue Engineering and Therapy,” *Macromol Biosci*, pp. 958–977, Jul. 2016, doi: 10.1002/mabi.201500396.
[67] T. Liu *et al.*, “Advanced Cardiac Patches for the Treatment of Myocardial Infarction,” *Circulation*, vol. 149, no. 25, pp. 2002–2020, Jun. 2024, doi: 10.1161/CIRCULATIONAHA.123.067097.
[68] M. Domenech, L. Polo-Corrales, J. E. Ramirez-Vick, and D. O. Freytes, “Tissue engineering strategies for myocardial regeneration: Acellular versus cellular scaffolds?” Dec. 01, 2016, *Mary Ann Liebert Inc.* doi: 10.1089/ten.teb.2015.0523.
[69] D. W. Y. Toong *et al.*, “Bioresorbable polymeric scaffold in cardiovascular applications,” May 02, 2020, *MDPI AG*. doi: 10.3390/ijms21103444.
[70] D. W. Y. Toong *et al.*, “Bioresorbable Polymeric Scaffold in Cardiovascular Applications,” *Int J Mol Sci*, vol. 21, no. 10, p. 3444, May 2020, doi: 10.3390/ijms21103444.
[71] Z. Cui, B. Yang, and R. K. Li, “Application of Biomaterials in Cardiac Repair and Regeneration,” *Engineering*, vol. 2, no. 1, pp. 141–148, Mar. 2016, doi: 10.1016/J.ENG.2016.01.028.
[72] M. O. Chrobak *et al.*, “Design of a Fibrin Microthread-Based Composite Layer for Use in a Cardiac Patch,” *ACS Biomater Sci Eng*, vol. 3, no. 7, pp. 1394–1403, Jul. 2017, doi: 10.1021/acsbiomaterials.6b00547.
[73] Y. Zhang *et al.*, “Recent Advances in Cardiac Patches: Materials, Preparations, and Properties,” Sep. 12, 2022, *American Chemical Society*. doi: 10.1021/acsbiomaterials.2c00348.
[74] P. Baei, S. Jalili-Firoozinezhad, S. Rajabi-Zeleti, M. Tafazzoli-Shadpour, H. Baharvand, and N. Aghdami, “Electrically conductive gold nanoparticle-chitosan thermosensitive

hydrogels for cardiac tissue engineering," *Materials Science and Engineering C*, vol. 63, pp. 131–141, Jun. 2016, doi: 10.1016/j.msec.2016.02.056.
[75] R. D. Levit *et al.*, "Cellular Encapsulation Enhances Cardiac Repair," *J Am Heart Assoc*, vol. 2, no. 5, Sep. 2013, doi: 10.1161/JAHA.113.000367.
[76] R. Gaetani *et al.*, "Epicardial application of cardiac progenitor cells in a 3D-printed gelatin/hyaluronic acid patch preserves cardiac function after myocardial infarction," *Biomaterials*, vol. 61, pp. 339–348, Aug. 2015, doi: 10.1016/j.biomaterials.2015.05.005.
[77] H. Peng *et al.*, "Polymer Cell Surface Coating Enhances Mesenchymal Stem Cell Retention and Cardiac Protection," *ACS Appl Bio Mater*, vol. 4, no. 2, pp. 1655–1667, Feb. 2021, doi: 10.1021/acsabm.0c01473.
[78] S. K. Asl, M. Rahimzadegan, and A. K. Asl, "Progress in cardiac tissue engineering and regeneration: Implications of gelatin-based hybrid scaffolds," *Int J Biol Macromol*, vol. 261, p. 129924, Mar. 2024, doi: 10.1016/j.ijbiomac.2024.129924.
[79] E. Rosellini, L. Lazzeri, S. Maltinti, F. Vanni, N. Barbani, and M. G. Cascone, "Development and characterization of a suturable biomimetic patch for cardiac applications," *J Mater Sci Mater Med*, vol. 30, no. 11, p. 126, Nov. 2019, doi: 10.1007/s10856-019-6327-6.
[80] B. Sun, L. Wang, W. Guo, S. Chen, Y. Ma, and D. Wang, "New treatment methods for myocardial infarction," *Front Cardiovasc Med*, vol. 10, Sep. 2023, doi: 10.3389/fcvm.2023.1251669.
[81] L. Altomare, S. Farè, and M. C. Tanzi, "Bio-Instructive Scaffolds for Muscle Regeneration," in *Bio-Instructive Scaffolds for Musculoskeletal Tissue Engineering and Regenerative Medicine*, Elsevier, 2017, pp. 161–186. doi: 10.1016/B978-0-12-803394-4.00007-0.
[82] T. Sugiura, N. Hibino, C. K. Breuer, and T. Shinoka, "Tissue-engineered cardiac patch seeded with human induced pluripotent stem cell derived cardiomyocytes promoted the regeneration of host cardiomyocytes in a rat model," *J Cardiothorac Surg*, vol. 11, no. 1, Dec. 2016, doi: 10.1186/s13019-016-0559-z.
[83] T. Chang *et al.*, "Biomaterials based cardiac patches for the treatment of myocardial infarction," Dec. 20, 2021, *Chinese Society of Metals*. doi: 10.1016/j.jmst.2021.03.062.
[84] A. R. Adhikari, B. P. Tilakaratne, D. Wijesundera, and W.-K. Chu, "A Study of Surface Modification of Poly(lactic-co-glycolic) Acid Using Argon Ion Irradiation," *J Surf Eng Mater Adv Technol*, vol. 04, no. 06, pp. 326–331, 2014, doi: 10.4236/jsemat.2014.46036.
[85] Y. Xing *et al.*, "Construction of engineered myocardial tissues in﷿vitro with cardiomyocyte-like cells and a polylactic-co-glycolic acid polymer," *Mol Med Rep*, Jun. 2019, doi: 10.3892/mmr.2019.10434.
[86] M. P Prabhakaran, D. Kai, L. Ghasemi-Mobarakeh, and S. Ramakrishna, "Electrospun biocomposite nanofibrous patch for cardiac tissue engineering," *Biomedical Materials*, vol. 6, no. 5, p. 055001, Oct. 2011, doi: 10.1088/1748-6041/6/5/055001.
[87] J. H. Wee *et al.*, "Stem cell laden nano and micro collagen/PLGA bimodal fibrous patches for myocardial regeneration," *Biomater Res*, vol. 26, no. 1, Sep. 2022, doi: 10.1186/s40824-022-00319-w.
[88] S. G. Kumbar, R. James, S. P. Nukavarapu, and C. T. Laurencin, "Electrospun nanofiber scaffolds: Engineering soft tissues," *Biomedical Materials*, vol. 3, no. 3, Sep. 2008, doi: 10.1088/1748-6041/3/3/034002.
[89] Y. Liu, Y. Xu, Z. Wang, D. Wen, W. Zhang, S. Schmull, H. Li, Y. Chen, S. Xue "Electrospun nanofibrous sheets of collagen/elastin/polycaprolactone improve cardiac repair after myocardial infarction," *Am J Transl Res* , vol. 8, no. 4, 2016.

[90] Y. He *et al.*, "Mussel-inspired conductive nanofibrous membranes repair myocardial infarction by enhancing cardiac function and revascularization," *Theranostics*, vol. 8, no. 18, pp. 5159–5177, 2018, doi: 10.7150/thno.27760.
[91] Dr Jackson Fyfe, "The multiple roles of the Extracellular Matrix," https://humanperformanceandhealth.org/blog/2019/12/01/the-multiple-roles-of-the-extracellular-matrix/, 2024.
[92] D. Bejleri *et al.*, "A Bioprinted Cardiac Patch Composed of Cardiac-Specific Extracellular Matrix and Progenitor Cells for Heart Repair," *Adv Healthc Mater*, vol. 7, no. 23, Dec. 2018, doi: 10.1002/adhm.201800672.
[93] T. W. Gilbert, T. L. Sellaro, and S. F. Badylak, "Decellularization of tissues and organs," Jul. 2006. doi: 10.1016/j.biomaterials.2006.02.014.
[94] I. Inci, A. Norouz Dizaji, C. Ozel, U. Morali, F. Dogan Guzel, and H. Avci, "Decellularized inner body membranes for tissue engineering: A review," Jul. 02, 2020, *Taylor and Francis Inc.* doi: 10.1080/09205063.2020.1751523.
[95] W. A. Oldenburg, T. Almerey, M. Selim, H. Farres, and A. G. Hakaim, "Durability of Carotid Endarterectomy with Bovine Pericardial Patch," *Ann Vasc Surg*, vol. 50, pp. 218–224, Jul. 2018, doi: 10.1016/j.avsg.2017.11.062.
[96] S. M. Kameli *et al.*, "Application of tissue-engineered pericardial patch in rat models of myocardial infarction," *J Biomed Mater Res A*, vol. 106, no. 10, pp. 2670–2678, Oct. 2018, doi: 10.1002/jbm.a.36464.
[97] Y. Dong, M. Hong, R. Dai, H. Wu, and P. Zhu, "Engineered bioactive nanoparticles incorporated biofunctionalized ECM/silk proteins based cardiac patches combined with MSCs for the repair of myocardial infarction: In vitro and in vivo evaluations," *Science of the Total Environment*, vol. 707, Mar. 2020, doi: 10.1016/j.scitotenv.2019.135976.
[98] A. D'Amore *et al.*, "Bi-layered polyurethane – Extracellular matrix cardiac patch improves ischemic ventricular wall remodeling in a rat model," *Biomaterials*, vol. 107, pp. 1–14, Nov. 2016, doi: 10.1016/j.biomaterials.2016.07.039.
[99] D. Steffens, D. I. Braghirolli, N. Maurmann, and P. Pranke, "Update on the main use of biomaterials and techniques associated with tissue engineering," Aug. 01, 2018, *Elsevier Ltd*. doi: 10.1016/j.drudis.2018.03.013.
[100] J. Xue, T. Wu, Y. Dai, and Y. Xia, "Electrospinning and electrospun nanofibers: Methods, materials, and applications," Apr. 24, 2019, *American Chemical Society*. doi: 10.1021/acs.chemrev.8b00593.
[101] K. Garg and G. L. Bowlin, "Electrospinning jets and nanofibrous structures," *Biomicrofluidics*, vol. 5, no. 1, Mar. 2011, doi: 10.1063/1.3567097.
[102] A. R. Alharbi, I. M. Alarifi, W. S. Khan, and R. Asmatulu, "Highly Hydrophilic Electrospun Polyacrylonitrile/ Polyvinypyrro-lidone Nanofibers Incorporated with Gentamicin as Filter Medium for Dam Water and Wastewater Treatment," *Journal of Membrane and Separation Technology*, vol. 5, no. 2, pp. 38–56, Jul. 2016, doi: 10.6000/1929-6037.2016.05.02.1.
[103] B. Fromager, E. Marhuenda, B. Louis, N. Bakalara, J. Cambedouzou, and D. Cornu, "Recent Advances in Electrospun Fibers for Biological Applications," *Macromol*, vol. 3, no. 3, pp. 569–613, Aug. 2023, doi: 10.3390/macromol3030033.
[104] A. Gilpin and Y. Yang, "Decellularization Strategies for Regenerative Medicine: From Processing Techniques to Applications," 2017, *Hindawi Limited*. doi: 10.1155/2017/9831534.
[105] G. S. Hussey, J. L. Dziki, and S. F. Badylak, "Extracellular matrix-based materials for regenerative medicine," Jul. 01, 2018, *Nature Publishing Group*. doi: 10.1038/s41578-018-0023-x.

[106] P. M. Crapo, T. W. Gilbert, and S. F. Badylak, “An overview of tissue and whole organ decellularization processes,” Apr. 2011. doi: 10.1016/j.biomaterials.2011.01.057.
[107] M. Parmaksiz, A. Dogan, S. Odabas, A. E. Elçin, and Y. M. Elçin, “Clinical applications of decellularized extracellular matrices for tissue engineering and regenerative medicine,” *Biomedical Materials (Bristol)*, vol. 11, no. 2, Mar. 2016, doi: 10.1088/1748-6041/11/2/022003.
[108] Y. Jiang *et al.*, “Myocardial repair of bioengineered cardiac patches with decellularized placental scaffold and human-induced pluripotent stem cells in a rat model of myocardial infarction,” *Stem Cell Res Ther*, vol. 12, no. 1, p. 13, Dec. 2021, doi: 10.1186/s13287-020-02066-y.
[109] T. T. A. Liguori, G. R. Liguori, J. A. van Dongen, L. F. P. Moreira, and M. C. Harmsen, “Bioactive decellularized cardiac extracellular matrix-based hydrogel as a sustained-release platform for human adipose tissue-derived stromal cell-secreted factors,” *Biomedical Materials*, vol. 16, no. 2, p. 025022, Mar. 2021, doi: 10.1088/1748-605X/abcff9.
[110] I. Allu, A. K. Sahi, M. Koppadi, S. Gundu, and A. Sionkowska, “Decellularization Techniques for Tissue Engineering: Towards Replicating Native Extracellular Matrix Architecture in Liver Regeneration,” *J Funct Biomater*, vol. 14, no. 10, p. 518, Oct. 2023, doi: 10.3390/jfb14100518.
[111] K. Ashtari *et al.*, “Electrically conductive nanomaterials for cardiac tissue engineering,” Apr. 01, 2019, *Elsevier B.V.* doi: 10.1016/j.addr.2019.06.001.
[112] B. Guo and P. X. Ma, “Conducting Polymers for Tissue Engineering,” *Biomacromolecules*, vol. 19, no. 6, pp. 1764–1782, Jun. 2018, doi: 10.1021/acs.biomac.8b00276.
[113] C.-H. Chen, J.-M. Wang, and W.-Y. Chen, “Conductive Polyaniline Doped with Dodecyl Benzene Sulfonic Acid: Synthesis, Characterization, and Antistatic Application,” *Polymers (Basel)*, vol. 12, no. 12, p. 2970, Dec. 2020, doi: 10.3390/polym12122970.
[114] Y. Li *et al.*, “Conductive biomaterials for cardiac repair: A review,” *Acta Biomater*, vol. 139, pp. 157–178, Feb. 2022, doi: 10.1016/j.actbio.2021.04.018.
[115] L. Wang, Y. Wu, T. Hu, B. Guo, and P. X. Ma, “Electrospun conductive nanofibrous scaffolds for engineering cardiac tissue and 3D bioactuators,” *Acta Biomater*, vol. 59, pp. 68–81, Sep. 2017, doi: 10.1016/j.actbio.2017.06.036.
[116] B. S. Spearman *et al.*, “Conductive interpenetrating networks of polypyrrole and polycaprolactone encourage electrophysiological development of cardiac cells,” *Acta Biomater*, vol. 28, pp. 109–120, Dec. 2015, doi: 10.1016/j.actbio.2015.09.025.
[117] R. Balint, N. J. Cassidy, and S. H. Cartmell, “Conductive polymers: Towards a smart biomaterial for tissue engineering,” *Acta Biomater*, vol. 10, no. 6, pp. 2341–2353, Jun. 2014, doi: 10.1016/j.actbio.2014.02.015.
[118] S. Jadoun, S. Jabin, and A. Verma, “Ionic liquid–polymer based nanocomposites and applications,” in *Ionic Liquids and Their Application in Green Chemistry*, Elsevier, 2023, pp. 97–112. doi: 10.1016/B978-0-323-95931-5.00007-5.
[119] M. Li, Y. Guo, Y. Wei, A. G. MacDiarmid, and P. I. Lelkes, “Electrospinning polyaniline-contained gelatin nanofibers for tissue engineering applications,” *Biomaterials*, vol. 27, no. 13, pp. 2705–2715, May 2006, doi: 10.1016/j.biomaterials.2005.11.037.
[120] M. C. Chen, Y. C. Sun, and Y. H. Chen, “Electrically conductive nanofibers with highly oriented structures and their potential application in skeletal muscle tissue engineering,” *Acta Biomater*, vol. 9, no. 3, pp. 5562–5572, 2013, doi: 10.1016/j.actbio.2012.10.024.
[121] I. Rajzer, M. Rom, E. Menaszek, and P. Pasierb, “Conductive PANI patterns on electrospun PCL/gelatin scaffolds modified with bioactive particles for bone tissue

engineering," *Mater Lett*, vol. 138, pp. 60–63, Jan. 2015, doi: 10.1016/j.matlet.2014.09.077.
[122] M. Beygisangchin, S. Abdul Rashid, S. Shafie, A. R. Sadrolhosseini, and H. N. Lim, "Preparations, Properties, and Applications of Polyaniline and Polyaniline Thin Films—A Review," *Polymers (Basel)*, vol. 13, no. 12, p. 2003, Jun. 2021, doi: 10.3390/polym13122003.
[123] M. Montgomery, B. Zhang, and M. Radisic, "Cardiac Tissue Vascularization," *J Cardiovasc Pharmacol Ther*, vol. 19, no. 4, pp. 382–393, Jul. 2014, doi: 10.1177/1074248414528576.
[124] M. Shibuya, "Vascular Endothelial Growth Factor (VEGF) and Its Receptor (VEGFR) Signaling in Angiogenesis: A Crucial Target for Anti- and Pro-Angiogenic Therapies," *Genes Cancer*, vol. 2, no. 12, pp. 1097–1105, Dec. 2011, doi: 10.1177/1947601911423031.
[125] T. Liu *et al.*, "Advanced Cardiac Patches for the Treatment of Myocardial Infarction," *Circulation*, vol. 149, no. 25, pp. 2002–2020, Jun. 2024, doi: 10.1161/CIRCULATIONAHA.123.067097.
[126] Y. Miyagi, L. L. Y. Chiu, M. Cimini, R. D. Weisel, M. Radisic, and R. K. Li, "Biodegradable collagen patch with covalently immobilized VEGF for myocardial repair," *Biomaterials*, vol. 32, no. 5, pp. 1280–1290, Feb. 2011, doi: 10.1016/j.biomaterials.2010.10.007.
[127] K. Huang *et al.*, "An off-the-shelf artificial cardiac patch improves cardiac repair after myocardial infarction in rats and pigs," *Sci Transl Med*, vol. 12, no. 538, Apr. 2020, doi: 10.1126/scitranslmed.aat9683.
[128] R. Rai *et al.*, "Bioactive Electrospun Fibers of Poly(glycerol sebacate) and Poly(ε-caprolactone) for Cardiac Patch Application," *Adv Healthc Mater*, vol. 4, no. 13, pp. 2012–2025, Sep. 2015, doi: 10.1002/adhm.201500154.
[129] M. Akram and A. Rashid, "Anti-coagulant activity of plants: mini review," Oct. 01, 2017, *Springer New York LLC*. doi: 10.1007/s11239-017-1546-5.
[130] S. Liu, J. Yu, M. Fu, X. Wang, and X. Chang, "Regulatory effects of hawthorn polyphenols on hyperglycemic, inflammatory, insulin resistance responses, and alleviation of aortic injury in type 2 diabetic rats," *Food Research International*, vol. 142, Apr. 2021, doi: 10.1016/j.foodres.2021.110239.
[131] Q. Chang, Z. Zuo, F. Harrison, and M. S. S. Chow, "Hawthorn," 2002. doi: 10.1177/00970002042006003.
[132] E. Koch and F. A. Malek, "Standardized extracts from hawthorn leaves and flowers in the treatment of cardiovascular disorders preclinical and clinical studies," 2011. doi: 10.1055/s-0030-1270849.
[133] J. Wang, X. Xiong, and B. Feng, "Effect of crataegus usage in cardiovascular disease prevention: An evidence-based approach," 2013, *Oxford University Press*. doi: 10.1155/2013/149363.
[134] A. S. Shatoor, A. Shati, S. M. Al Humayed, A. K. Shatoor, N. M. Alhawiti, and S. A. Alqahtani, "The hypocoagulant effect of Crataegus aronia in rats entails vitamin K-dependent and vitamin K-independent effects," *J Food Biochem*, vol. 44, no. 1, Jan. 2020, doi: 10.1111/jfbc.13094.
[135] R. Jayalakshmi, C. J. Thirupurasundari, and S. N. Devaraj, "Pretreatment with alcoholic extract of shape Crataegus oxycantha (AEC) activates mitochondrial protection during isoproterenol - Induced myocardial infarction in rats," *Mol Cell Biochem*, vol. 292, no. 1–2, pp. 59–67, Nov. 2006, doi: 10.1007/s11010-006-9218-3.

[136] D. Sönmezer, F. Latifoglu, G. Toprak, A. Düzler, and I. A. Işoglu, "Pericardial fluid and vascular tissue engineering: A preliminary study," *Biomed Mater Eng*, vol. 32, no. 2, pp. 101–113, 2021, doi: 10.3233/BME-196014.
[137] E. Pagoulatou *et al.*, "Biomechanical and structural changes following the decellularization of bovine pericardial tissues for use as a tissue engineering scaffold," *J Mater Sci Mater Med*, vol. 23, no. 6, pp. 1387–1396, 2012, doi: 10.1007/s10856-012-4620-8.
[138] S. Zouhair *et al.*, "A comprehensive comparison of bovine and porcine decellularized pericardia: New insights for surgical applications," *Biomolecules*, vol. 10, no. 3, Mar. 2020, doi: 10.3390/biom10030371.
[139] Y. E. Arslan, B. Efe, and T. Sezgin Arslan, "A novel method for constructing an acellular 3D biomatrix from bovine spinal cord for neural tissue engineering applications," *Biotechnol Prog*, vol. 35, no. 4, Jul. 2019, doi: 10.1002/btpr.2814.
[140] M. Kimicata *et al.*, "Assessment of decellularized pericardial extracellular matrix and poly(propylene fumarate) biohybrid for small-diameter vascular graft applications," *Acta Biomater*, vol. 110, pp. 68–81, Jul. 2020, doi: 10.1016/j.actbio.2020.04.013.
[141] F. C. Bayram, M. F. Kapçı, A. Yuruk, I. A. Isoglu, and B. Bal, "Investigations of strain rate, size, and crack length effects on the mechanical response of polycaprolactone electrospun membranes," *Proceedings of the Institution of Mechanical Engineers, Part E: Journal of Process Mechanical Engineering*, vol. 235, no. 6, pp. 1957–1970, Dec. 2021, doi: 10.1177/09544089211024065.
[142] A. Yürük Durukan and I. A. Işoğlu, "3-Sulfopropyl methacrylate based cryogels as potential tissue engineering scaffolds," *Materials Technology*, vol. 35, no. 13–14, pp. 853–862, Dec. 2020, doi: 10.1080/10667857.2019.1706271.
[143] B. Bal, I. B. Tugluca, N. Koc, and I. A. Isoglu, "On the detailed mechanical response investigation of PHBV/PCL and PHBV/PLGA electrospun mats," *Mater Res Express*, vol. 6, no. 6, Mar. 2019, doi: 10.1088/2053-1591/ab0eaa.
[144] M. Zamanifard, M. T. Khorasani, M. Daliri, and M. Parvazinia, "Preparation and modeling of electrospun polyhydroxybutyrate/polyaniline composite scaffold modified by plasma and printed by an inkjet method and its cellular study," *J Biomater Sci Polym Ed*, vol. 31, no. 12, pp. 1515–1537, 2020, doi: 10.1080/09205063.2020.1764162.
[145] T. H. Qazi *et al.*, "Development and characterization of novel electrically conductive PANI-PGS composites for cardiac tissue engineering applications," *Acta Biomater*, vol. 10, no. 6, pp. 2434–2445, 2014, doi: 10.1016/j.actbio.2014.02.023.
[146] J. H. Yoo, Y. Liu, and H. S. Kim, "Hawthorn fruit extract elevates expression of Nrf2/HO-1 and improves lipid profiles in ovariectomized rats," *Nutrients*, vol. 8, no. 5, May 2016, doi: 10.3390/nu8050283.
[147] A. Yuruk, S. D. Isoglu, and I. A. Isoglu, "Preparation and Characterization of Viburnum Opulus Containing Electrospun Membranes as Antibacterial Wound Dressing," *Fibers and Polymers*, vol. 24, no. 11, pp. 3761–3774, Nov. 2023, doi: 10.1007/s12221-023-00360-z.
[148] I. A. Isoglu and N. Koc, "Centella Asiatica Extract Containing Bilayered Electrospun Wound Dressing," *Fibers and Polymers*, vol. 21, no. 7, pp. 1453–1465, Jul. 2020, doi: 10.1007/s12221-020-9956-y.
[149] G. Lan *et al.*, "Chitosan/gelatin composite sponge is an absorbable surgical hemostatic agent," *Colloids Surf B Biointerfaces*, vol. 136, pp. 1026–1034, Dec. 2015, doi: 10.1016/j.colsurfb.2015.10.039.
[150] B. M. Vickerman, C. P. O'Banion, X. Tan, and D. S. Lawrence, "Light-Controlled Release of Therapeutic Proteins from Red Blood Cells," *ACS Cent Sci*, vol. 7, no. 1, pp. 93–103, Jan. 2021, doi: 10.1021/acscentsci.0c01151.

[151] A. Yuruk, S. D. Isoglu, and I. A. Isoglu, “Preparation and Characterization of Viburnum Opulus Containing Electrospun Membranes as Antibacterial Wound Dressing,” *Fibers and Polymers*, Nov. 2023, doi: 10.1007/s12221-023-00360-z.
[152] S. Kamiloglu, G. Sari, T. Ozdal, and E. Capanoglu, “Guidelines for cell viability assays,” *Food Front*, vol. 1, no. 3, pp. 332–349, Sep. 2020, doi: 10.1002/fft2.44.
[153] M. Shah, P. Kc, and G. Zhang, “In Vivo Assessment of Decellularized Porcine Myocardial Slice as an Acellular Cardiac Patch,” *ACS Appl Mater Interfaces*, vol. 11, no. 27, pp. 23893–23900, Jul. 2019, doi: 10.1021/acsami.9b06453.
[154] L. A. Reis, L. L. Y. Chiu, N. Feric, L. Fu, and M. Radisic, “Biomaterials in myocardial tissue engineering,” *J Tissue Eng Regen Med*, vol. 10, no. 1, pp. 11–28, Jan. 2016, doi: 10.1002/term.1944.
[155] S. Saghebasl, A. Akbarzadeh, A. M. Gorabi, N. Nikzamir, M. SeyedSadjadi, and E. Mostafavi, “Biodegradable functional macromolecules as promising scaffolds for cardiac tissue engineering,” *Polym Adv Technol*, vol. 33, no. 7, pp. 2044–2068, Jul. 2022, doi: 10.1002/pat.5669.
[156] C. Cristallini *et al.*, “Micro- and Macrostructured PLGA/Gelatin Scaffolds Promote Early Cardiogenic Commitment of Human Mesenchymal Stem Cells In Vitro,” *Stem Cells Int*, vol. 2016, pp. 1–16, 2016, doi: 10.1155/2016/7176154.
[157] M. A. Heuschkel *et al.*, “In vitro evaluation of bovine pericardium after a soft decellularization approach for use in tissue engineering,” *Xenotransplantation*, vol. 26, no. 2, Mar. 2019, doi: 10.1111/xen.12464.
[158] L. Wollmann *et al.*, “Characterization of decellularized human pericardium for tissue engineering and regenerative medicine applications,” *Arq Bras Cardiol*, vol. 113, no. 1, pp. 11–17, Jul. 2019, doi: 10.5935/abc.20190094.
[159] F. Chen *et al.*, “Crosslinked Decellularized Porcine Pericardium as a Substrate for Conjunctival Reconstruction,” *Stem Cells Int*, vol. 2022, 2022, doi: 10.1155/2022/7571146.
[160] F. Stieglmeier, M. Grab, F. König, J. Büch, C. Hagl, and N. Thierfelder, “Mapping of bovine pericardium to enable a standardized acquirement of material for medical implants,” *J Mech Behav Biomed Mater*, vol. 118, Jun. 2021, doi: 10.1016/j.jmbbm.2021.104432.
[161] L. Laker, P. M. Dohmen, and F. E. Smit, “Synergy in a detergent combination results in superior decellularized bovine pericardial extracellular matrix scaffolds,” *J Biomed Mater Res B Appl Biomater*, vol. 108, no. 6, pp. 2571–2578, Aug. 2020, doi: 10.1002/jbm.b.34588.
[162] N. Jadidi, B. Adib, and F. B. Malihi, “Synergism and performance optimization in liquid detergents containing binary mixtures of anionic-nonionic, and anionic-cationic surfactants,” *J Surfactants Deterg*, vol. 16, no. 1, pp. 115–121, Jan. 2013, doi: 10.1007/s11743-012-1371-y.
[163] S. Zouhair *et al.*, “Preservation strategies for decellularized pericardial scaffolds for off-the-shelf availability,” *Acta Biomater*, vol. 84, pp. 208–221, Jan. 2019, doi: 10.1016/j.actbio.2018.10.026.
[164] M. Todesco *et al.*, “A New Detergent for the Effective Decellularization of Bovine and Porcine Pericardia,” *Biomimetics*, vol. 7, no. 3, Sep. 2022, doi: 10.3390/biomimetics7030104.
[165] J. Hülsmann *et al.*, “Transplantation material bovine pericardium: Biomechanical and immunogenic characteristics after decellularization vs. glutaraldehyde-fixing,” *Xenotransplantation*, vol. 19, no. 5, pp. 286–297, Sep. 2012, doi: 10.1111/j.1399-3089.2012.00719.x.

[166] N. V. Shchotkina *et al.*, “Optimized Method of Bovine Pericardium Decellularization for Tissue Engineering,” *Wiad Lek*, vol. 74, no. 4, pp. 815–820, 2021, doi: 10.36740/wlek202104101.
[167] B. Mendoza-Novelo *et al.*, “Decellularization of pericardial tissue and its impact on tensile viscoelasticity and glycosaminoglycan content,” *Acta Biomater*, vol. 7, no. 3, pp. 1241–1248, 2011, doi: 10.1016/j.actbio.2010.11.017.
[168] O. Ngamna, A. Morrin, A. J. Killard, S. E. Moulton, M. R. Smyth, and G. G. Wallace, “Inkjet printable polyaniline nanoformulations,” *Langmuir*, vol. 23, no. 16, pp. 8569–8574, Jul. 2007, doi: 10.1021/la700540g.
[169] M. Khalid, A. Maria Borges Honorato, and H. Varela, “Polyaniline: Synthesis Methods, Doping and Conduction Mechanism”, doi: 10.5772/intechopen.79089.
[170] M. A. E. Hafizah, A. F. Riyadi, A. Manaf, and Andreas, “Particle Size Reduction of Polyaniline Assisted by Anionic Emulsifier of Sodium Dodecyl Sulphate (SDS) Through Emulsion Polymerization,” in *IOP Conference Series: Materials Science and Engineering*, Institute of Physics Publishing, 2019. doi: 10.1088/1757-899X/515/1/012080.
[171] M. Zamanifard, M. T. Khorasani, M. Daliri, and M. Parvazinia, “Preparation and modeling of electrospun polyhydroxybutyrate/polyaniline composite scaffold modified by plasma and printed by an inkjet method and its cellular study,” *J Biomater Sci Polym Ed*, vol. 31, no. 12, pp. 1515–1537, Aug. 2020, doi: 10.1080/09205063.2020.1764162.
[172] V. Kumar, T. Yokozeki, T. Goto, and T. Takahashi, “Synthesis and characterization of PANI-DBSA/DVB composite using roll-milled PANI-DBSA complex,” *Polymer (Guildf)*, vol. 86, pp. 129–137, Mar. 2016, doi: 10.1016/j.polymer.2016.01.054.
[173] K. Pal, A. T. Paulson, and D. Rousseau, “Biopolymers in Controlled-Release Delivery Systems,” in *Modern Biopolymer Science: Bridging the Divide between Fundamental Treatise and Industrial Application*, Elsevier, 2009, pp. 519–557. doi: 10.1016/B978-0-12-374195-0.00016-1.
[174] Q. Yin *et al.*, “A Conductive Bioengineered Cardiac Patch for Myocardial Infarction Treatment by Improving Tissue Electrical Integrity,” *Adv Healthc Mater*, vol. 12, no. 1, Jan. 2023, doi: 10.1002/adhm.202201856.
[175] J. Zhang, X. Chai, F. Zhao, G. Hou, and Q. Meng, “Food Applications and Potential Health Benefits of Hawthorn,” Sep. 01, 2022, *MDPI*. doi: 10.3390/foods11182861.
[176] H. Rao, P. Li, H. Wu, C. Liu, W. Peng, and W. Su, “Simultaneous determination of six compounds in destructive distillation extracts of hawthorn seed by GC-MS and evaluation of their antimicrobial activity,” *Molecules*, vol. 24, no. 23, Nov. 2019, doi: 10.3390/molecules24234328.
[177] J. Wu, W. Peng, R. Qin, and H. Zhou, “Crataegus pinnatifida: Chemical Constituents, Pharmacology, and Potential Applications,” Feb. 2014. doi: 10.3390/molecules19021685.
[178] R. J. Van Putten, J. C. Van Der Waal, E. De Jong, C. B. Rasrendra, H. J. Heeres, and J. G. De Vries, “Hydroxymethylfurfural, a versatile platform chemical made from renewable resources,” Mar. 13, 2013. doi: 10.1021/cr300182k.
[179] W. Y. Jin *et al.*, “Antiplatelet and antithrombotic effect of Phyllostachys pubescens leaves and Mume Fructus combination,” *Integr Med Res*, vol. 2, no. 2, pp. 70–75, Jun. 2013, doi: 10.1016/j.imr.2013.04.005.
[180] R. S. Al-Moghrabi, A. M. Abdel-Gaber, and H. T. Rahal, “A comparative study on the inhibitive effect of Crataegus oxyacantha and Prunus avium plant leaf extracts on the corrosion of mild steel in hydrochloric acid solution,” *International Journal of Industrial Chemistry*, vol. 9, no. 3, pp. 255–263, Sep. 2018, doi: 10.1007/s40090-018-0154-3.

[181] C. Dwivedi *et al.*, "In vivo biocompatibility of electrospun biodegradable dual carrier (Antibiotic + growth factor) in a mouse model—implications for rapid wound healing," *Pharmaceutics*, vol. 11, no. 4, Apr. 2019, doi: 10.3390/pharmaceutics11040180.
[182] J. Hu, B. Ai, S. Zhu, Z. Wang, H. Xia, and W. Jia, "Electrospun PLGA and PLGA/gelatin scaffolds for tubularized urethral replacement: Studies in vitro and in vivo," *J Biomater Appl*, vol. 36, no. 6, pp. 956–964, Jan. 2022, doi: 10.1177/08853282211030904.
[183] N. N. Akşit, S. Gürdap, S. D. İşoğlu, and İ. A. İşoğlu, "Preparation of antibacterial electrospun poly(D, L-lactide-co-glycolide)/gelatin blend membranes containing Hypericum capitatum var. capitatum," *International Journal of Polymeric Materials and Polymeric Biomaterials*, vol. 70, no. 11, pp. 797–809, 2021, doi: 10.1080/00914037.2020.1765354.
[184] I. Garcia-Orue *et al.*, "Novel nanofibrous dressings containing rhEGF and Aloe vera for wound healing applications," *Int J Pharm*, vol. 523, no. 2, pp. 556–566, May 2017, doi: 10.1016/j.ijpharm.2016.11.006.
[185] R. M. Nezarati, M. B. Eifert, and E. Cosgriff-Hernandez, "Effects of humidity and solution viscosity on electrospun fiber morphology," *Tissue Eng Part C Methods*, vol. 19, no. 10, pp. 810–819, Oct. 2013, doi: 10.1089/ten.tec.2012.0671.
[186] F. Ghorbani, H. Nojehdehyan, A. Zamanian, M. Gholipourmalekabadi, and M. Mozafari, "Synthesis, physico-chemical characteristics and cellular behavior of poly (lactic-co-glycolic acid)/gelatin nanofibrous scaffolds for engineering soft connective tissues," *Adv Mater Lett*, vol. 7, no. 2, pp. 163–169, Feb. 2016, doi: 10.5185/amlett.2016.6003.
[187] A. Asiri, S. Saidin, M. H. Sani, and R. H. Al-Ashwal, "Epidermal and fibroblast growth factors incorporated polyvinyl alcohol electrospun nanofibers as biological dressing scaffold," *Sci Rep*, vol. 11, no. 1, Dec. 2021, doi: 10.1038/s41598-021-85149-x.
[188] F. Khan *et al.*, "Encapsulation of 5-flurouracil into PLGA nanofibers and enhanced anticancer effect in combination with Ajwa-Dates-Extract (Phoenix dactylifera L.)," *J Biomed Nanotechnol*, vol. 14, no. 3, pp. 553–563, Mar. 2018, doi: 10.1166/jbn.2018.2515.
[189] D. Kai, M. P. Prabhakaran, G. Jin, L. Tian, and S. Ramakrishna, "Potential of VEGF-encapsulated electrospun nanofibers for in vitro cardiomyogenic differentiation of human mesenchymal stem cells," *J Tissue Eng Regen Med*, vol. 11, no. 4, pp. 1002–1010, Apr. 2017, doi: 10.1002/term.1999.
[190] D. I. Braghirolli, V. E. Helfer, P. C. Chagastelles, T. P. Dalberto, D. Gamba, and P. Pranke, "Electrospun scaffolds functionalized with heparin and vascular endothelial growth factor increase the proliferation of endothelial progenitor cells," *Biomedical Materials (Bristol)*, vol. 12, no. 2, Mar. 2017, doi: 10.1088/1748-605X/aa5bbc.
[191] M. Sadri, S. Arab-Sorkhi, H. Vatani, and A. Bagheri-Pebdeni, "New wound dressing polymeric nanofiber containing green tea extract prepared by electrospinning method," *Fibers and Polymers*, vol. 16, no. 8, pp. 1742–1750, Aug. 2015, doi: 10.1007/s12221-015-5297-7.
[192] F. Cheng, J. Gao, L. Wang, and X. Hu, "Composite chitosan/poly(ethylene oxide) electrospun nanofibrous mats as novel wound dressing matrixes for the controlled release of drugs," *J Appl Polym Sci*, vol. 132, no. 24, Jun. 2015, doi: 10.1002/app.42060.
[193] R. Sedghi and A. Shaabani, "Electrospun biocompatible core/shell polymer-free core structure nanofibers with superior antimicrobial potency against multi drug resistance organisms," *Polymer (Guildf)*, vol. 101, pp. 151–157, Sep. 2016, doi: 10.1016/j.polymer.2016.08.060.
[194] X. Chen *et al.*, "Electrospun poly(l-lactic acid-co-ε-caprolactone) fibers loaded with heparin and vascular endothelial growth factor to improve blood compatibility and

endothelial progenitor cell proliferation," *Colloids Surf B Biointerfaces*, vol. 128, pp. 106–114, Apr. 2015, doi: 10.1016/j.colsurfb.2015.02.023.
[195] C. Del Gaudio *et al.*, "Induction of angiogenesis using VEGF releasing genipin-crosslinked electrospun gelatin mats," *Biomaterials*, vol. 34, no. 31, pp. 7754–7765, Oct. 2013, doi: 10.1016/j.biomaterials.2013.06.040.
[196] K. Nagase *et al.*, "Local Release of VEGF Using Fiber Mats Enables Effective Transplantation of Layered Cardiomyocyte Sheets," *Macromol Biosci*, vol. 17, no. 8, Aug. 2017, doi: 10.1002/mabi.201700073.
[197] G. An, W. B. Zhang, D. K. Ma, B. Lu, G. J. Wei, Y. Guang, C. H. Ru, Y. S. Wang, "Influence of VEGF/BMP-2 on the proliferation and osteogenetic differentiation of rat bone mesenchymal stem cells on PLGA/gelatin composite scaffold," *Eur Rev Med Pharmacol Sci*, vol. 21, no. 10, 2017.
[198] Z. Mokhames, Z. Rezaie, A. Ardeshirylajimi, A. Basiri, M. Taheri, and M. D. Omrani, "VEGF-incorporated PVDF/collagen nanofibrous scaffold for bladder wall regeneration and angiogenesis," *International Journal of Polymeric Materials and Polymeric Biomaterials*, vol. 70, no. 8, pp. 521–529, 2021, doi: 10.1080/00914037.2020.1740985.
[199] H. M. Eltaher, S. S. Said, and L. K. El-Khordagui, "Drug delivery for cardiac regeneration," in *Applications of Nanocomposite Materials in Drug Delivery*, Elsevier, 2018, pp. 283–321. doi: 10.1016/B978-0-12-813741-3.00013-3.
[200] I. Pawlaczyk-Graja, "Polyphenolic-polysaccharide conjugates from flowers and fruits of single-seeded hawthorn (Crataegus monogyna Jacq.): Chemical profiles and mechanisms of anticoagulant activity," *Int J Biol Macromol*, vol. 116, pp. 869–879, Sep. 2018, doi: 10.1016/j.ijbiomac.2018.05.101.
[201] W. Song, Q. Zeng, X. Yin, L. Zhu, T. Gong, and C. Pan, "Preparation and anticoagulant properties of heparin-like electrospun membranes from carboxymethyl chitosan and bacterial cellulose sulfate," *Int J Biol Macromol*, vol. 120, pp. 1396–1405, Dec. 2018, doi: 10.1016/j.ijbiomac.2018.09.133.
[202] C. J. Tsao *et al.*, "Electrospun Patch Functionalized with Nanoparticles Allows for Spatiotemporal Release of VEGF and PDGF-BB Promoting in Vivo Neovascularization," *ACS Appl Mater Interfaces*, vol. 10, no. 51, pp. 44344–44353, Dec. 2018, doi: 10.1021/acsami.8b19975.
[203] J. Wu *et al.*, "Infarct stabilization and cardiac repair with a VEGF-conjugated, injectable hydrogel," *Biomaterials*, vol. 32, no. 2, pp. 579–586, Jan. 2011, doi: 10.1016/j.biomaterials.2010.08.098.
[204] C. Lallemand *et al.*, "Quantification of Bevacizumab Activity Following Treatment of Patients With Ovarian Cancer or Glioblastoma," *Front Immunol*, vol. 11, Oct. 2020, doi: 10.3389/fimmu.2020.515556.
[205] L. Wang *et al.*, "Development of a robust reporter-based assay for the bioactivity determination of anti-VEGF therapeutic antibodies," *J Pharm Biomed Anal*, vol. 125, pp. 212–218, Jun. 2016, doi: 10.1016/j.jpba.2016.03.042.
[206] C. O. Çakır, M. T. Ozturk, and K. Tuzlakoglu, "Design of antibacterial bilayered silk fibroin-based scaffolds for healing of severe skin damages," *Materials Technology*, vol. 33, no. 10, pp. 651–658, Aug. 2018, doi: 10.1080/10667857.2018.1492209.
[207] I. A. İşoğlu, C. Demirkan, M. G. Şeker, K. Tuzlakoğlu, and S. D. İşoğlu, "Antibacterial Bilayered Skin Patches Made of HPMA and Quaternary Poly(4-vinyl pyridine)," *Fibers and Polymers*, vol. 19, no. 11, pp. 2229–2236, Nov. 2018, doi: 10.1007/s12221-018-8480-9.
[208] S. Tamburaci, B. Cecen, O. Ustun, B. U. Ergur, H. Havitcioglu, and F. Tihminlioglu, "Production and Characterization of a Novel Bilayer Nanocomposite Scaffold Composed of Chitosan/Si-nHap and Zein/POSS Structures for Osteochondral Tissue Regeneration,"

ACS Appl Bio Mater, vol. 2, no. 4, pp. 1440–1455, Apr. 2019, doi: 10.1021/acsabm.8b00700.
[209] X. Mo, H. Iwata, and Y. Ikada, "A tissue adhesives evaluated in vitro and in vivo analysis," *J Biomed Mater Res A*, vol. 94, no. 1, pp. 326–332, Jul. 2010, doi: 10.1002/jbm.a.32788.
[210] W. Zhang *et al.*, "Functionalized Multiarmed Polycaprolactones as Biocompatible Tissue Adhesives," *ACS Appl Mater Interfaces*, vol. 12, no. 15, pp. 17314–17320, Apr. 2020, doi: 10.1021/acsami.0c03478.
[211] N. Artzi, T. Shazly, A. B. Baker, A. Bon, and E. R. Edelman, "Aldehyde-amine chemistry enables modulated biosealants with tissue-specific adhesion," *Advanced Materials*, vol. 21, no. 32–33, pp. 3399–3403, Sep. 2009, doi: 10.1002/adma.200900340.
[212] M. Boffito, C. Tonda-Turo, and G. Ciardelli, "Design of electrospun fibrous patches for myocardium regeneration," in *Electrofluidodynamic Technologies (EFDTs) for Biomaterials and Medical Devices: Principles and Advances*, Elsevier Inc., 2018, pp. 221–250. doi: 10.1016/B978-0-08-101745-6.00012-8.
[213] Q. Z. Chen *et al.*, "Characterisation of a soft elastomer poly(glycerol sebacate) designed to match the mechanical properties of myocardial tissue," *Biomaterials*, vol. 29, no. 1, pp. 47–57, Jan. 2008, doi: 10.1016/j.biomaterials.2007.09.010.
[214] M. H. Norahan, M. Pourmokhtari, M. R. Saeb, B. Bakhshi, M. Soufi Zomorrod, and N. Baheiraei, "Electroactive cardiac patch containing reduced graphene oxide with potential antibacterial properties," *Materials Science and Engineering C*, vol. 104, Nov. 2019, doi: 10.1016/j.msec.2019.109921.
[215] J. S. Yoo, Y. J. Kim, S. H. Kim, and S. H. Choi, "Study on genipin: A new alternative natural crosslinking agent for fixing heterograft tissue," *Korean Journal of Thoracic and Cardiovascular Surgery*, vol. 44, no. 3, pp. 197–207, Jun. 2011, doi: 10.5090/kjtcs.2011.44.3.197.
[216] W. Jang, S. Choi, S. H. Kim, E. Yoon, H. G. Lim, and Y. J. Kim, "A comparative study on mechanical and biochemical properties of bovine pericardium after single or double crosslinking treatment," *Korean Circ J*, vol. 42, no. 3, pp. 154–163, 2012, doi: 10.4070/kcj.2012.42.3.154.
[217] Y. Yao *et al.*, "Multifunctional elastomer cardiac patches for preventing left ventricle remodeling after myocardial infarction in vivo," *Biomaterials*, vol. 282, Mar. 2022, doi: 10.1016/j.biomaterials.2022.121382.
[218] B. Kaczmarek-Szczepańska, O. Miłek, M. Michalska-Sionkowska, and A. M. Osyczka, "Bio-studies of scaffolds based on chitosan/tannic acid cross-linked by glyoxal," *Mater Lett*, vol. 292, Jun. 2021, doi: 10.1016/j.matlet.2021.129667.
[219] L. Yang *et al.*, "Preparation of pu/fibrin vascular scaffold with good biomechanical properties and evaluation of its performance in vitro and in vivo," *Int J Nanomedicine*, vol. 15, pp. 8697–8715, 2020, doi: 10.2147/IJN.S274459.
[220] A. Ghebleh and A. Z. Kharazi, "Fabrication and in vitro assessment of a biomimetic tri-layer PGS/PCL scaffold loaded with Heparin and PRP for tissue engineering of vascualar grafts," 2022, doi: 10.21203/rs.3.rs-2104007/v1.
[221] K. S. Venkataprasanna *et al.*, "Fabrication of Chitosan/PVA/GO/CuO patch for potential wound healing application," *Int J Biol Macromol*, vol. 143, pp. 744–762, Jan. 2020, doi: 10.1016/j.ijbiomac.2019.10.029.
[222] J.-M. Lü *et al.*, "Current advances in research and clinical applications of PLGA-based nanotechnology," *Expert Rev Mol Diagn*, vol. 9, no. 4, pp. 325–341, May 2009, doi: 10.1586/erm.09.15.

[223] Y. Wu, L. Wang, B. Guo, and P. X. Ma, "Interwoven Aligned Conductive Nanofiber Yarn/Hydrogel Composite Scaffolds for Engineered 3D Cardiac Anisotropy," *ACS Nano*, vol. 11, no. 6, pp. 5646–5659, Jun. 2017, doi: 10.1021/acsnano.7b01062.
[224] Y. Eitan, U. Sarig, N. Dahan, and M. Machluf, "Acellular Cardiac Extracellular Matrix as a Scaffold for Tissue Engineering: In Vitro Cell Support, Remodeling, and Biocompatibility."
[225] S. Saravanan *et al.*, "Graphene Oxide-Gold Nanosheets Containing Chitosan Scaffold Improves Ventricular Contractility and Function After Implantation into Infarcted Heart," *Sci Rep*, vol. 8, no. 1, Dec. 2018, doi: 10.1038/s41598-018-33144-0.
[226] A.-L. Papa *et al.*, "Dispersion of titanate nanotubes for nanomedicine: comparison of PEI and PEG nanohybrids," *Dalton Transactions*, vol. 44, no. 2, pp. 739–746, 2015, doi: 10.1039/C4DT02552K.
[227] K. R. Tang-Quan, N. A. Mehta, L. C. Sampaio, and D. A. Taylor, "Whole cardiac tissue bioscaffolds," in *Advances in Experimental Medicine and Biology*, vol. 1098, Springer New York LLC, 2018, pp. 85–114. doi: 10.1007/978-3-319-97421-7_5.
[228] K. Roshanbinfar, L. Vogt, F. Ruther, J. A. Roether, A. R. Boccaccini, and F. B. Engel, "Nanofibrous Composite with Tailorable Electrical and Mechanical Properties for Cardiac Tissue Engineering," *Adv Funct Mater*, vol. 30, no. 7, Feb. 2020, doi: 10.1002/adfm.201908612.
[229] X. P. Li *et al.*, "High-aspect-ratio water-dispersed gold nanowires incorporated within gelatin methacrylate hydrogels for constructing cardiac tissues: In vitro," *J Mater Chem B*, vol. 8, no. 32, pp. 7213–7224, Aug. 2020, doi: 10.1039/d0tb00768d.
[230] Y. Xing *et al.*, "Construction of engineered myocardial tissues in vitro with cardiomyocyte-like cells and a polylactic-co-glycolic acid polymer," *Mol Med Rep*, vol. 20, no. 3, pp. 2403–2409, 2019, doi: 10.3892/mmr.2019.10434.
[231] P. Benzoni *et al.*, "Biomanufacturing of a Chitosan/Collagen Scaffold to Drive Adhesion and Alignment of Human Cardiomyocyte Derived from Stem Cells," in *Procedia CIRP*, Elsevier B.V., 2016, pp. 113–120. doi: 10.1016/j.procir.2015.09.004.
[232] Z. Fang *et al.*, "Flexible Conductive Decellularized Fish Skin Matrix as a Functional Scaffold for Myocardial Infarction Repair," *Macromol Biosci*, vol. 23, no. 12, Dec. 2023, doi: 10.1002/mabi.202300207.
[233] K. L. Fujimoto *et al.*, "Placement of an elastic biodegradable cardiac patch on a subacute infarcted heart leads to cellularization with early developmental cardiomyocyte characteristics," *J Card Fail*, vol. 18, no. 7, pp. 585–595, Jul. 2012, doi: 10.1016/j.cardfail.2012.05.006.
[234] K. L. Fujimoto, A. Yamawaki-Ogata, K. Uto, A. Usui, Y. Narita, and M. Ebara, "Long term efficacy and fate of a right ventricular outflow tract replacement using an elastomeric cardiac patch consisting of caprolactone and D,L-lactide copolymers," *Acta Biomater*, vol. 123, pp. 222–229, Mar. 2021, doi: 10.1016/j.actbio.2021.01.022.
[235] H. E. M. Mewhort, J. D. Turnbull, H. C. Meijndert, J. M. C. Ngu, and P. W. M. Fedak, "Epicardial infarct repair with basic fibroblast growth factor-enhanced CorMatrix-ECM biomaterial attenuates postischemic cardiac remodeling," *Journal of Thoracic and Cardiovascular Surgery*, vol. 147, no. 5, pp. 1650–1659, 2014, doi: 10.1016/j.jtcvs.2013.08.005.
[236] D. Kai *et al.*, "Stem cell-loaded nanofibrous patch promotes the regeneration of infarcted myocardium with functional improvement in rat model," *Acta Biomater*, vol. 10, no. 6, pp. 2727–2738, 2014, doi: 10.1016/j.actbio.2014.02.030.
[237] S. J. Joggerst and A. K. Hatzopoulos, "Stem cell therapy for cardiac repair: benefits and barriers," *Expert Rev Mol Med*, vol. 11, p. e20, Jul. 2009, doi: 10.1017/S1462399409001124.

CURRICULUM VITAE

2012 – 2016	B.Sc., Biomedical Engineering, Namık Kemal University, Tekirdağ, TÜRKİYE
2018 – 2024	PhD, Bioengineering, Abdullah Gül University, Kayseri, TÜRKİYE
2018-2022	Doctorate Scholarship, The Council of Higher Education (YÖK) 100/2000, TÜRKİYE
2019	Bursary, FEBS Young Scientist Travel Grant for 47th FEBS Congress, POLAND
2021-2025	Doctorate Scholarship, The Scientific and Technological Research Council of Turkey (TÜBİTAK BİDEB 2211- A), TÜRKİYE
2023	Bursary, FEBS Young Scientist Travel Grant for 44th FEBS Congress, FRANCE

SELECTED PUBLICATIONS AND PRESENTATIONS

J1) Yuruk A., Isoglu I. A. (2019). "3-Sulfopropyl methacrylate based cryogels as potential tissue engineering scaffolds", Materials Technology, 1-10., Doi:10.1080/10667857.2019.1706271.

J2) Bayram, F. C., Kapci, M. F., Yuruk, A., Isoglu, I. A., & Bal, B. (2021). Investigations of strain rate, size, and crack length effects on the mechanical response of polycaprolactone electrospun membranes. Proceedings of the Institution of Mechanical Engineers, Part E: Journal of Process Mechanical Engineering, 235(6), 1957-1970.

J3) Yuruk, A., Isoglu, S. D., & Isoglu, I. A. (2023). Preparation and Characterization of Viburnum Opulus Containing Electrospun Membranes as Antibacterial Wound Dressing. Fibers and Polymers, 24(11), 3761-3774.

C1) Yuruk A., Isoglu I. A. (2018) "Highly Porous Sulfoproply Methachrylate-Based Cryogels as Biomaterials", Oral Presentation, 14th Nanoscience and Technology Symposium-NanoTR, İzmir, Türkiye.

C2) Yuruk A., Isoglu I. A. (2019) “Synthesis and Characterization of 4-VP/SPMA cryogels”, Posters. FEBS Open Bio, 9: 65-431. P-20-020. https://do.org/10.1002/2211-5463.12675.

C3) Yuruk, A., Isoglu, S.D. & Isoglu, I.A. (2023) “Investigation of a novel antibacterial wound dressing PCL/gelatin membranes with Viburnum opulus plant extract”. Posters. FEBS Open Bio, 13: 61-258, P-03.1-02.

C4) Yuruk, A., Isoglu, S.D. & Isoglu, I.A. (2023) “A Novel Antibacterial Polymeric Wound Dressing Membranes for Wound Healing Applications”, Oral Presentation, 17th Nanoscence and Technology Symposum-NanoTR17, İzmir, Türkiye.